


Spring 5-14-2016

# Structural Analysis of Transient Receptor Potential Vanilloid Type 1 (TRPV1) Channel Protein and Proline Mimics using Computational Techniques

Kelly A. Raymond  
kelly.raymond@student.shu.edu

Follow this and additional works at: <https://scholarship.shu.edu/dissertations>

 Part of the [Biochemistry, Biophysics, and Structural Biology Commons](#), and the [Physical Chemistry Commons](#)

---

## Recommended Citation

Raymond, Kelly A., "Structural Analysis of Transient Receptor Potential Vanilloid Type 1 (TRPV1) Channel Protein and Proline Mimics using Computational Techniques" (2016). *Seton Hall University Dissertations and Theses (ETDs)*. 2184.  
<https://scholarship.shu.edu/dissertations/2184>

# Structural Analysis of Transient Receptor Potential Type 1 (TRPV1) Channel Protein and Proline Mimics using Computational Techniques

A Dissertation  
Submitted to the Department of  
Chemistry and Biochemistry of  
Seton Hall University

By  
Kelly A. Raymond  
May 2016

In partial Fulfillment of the  
Requirements of the Degree  
Of  
Doctorate of Chemistry

Accepted by:

Dr. Stephen Kelty  
Dr. Cecilia Marzabadi  
Dr. Sergiu Gorun  
Dr. David Sabatino  
Dr. Yufeng Wei  
Dr. Monika Raj


© 2016 *Kelly A. Raymond*

APPROVAL FOR SUCCESSFUL DEFENSE

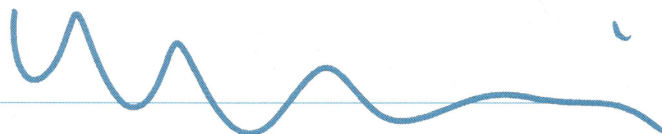
Doctoral Candidate, Kelly A. Raymond, has successfully defended and made the required modifications to the text of the doctoral dissertation for the Ph.D. during Spring Semester 2016.

Dissertation Committee

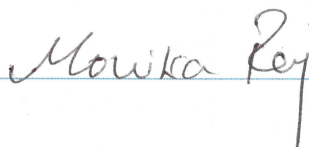
Dr. Stephen Kelty  
Mentor



Dr. Yufeng Wei  
Committee Member



Dr. Monika Raj  
Committee Member



Dr. Cecilia Marzabadi  
Chair, Department of Chemistry and Biochemistry



## Acknowledgments

I would like to thank my advisor Dr. Stephen Kelty for his assistance, guidance, and support throughout this journey. You have taught me to think critically, to believe in myself and to always push myself. I am forever thankful for allowing me to join your fantastic group and for providing me with life lessons that I will carry with me beyond Seton Hall University.

To Dr. Yufeng Wei, you saw something in me that I did not see in myself. Thank you for your patience, guidance and for giving me this project. I learned so much about science, computers, multi-tasking and scientific writing from you.

To Dr. Monika Raj, thank you for your guidance and assistance throughout this process.

My sincere gratitude is given to my boss, Devin Wigington. Thank you for helping me, supporting me, and for inspiring me to never give up. Most importantly, thank you for teaching me how to think critically and work independently.

I would not be where I am today without my mom, sisters and brother. Thank you Mom, Colleen, Kaitlyn, Kara and Michael for always believing in me and for your unconditional love and support. Mom, thank you for teaching me at an early age that I can do anything and for showing me how to be a loving mother. Thank you to my in-

laws (Chris, Jeff, Kim and George) for welcoming me into your family and assisting me on this journey. Thank you to Amy Chiasson, Valerie Fischetti, and Natalie Simsik for being my best friends, my constant voices of reason, and for always holding my hand when I needed an extra support.

To my nieces: Madison, Stella, Scarlett and Mallory you are beautiful, smart and kind. Remember that you capable of greatness and you can do anything you want to in life. Thank you for inspiring me everyday. To Maddox, thank you for reminding me to anyways smile.

Finally, I would like to recognize the two most important people in my life, my husband Dave and my son Colin. Dave, thank you for teaching me Linux command line, for your patience, understanding and for always pushing me to be the best version of myself. Thank you to my sweet son for being my inspiration and my biggest fan. Thank you both for teaching me what unconditional love really means.

## **Dedication**

For my mother, Mary Russell; my husband, David Raymond; and my son, Colin  
Raymond

## Table of Contents

<i>Acknowledgments</i> .....	<i>iv</i>
<i>Dedication</i> .....	<i>vi</i>
<i>List of Tables</i> .....	<i>x</i>
<i>List of Figures</i> .....	<i>xi</i>
<i>Abbreviations</i> .....	<i>xiii</i>
<b>CHAPTER I</b> .....	<b>1</b>
<i>Molecular Dynamics Simulations of Transient Receptor Potential Vanilloid Type 1</i> .....	<b>1</b>
<b>Abstract</b> .....	<b>2</b>
<b>1.1 Introduction</b> .....	<b>3</b>
1.1.1 TRPV1 Structure.....	6
1.1.2 Phosphatidylinositol 4,5-bisphosphate .....	9
<b>1.2 Methodology</b> .....	<b>10</b>
1.2.1 Rational for Studying TRPV1.....	10
1.2.2 Project Objectives .....	12
<b>1.3 Publication</b>	
<b><i>Characterization of temperature-sensing and PIP<sub>2</sub>-regulation of TRPV1 ion channel at the C-terminal domain using NMR spectroscopy and Molecular Dynamics Simulations</i></b> .....	<b>13</b>
1.3.1 Abstract.....	13
1.3.2 Introduction.....	14
1.3.3 Materials and Methods.....	18
1.3.3.1 Peptide Synthesis .....	18
1.3.3.2 NMR Sample Preparation.....	19
1.3.3.3 NMR Spectroscopy.....	19
1.3.3.4 Molecular Dynamics Simulations .....	20
1.3.4 Results.....	21
1.3.4.1 NMR spectroscopy of TRPV1 temperature-sensing segment.....	21
1.3.4.2 NMR spectroscopy of TRPV1 PIP <sub>2</sub> -binding segment.....	23
1.3.4.3 Molecular dynamics simulations of TRPV1 C-terminal domain.....	25
1.3.5 Discussion.....	27
1.3.6 Concluding Remarks.....	29
1.3.7 Acknowledgments.....	31
<b>1.4 Structural Affect on C-terminal Domain of TRPV1 at Varying Temperature</b> .....	<b>32</b>
1.4.1 Methodology .....	32



1.4.2	Lipid Membrane Generation.....	36
1.4.3	Protein Insertion.....	37
1.4.4	Molecular Dynamics Simulations.....	39
1.4.5	C-terminal domain Experiment Results.....	43
<b>1.5</b>	<b><i>C-terminal Domain Experiments with PIP<sub>2</sub></i></b> .....	<b>44</b>
1.5.1	PIP <sub>2</sub> insertion with C-TERMINAL DOMAIN and S6 helix.....	44
1.5.2	AutoDock.....	45
	1.5.2.1 AutoDock Experiment Rationale and Methodology.....	45
	1.5.2.2 AutoDock Results.....	45
	1.5.2.3 AutoDock Result Table.....	46
	1.5.2.4 AutoDock Discussion.....	46
<b>1.6</b>	<b><i>Temperature and PIP<sub>2</sub> Binding Experiments Utilizing the Complete Tetramer</i></b> .....	<b>47</b>
1.6.1	Introduction.....	47
1.6.2	Methodology and Experiments.....	48
	1.6.2.1 C-terminal domain attachment to Transmembrane Domain.....	48
	1.6.2.2 Lipid Membrane Generation.....	50
	1.6.2.3 Protein Insertion into Lipid Membrane.....	54
	1.6.2.4 Solvation and Ionization.....	55
1.6.3	Simulation Results.....	59
	1.6.3.1 Control Results.....	59
	1.6.3.2 Simulations of Complete Structure.....	61
	1.6.3.3 Results from PIP <sub>2</sub> experiments.....	63
<b>1.7</b>	<b><i>Additional and Future Experiments</i></b> .....	<b>64</b>
<b>1.8</b>	<b><i>Concluding Remarks</i></b> .....	<b>64</b>
<b>CHAPTER II</b>	<b>.....</b>	<b>66</b>
	<i>Structural Analysis of Proline Mimics using Computational Techniques</i> .....	66
	Abstract Chapter II.....	67
<b>2.1</b>	<b><i>Introduction</i></b> .....	<b>68</b>
2.1.1	Proline Conformations.....	69
2.1.2	Pseudoproline and β-Turns.....	70
2.1.3	Proline Mimic.....	71
<b>2.2</b>	<b><i>Rationale for Studying Peptides</i></b> .....	<b>72</b>
<b>2.3</b>	<b><i>Methodology</i></b> .....	<b>73</b>
2.3.1	Amino Acid, Peptide Generation and GAMESS Analysis.....	73
2.3.2	Structure Analysis.....	79
	2.3.2.1 Ramachandran Plot.....	79
	2.3.2.2 Peptide Ramachandran Plots.....	82
	2.3.2.3 Results Ramachandran Plots.....	85

<b>2.4 Concluding Remarks</b> .....	87
<b>References</b> .....	88

## List of Tables

<i>Table 1: Modeller Results</i> .....	34
<i>Table 2: AutoDock Result Table</i> .....	46
<i>Table 3: Box size for PBC</i> .....	59
<i>Table 4: Temperature gradient in Configuration File</i> .....	62
<i>Table 5: GAMESS Input</i> .....	74
<i>Table 6: GAMESS Result Table- Proline</i> .....	75
<i>Table 7: GAMESS Result TablePseudoproline</i> .....	75
<i>Table 8: GAMESS Result Table Proline Mimic</i> .....	76

## List of Figures

<i>Figure 1: Structure of Capsaicin</i> .....	5
<i>Figure 2: Vanillyl Functional Group</i> .....	5
<i>Figure 3: TRPV1 Structure</i> .....	6
<i>Figure 4: Overlaid NOSEY Spectra of TRPV1 Q727-752</i> .....	22
<i>Figure 5: NOESY Spectra of mTRPV1 778-819</i> .....	24
<i>Figure 6: Sequence alignment of human TRPV1 C-terminal domain</i> .....	25
<i>Figure 7: Computational Models of TRPV1 C-TERMINAL DOMAIN at 298K</i> .....	27
<i>Figure 8: TRPV1 created S6 <math>\alpha</math> helix created using PyMOL</i> .....	33
<i>Figure 9: TRPV1 created S6 <math>\alpha</math> helix displayed in VMD</i> .....	33
<i>Figure 10: Overlay of C-TERMINAL DOMAIN structures 1,3, and 4</i> .....	35
<i>Figure 11: C-TERMINAL DOMAIN highlighting secondary structure motifs</i> .....	35
<i>Figure 12: Lipid Membrane created by CHARMM-GUI</i> .....	36
<i>Figure 13: Solvated and Ionized C-terminal Domain inserted into a Lipid Membrane</i> .....	39
<i>Figure 14: Simulation RMSD</i> .....	40
<i>Figure 15: C-TERMINAL DOMAIN highlighting the secondary structure and temperature sensing region</i> .....	41
<i>Figure 16: Overlay of C-TERMINAL DOMAIN at 300K(red) and 400K(green)</i> .....	42
<i>Figure 17: Overlay of C-TERMINAL DOMAIN 400K starting frame (red) and ending frame (pink)</i> ...	43
<i>Figure 18: C-TERMINAL DOMAIN and S6 helix complex with the addition of 1 molecule of PIP<sub>2</sub></i> .....	44
<i>Figure 19: AutoDock binding study results</i> .....	45
<i>Figure 20: Top View of 3J5P</i> .....	48
<i>Figure 21: Side View of 3J5P</i> .....	48
<i>Figure 22: Representation of the most thermodynamically stable C-TERMINAL DOMAIN</i> .....	49
<i>Figure 23: The completed TRPV1 transmembrane section plus four C-TERMINAL DOMAIN</i> .....	50
<i>Figure 24: Original topology file for PIP<sub>2</sub></i> .....	51
<i>Figure 25: Updated topology file for PIP<sub>2</sub></i> .....	52
<i>Figure 26: Lipid Membrane with PIP<sub>2</sub></i> .....	53
<i>Figure 27: Transmembrane section inserted into lipid membrane</i> .....	54
<i>Figure 28: Solvation parameters obtained from VMD</i> .....	55
<i>Figure 29: Snapshot of complete TRPV1 structure visualized using VMD</i> .....	56
<i>Figure 30: Snapshot of complete TRPV1 structure with water removed</i> .....	57
<i>Figure 31: Snapshot of complete TRPV1 structure with water removed top view</i> .....	57
<i>Figure 32: VMD snapshot final control structure without PIP<sub>2</sub></i> .....	58
<i>Figure 33: Snapshot of complete TPRV1 control structure with water removed</i> .....	58

<i>Figure 34: Snapshot of overlay containing final frame of simulations performed at 300K and 400K ...</i>	<i>60</i>
<i>Figure 35: RMSD of compliation of simulations performed at 300K and 400K.....</i>	<i>61</i>
<i>Figure 36: Snapshot of TRPV1 and PIP<sub>2</sub> in 10ns simulation.....</i>	<i>63</i>
<i>Figure 37: Proline Structure .....</i>	<i>69</i>
<i>Figure 38: Proline amino acid in trans configuration .....</i>	<i>70</i>
<i>Figure 39:: Pseudoproline trans isomer.....</i>	<i>70</i>
<i>Figure 40: <math>\beta</math>-turn example.....</i>	<i>71</i>
<i>Figure 41: Proline Mimics Cis and Trans isomers .....</i>	<i>72</i>
<i>Figure 42: Structure of Proline highlighting potential confirmations .....</i>	<i>73</i>
<i>Figure 43: Structure of Pseudoproline .....</i>	<i>73</i>
<i>Figure 44: Structure of Proline Mimic .....</i>	<i>74</i>
<i>Figure 45: Avogadro created peptide, GPG.....</i>	<i>77</i>
<i>Figure 46: Avogadro created peptide, GPseudoprolineG.....</i>	<i>77</i>
<i>Figure 47: Avogadro created peptide, GProlineMimicG.....</i>	<i>78</i>
<i>Figure 48: Avogadro created peptide, GGPPGG.....</i>	<i>78</i>
<i>Figure 49: Avogadro created peptide, GGS GG.....</i>	<i>78</i>
<i>Figure 50: Avogadro created peptide, GGProlinMimicGG.....</i>	<i>79</i>
<i>Figure 51: Angles <math>\phi</math> and <math>\psi</math> present in a peptide backbone.....</i>	<i>80</i>
<i>Figure 52: Ramachandran Plot Example.....</i>	<i>81</i>
<i>Figure 53: Ramachandran plot focused on Proline in GGPPGG peptide .....</i>	<i>82</i>
<i>Figure 54: Ramachandran plot for serine present in GGS GG peptide.....</i>	<i>83</i>
<i>Figure 55: Ramachandran plot for proline mimi present in GGMimicGG peptide.....</i>	<i>84</i>
<i>Figure 56: Contour plot based on proline mimic Ramachandran Plot.....</i>	<i>85</i>
<i>Figure 57: Ramachandran plot focusing on <math>\beta</math>-hairpin turn .....</i>	<i>86</i>
<i>Figure 58: Figure illustrating <math>\phi</math> and <math>\Psi</math> angles of proline mimic structure .....</i>	<i>86</i>

## Abbreviations

Transient Receptor Potential	TRP
Molecular Dynamics	MD
Nuclear Magnetic Resonance	NMR
Nuclear Overhauser Effect	NOE
Phosphatidylinositol-4,5-bisphosphate	PIP <sub>2</sub>
C-terminal domain	CTD
Transient Receptor Potential Vanilloid Type 1	TRPV1
Solid phase peptide synthesis	SPPS

# CHAPTER I

*Molecular Dynamics Simulations of Transient Receptor Potential*

*Vanilloid Type 1*

## Abstract

The Transient Receptor Potential (TRP) family of ion channels encompasses more than 30 members, which are expressed in many different tissues and cell types.<sup>1</sup> Transient Receptor Potential Vanilloid Type 1 (TRPV1) is part of the TRP family gated by vanilloids, heat and protons.<sup>2</sup> Molecular modeling will be used in order to obtain structural and functional data on TRPV1 in its membrane bound environment. In particular, the transmembrane and C-terminal domain regions of TRPV1 are of particular interest. The S1-S4 region of the channel is the putative ligand-binding segment, while the C-terminal domain is suggested to respond to temperature and is regulated by phosphatidylinositides (PIP<sub>2</sub>). Despite the crucial roles in mediating signal transductions at both peripheral and central nervous systems, TRP channels are poorly understood in the context of structures and mechanisms.<sup>4</sup> A molecular model of the published transmembrane section of TRPV1 along with the putative, unstructured C-terminal domain was created using their respective homology models and inserted into their membranes.<sup>5</sup> Simulations were performed using both a lipid membrane containing PIP<sub>2</sub> and one without PIP<sub>2</sub> in order to determine its role in TRPV1 activation/deactivation. Molecular dynamics simulations could provide pivotal information about ligand binding, voltage sensing, interaction with heat/cold and proton binding for TRPV1. MD simulations alluded to the fact that when both temperature and PIP<sub>2</sub> are present a greater degree of conformational change is observed. A greater understanding of the structure of TRPV1 could provide important details on how to alleviate certain diseases such as pain, asthma and diabetes.



## ***1.1 Introduction***

Transient Receptor Potential Ion channel proteins are comprised of more than 30 different proteins and are expressed in many different tissues and cell types.<sup>1</sup> The TRP family of ion channel membrane proteins are structurally and mechanically related to voltage-activated channels.<sup>68</sup> TRP channels play vital roles in intracellular calcium homeostasis, nociception, cellular chemotaxis, neuronal guidance and neurite extension, calcium transport, and immune response.<sup>2</sup> In addition, this family of proteins are involved in the detection of sensory stimuli, which allows humans to be able to taste sweet, bitter and umami tastes as well as distinguish between warmth, heat and cold.<sup>2</sup> In addition, it is involved in the detection and integration of painful chemical and thermal stimuli.

TRP channels are members of a genetically conserved superfamily made up of seven different subfamilies; each of which contains proteins that function as an ion channel.<sup>1</sup> The seven different subfamilies are: canonical, vanilloid, melastatin, polycystin, mucolipin, ankyrin and NOMPC-like more commonly referred to as TRPC, TRPV, TRPM, TRPP, TRPML, TRPA, and TRPN, respectively. The seven subfamilies are all ion channels; some are non-selective cation channels while others have an affinity for  $\text{Ca}^{2+}$  or  $\text{Mg}^{2+}$ .<sup>69,70</sup> Several TRP channels are easily activated by changes in temperature and are known as thermo TRP channels.<sup>71</sup> Several examples of thermo TRP channels include four different but structurally and genetically similar vanilloid channels known as Receptor Potential Vanilloid Type 1, TRPV1, as well as TRPV2, TRPV3, TRPV4. TRPV channels well-studied non-selective cation channels potentiated by heat.<sup>72</sup> Specifically, temperatures greater than 25°C activate the

vanilloid channels. Temperatures of varying degrees activate each member of the vanilloid family.<sup>2</sup> Specifically, TRPV1 is activated by temperatures greater than 43°C, while TRPV2, which sequence is 50% identical to V1 is activated by temperatures greater than 52°C.<sup>2</sup> Temperatures greater than 31°C activates V3 while V4 is activated by temperatures greater than 25°C.<sup>2</sup> The vanilloid subfamily obtained the name vanilloid receptor because the channel activation ligand capsaicin contains a vanillyl functional group. Capsaicin, 8-methyl-*N*-vanillyl-6-nonenamide, is the hydrophobic pungent ingredient present in various types of chili peppers, which leads to a burning sensation when chili peppers are consumed.<sup>73</sup> TRPV1 membrane protein is encoded by the *TRPV1* gene and is also activated by agonist allyl isothiocyanate spicy ingredient in wasabi, horseradish and mustard.<sup>80</sup> Allyl isothiocyanate activates both TRPV1 as well as another TRP channel TRPA1.<sup>81</sup> Acidic conditions can also activate the TRPV1 cation channel.<sup>16</sup> In addition to low pH other endogenous activators of TRPV1 include: endocannabinoid anandamide, *N*-oleyl-dopamine, and *N*-arachidonoyl-dopamine.<sup>88</sup> TRPV1, like other TRPV members, is a non-selective cation channel, however, it has a high permeability to calcium ions.<sup>76,77</sup>

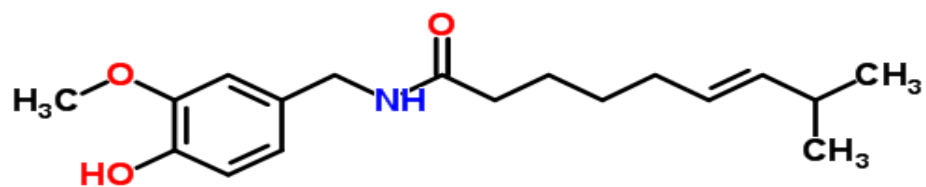


Figure 1: Structure of Capsaicin created using ChemSpider<sup>84</sup>

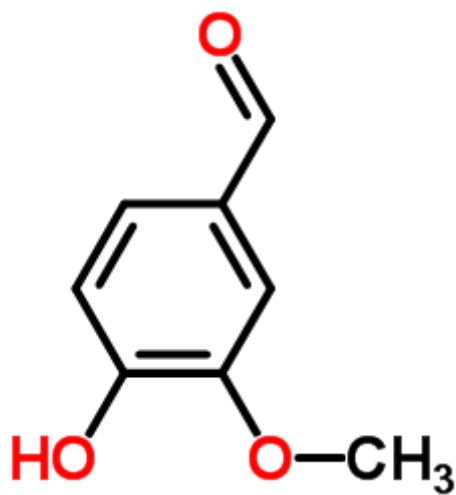


Figure 2: Vanillyl Functional Group created using ChemSpider<sup>84</sup>

### 1.1.1 TRPV1 Structure

TRPV1 is a transmembrane protein containing an intracellular N and C terminal region. The transmembrane domain is comprised of six transmembrane helices (S1-S6) and additional short amphipathic stretch between helices 5 and 6 flanked between the C-terminal and N-terminal domains.<sup>4</sup> TRPV1 sequence below was obtained using the PDB structure information published under PDB 3J5P.<sup>5</sup>

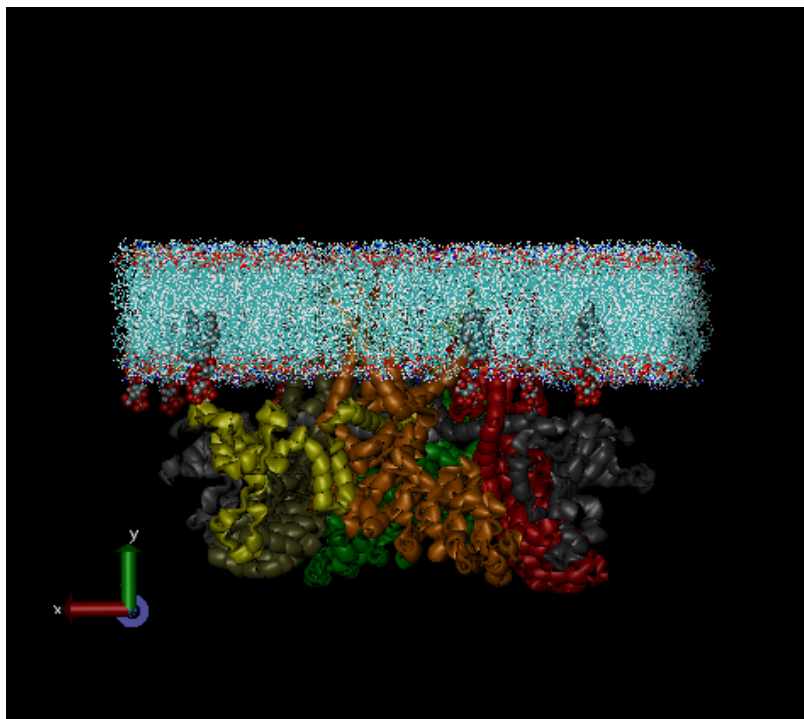


Figure 3: TRPV1 Structure created using VMD.<sup>47</sup>

The N-terminal domain is comprised of six helices dominated ankyrin repeats, totaling approximately 400 residues.<sup>6</sup> In 2007, the structure of an individual, 33 amino acid residue ankyrin molecules from TRPV1 was published using x-ray

crystallography (PDB 2PNN).<sup>7</sup> The cytosolic ankyrin repeats are theorized to play a role in protein-protein interactions, as well as the repeats contain the binding site for both ATP and calmodulin, a calcium binding protein.<sup>7</sup>

The cytosolic C-terminus is comprised of approximately 150 amino acid residues. Although a high-resolution structure of TRPV1 ion channel was determined using cryo-EM (PDB 3J5P) a majority of the C-terminus was not included, specifically residues 684-839.<sup>4,5</sup> The portions of the C-terminal domain that were included did provide detailed information about the TRP domain  $\alpha$ -helix and a  $\beta$  strand close to the end of the minimal construct.<sup>4</sup> This implies that the largely unstructured C-terminal domain could undergo significant conformational change upon activation or ligand binding.<sup>4</sup> It is well established that TRPV1 is potentiated by heat. Additionally, it is well known that another thermo TRP channel protein, TRPM8, is activated by cold.<sup>81</sup> Studies have shown that the removal of portions of the C-terminal domain of TRPV1 result in a reduction in heat sensitivity. Furthermore, the complete removal of the C-terminal domain resulted in a complete loss of channel function.<sup>10,11</sup> The C-terminus, particularly residues 684-721, act as a molecular determinant of heat activation energy responsible for inter-subunit interactions near the channel gate that contribute to the coupling of stimulus leading to the channel opening. In addition to its role in thermal sensitivity, the C-terminal domain also contains a potentially inhibitory, possibly activating phosphatidylinositol-4,5-bisphosphate (PIP<sub>2</sub>) binding site.<sup>12</sup> A potential binding site for PIP<sub>2</sub> on the C-terminal domain could be the conserved positively charged clusters that

interact with the negatively charged inositol head group.

In addition, TRPV1 is a homotetramer composed of four identical subunits each with a transmembrane domain comprised of six helices (S1-S6).<sup>75</sup> The six transmembrane domains contain an additional short amphipathic stretch between transmembrane 5 and 6. The channel-forming region of the molecule is formed with the helices 5, helices 6 and the amphipathic stretch. The additional helices S1-S4 make up the voltage-sensing region.<sup>13</sup>

TRPV1 is a transmembrane protein, which is inserted into an asymmetric lipid bilayer. Located on the extracellular side of the membrane is palmitoyl-oleoyl phosphatidylcholine, POPC. A mixture of palmitoyl-oleoyl phosphatidylethanolamine and palmitoyl-oleoyl phosphatidylserine, POPE and POPS, respectively are located on the intracellular side of the membrane. The ratio of POPE to POPS on the intracellular side is 2:1. In addition, the intracellular side of the membrane also contains 4% of a minor phospholipid PIP<sub>2</sub>. POPE and POPC are neutral while POPS contains a carboxyl group and therefore carries a -1 charge.

Prior to high-resolution cryo-EM structure determination of TRPV1, structure information pertaining to TRPV1 was inferred from potassium voltage-gated channels such as K<sub>v</sub>1.2. Potassium channels represent a complex class of voltage-gated ion channels in regards to both structure and function. Potassium voltage-gated channel subfamily A member 2, K<sub>v</sub>1.2, is a voltage dependent potassium ion channel, whose transmembrane sequence is most homologous to TRP channels, and will be used as the template to build homology models for subsequent molecular dynamic simulations

of transmembrane segment of TRPV1.<sup>8</sup>  $K_v$  channels are homotetramers made up of four voltage sensors and one pore domain.<sup>82</sup> The transmembrane region of the TRP family of proteins resembles that of the  $K_v$  channels by sequence; this section of both molecules is hypothesized to play a role in voltage gating.<sup>82</sup> In the transmembrane S1-S4 domain there is a 24.8% similarity in residues between TRPV1 and  $K_v1.2$ .<sup>36</sup> A sequence alignment was created between TRPV1 and  $K_v1.2$  using the information provided in the structure published under PDB bank structure 2A79.<sup>36</sup>

### **1.1.2 Phosphatidylinositol 4,5-bisphosphate**

Phosphatidylinositol 4,5-bisphosphate, or  $PIP_2$ , is comprised of an inositol head group and two fatty acid chains joined by a glycerol group. The two most common fatty acids are stearate and arachidonate and it can carry a charge of -3, -4 or -5. For the purpose of this project, a formal charge of -4 will be utilized since this is the presumed charge at physiological pH. While it is widely accepted that TRPV1 is potentiated by heat, the role that  $PIP_2$  is still widely debated.  $PIP_2$  acts as a second messenger phospholipid and breaks down into several different lipid messengers. The potential mechanism for TRPV1 sensation by  $PIP_2$  hydrolysis after phospholipase C activation is as follows: Phospholipase C (PLC) catalyzes the hydrolysis of  $PIP_2$  to inositol trisphosphate  $IP_3$  and diacylglycerol (DAG).  $IP_3$  is released as a soluble structure into the cytosol then diffuses through the cytosol to bind to  $IP_3$  receptors, such as calcium channels present in the endoplasmic reticulum (ER). This causes the cytosolic concentration of calcium to increase, causing a cascade of intracellular changes and activity. Throughout this process, DAG remains bound to the lipid

membrane. Calcium and DAG together activate protein kinase C, which goes on to phosphorylate other molecules, leading to altered cellular activity.<sup>4</sup> This results in the ability to taste as well as tumor promotion.

Once PIP<sub>2</sub> is cleaved by PLC and depleted the channel is either activated or deactivated with conflicting studies showing the potential for either scenario. Stein et al. has suggested the following potential activation scenario: NGF binding to trkK leads to P13K activation.<sup>9</sup> PI3K converts PIP<sub>2</sub> to PIP<sub>3</sub>, which leads to increase in TRPV1 channels in plasma membrane.<sup>9</sup>

In addition, while it hypothesized that PIP<sub>2</sub> interacts with a patch of positively charged amino acid residues on the C-terminus through electrostatic interactions this has not been proven. Recently in the literature a group published information reporting that channel activation is inhibited by PIP<sub>2</sub> and TRPM8 is activated by PIP<sub>2</sub>.<sup>28</sup> In this study, the terminal end of the C-terminus is responsible for PIP<sub>2</sub> binding; this region is not conserved between different TRP channels.<sup>28</sup> The study found that at low capsaicin concentration and low pH the channel was inhibited by PIP<sub>2</sub> binding.<sup>28</sup> However at high concentrations of capsaicin the PIP<sub>2</sub> does not inactivate the channel.<sup>26</sup>

## ***1.2 Methodology***

### **1.2.1 Rational for Studying TRPV1**

TRPV1 can be activated by increased temperature, low pH, or by ligands such as capsaicin or calmodulin.<sup>2</sup> Strict coupling occurs when only one of these activators



is required to induce a structural change resulting in the channel opening.<sup>2</sup> If for instance both an increase in temperature and capsaicin are required for channel activation, then that is referred to as allosteric coupling. Performing structural analysis on TRPV1 may provide insight as to which coupling mechanism is required in order to activate the channel.

TRPV1 has been implicated in a wide variety of cellular and physiological processes, including noxious physical and chemical stimuli detection, making it a promising target for pain-relieving drugs.<sup>15</sup> Neurons containing TRPV1 channels can be rendered insensitive to further painful stimuli through receptor desensitization in response to some agonists such as capsaicin. The result is a generalized lack of responsiveness of TRPV1 to further harmful stimuli. Therefore, updating important structure-function data through MD simulations could provide vital information about TRPV1 desensitization.

Thirdly, contradicting studies have reported PIP<sub>2</sub> either activates or deactivates TRPV1. Understanding the mechanism of PIP<sub>2</sub> and its role in TRPV1 activation or deactivation is vital to obtaining overall TRPV1 structure and function information.

Lastly, since the early 1900's capsaicin has been used to treat localized pain.<sup>16</sup> Understanding how TRPV1 activation occurs could provide pivotal information on how pain is treated and alleviated. In addition, thermo TRP channels have the ability to integrate multiple stimuli, and temperature activation thresholds can be shifted in response to allogeneic substances, phospholipid signaling molecules, phosphorylation states, mild acidic conditions, and membrane voltage. Moreover, the lack of knowledge on the detailed mechanisms and structures of TRP channels, particularly

the C-terminal domain, severely hampers the ability to understand the mechanistic role of TRP channels in nociception and the development of drugs to target TRP channels.<sup>4, 43</sup> A greater understanding of both the C-terminal domain and complete TRPV1 structure is necessary for drug discovery treatment of pain, bladder, and gastrointestinal diseases.<sup>44</sup>

### **1.2.2 Project Objectives**

The overall project objectives are to obtain imperative structure information on TRPV1 through MD simulations.

MD simulations and basic structural analysis were performed utilizing a thermodynamically stable C-terminal domain obtained using a homology model at varying temperatures. In this study, we describe our initial structural characterization of the TRPV1 C-terminal domain, the putative temperature sensing and PIP<sub>2</sub>-regulatory domain, using NMR spectroscopy and molecular dynamics simulations.

A homology model generated C-terminal domain monomer was combined with an S6  $\alpha$ -helix and inserted into a lipid membrane. The objective of this study was to determine if a conformational change would occur in the presence of high temperatures (400K) and if temperature alone could potentiate a conformational change. In addition, we were curious to see if a greater degree of change would be observed if both PIP<sub>2</sub> and increased temperature were included in the simulation. Additionally, binding experiments were performed utilizing AutoDock in order to determine if a binding pocket exists between PIP<sub>2</sub> and positively charged amino acids in the C-terminal domain.

Lastly, a complete tetramer TRPV1 model was created. Through MD simulations performed with and without functional ligand PIP<sub>2</sub> at varying temperatures could provide meaningful insight into the mechanism of TRPV1 channel activation.

### ***1.3 Publication Characterization of temperature-sensing and PIP<sub>2</sub>-regulation of TRPV1 ion channel at the C-terminal domain using NMR spectroscopy and Molecular Dynamics Simulations***

Kelly A. Raymond<sup>†</sup>, Edward C. Twomey<sup>†</sup>, and Yufeng Wei<sup>\*†‡</sup>

<sup>†</sup> Department of Chemistry and Biochemistry, Seton Hall University, South Orange, NJ 07079-2694, USA

<sup>‡</sup> Spectroscopy Resource Center, The Rockefeller University, New York, NY 10065-6399, USA

#### **1.3.1 Abstract**

Transient receptor potential (TRP) channels are receptors of stimulating signals, such as temperature, taste, odor, and chemo- and mechano-stimuli. Temperature sensing TRP channels coincidentally function as pain receptors, and are potential targets for substances of abuse, including alcohol and illicit drugs. TRP vanilloid type 1 (TRPV1) channel is activated by heat (>43 °C) and capsaicin under the tight regulation of membrane-associated second messenger, PIP<sub>2</sub> (phosphatidylinositol-4,5-bisphosphate), responds to noxious stimuli and inflammatory substances, and could potentially modulate effects of alcohol and drugs of abuse. Despite the crucial roles in mediating signal transductions at both peripheral and central nervous systems, TRP

channels are poorly understood in the context of structures and mechanisms. In this study, we describe our initial structural characterization of the TRPV1 C-terminal domain, the putative temperature sensing and PIP<sub>2</sub>-regulatory domain, using NMR spectroscopy and molecular dynamics simulations. Both experimental and computational models suggest the C-terminal domain is intrinsically unstructured at room temperature with and without lipid bicelles. Elevated temperature and PIP<sub>2</sub>-binding can induce substantial conformational changes and formation of considerable secondary structural components in the C-terminal domain, which could be transduced to the transmembrane domain to potentially sensitize the channel.

### **1.3.2 Introduction**

TRP channels are generally described as the vanguard of our sensory systems that respond to a variety of intra- and intercellular stimuli.<sup>2,16</sup> Thermo TRP channels are activated by distinct physiological temperatures, and are involved in converting thermal information into chemical and electrical signals within the sensory nervous system. The homologous related TRPV1, TRPV2, TRPV3, and TRPV4 are activated by increased temperature, while TRPM8 and TRPA1, the more distinctly related TRP channels, are activated upon cooling.<sup>17,18</sup> In addition to temperature, these channels can be activated by a number of agonists. For example, capsaicin, the pungent extract of hot peppers, can activate TRPV1; menthol, the cooling compound extracted from the mint plant, directly activates TRPM8; and mustard oil and cinnamaldehyde from the cinnamon oil specifically activate TRPA1.<sup>2,18</sup>

Coincidentally, thermo TRP channels are receptors of noxious stimuli, leading to acute nociceptive pain, a protective warning of damage.<sup>19,20</sup> However, many pathological conditions lead to changes in the expression level and/or sensitivity of nociceptive TRP channels, characterized as hyperesthesia. These pathological conditions include inflammations (inflammatory pain) and damage or lesions to the nervous system (neuropathic pain).<sup>21</sup> Recent research also suggests that alcohol can modulate thermo TRP channel activities. TRPM8 activity is inhibited by high concentration of ethanol,<sup>22</sup> while TRPV1 and TRPA1 are activated and potentiated by ethanol.<sup>23-25</sup> Using TRPV1 knockout mice, the roles of TRPV1 in the avoidance of the adverse alcohol taste and alcohol-induced intoxication were established.<sup>26,27</sup>

Most recently, high-resolution structures of TRPV1 ion channel were determined using state-of-the-art single particle cryo-electron microscopy (cryo-EM) technique, and distinct conformations were revealed upon activation of the channel.<sup>28, 29</sup> These structures contain amazingly detailed information on the arrangement of the transmembrane segments, including the ion passage pore, and the cytosolic N-terminal domain, including the ankyrin repeats. However, the TRPV1 structure (PDB ID: 3J5P)<sup>28</sup> was obtained using a minimal functional construct composed of residues 110-603 and 627-764, which lacks about half of the cytosolic C-terminal domain (residues 684-839).<sup>28</sup> In addition, this structure lacked electron density in the C-terminal region with the exceptions of the TRP domain  $\alpha$ -helix and a  $\beta$ -strand close to the end of the minimal construct. This observation strongly suggested a largely unstructured C-terminal domain that could undergo significant conformational change upon activation or ligand binding.

The intrinsically disordered C-terminal domain of TRPV1 is functionally critical. It has been suggested that the cytosolic C-terminal domains of thermo TRPs are functionally important in mediating TRP channel activities. Swapping mutagenesis experiments indicated that the C-terminal domains of TRPV1 and TRPM8 determine the activation phenotype by temperature of these channels.<sup>30</sup> It is also determined that a region located outside the TRP domain comprising the TRPV1 C-terminal amino acids Q727 to W752 (corresponding TRPM8 C-terminal amino acids K1030 to W1055) is the minimal portion to show temperature sensitivity (heat or cold), and deletion of 11 residues, comprising TRPV1 C741 to W752, results in losing channel thermal sensitivity while retaining voltage sensitivity.<sup>31</sup> The minimal construct used to obtain the TRPV1 structure contained this temperature-sensing segment (residues 727-752), and the minimal construct was reported to respond to heat.<sup>28</sup>

PIP<sub>2</sub> (phosphatidylinositol-4, 5-bisphosphate) is an essential modulator for TRP channels, as well as a wide range of other ion channels.<sup>9</sup> PIP<sub>2</sub> activates TRPM8, and activation of phospholipase C (PLC) and subsequent depletion of PIP<sub>2</sub> desensitize the channel.<sup>33,34</sup> On the other hand, TRPV1 is desensitized by PIP<sub>2</sub>, and depletion of cellular PIP<sub>2</sub> upon activation of PLC activates TRPV1.<sup>9</sup> However, the role of PIP<sub>2</sub> on TRPV1 modulation is still controversial, as experiments also show that PIP<sub>2</sub> sensitizes TRPV1 and that depletion leads to desensitization.<sup>35,36</sup> A dual regulatory role is also suggested.<sup>37</sup> It has been suggested that the conserved positively charged clusters in the C-terminal domain of TRP channels are responsible for PIP<sub>2</sub> binding. The putative PIP<sub>2</sub> binding site for TRPM8 is on the very proximal C-terminal TRP domain (K995,

R998, K1008), whereas in TRPV1, it is located on the more distal C-terminal region after the TRP domain (R786, K789, R798).<sup>3,37</sup> A homology model of TRPV1, built upon the crystal structures of Kv1.2 and HCN2 as templates for transmembrane and C-terminal regions, respectively, suggests that PIP<sub>2</sub> aliphatic chains are located near the voltage-sensor modules, while the PIP<sub>2</sub> polar head group is interacting with a cluster of positive charges located in the proximal C-terminal region, including residues K694, K698, K701, and K710, as well as with amino acids R575 and R579 located in the S4-S5 linker helix.<sup>3,38,39</sup> The C-terminal domain in this homology model, however, did not seem to agree with the recent cryo-EM structure, which indicated a mostly unstructured C-terminal domain with an  $\alpha$ -helical TRP domain and a  $\beta$ -strand in the temperature sensor, while the homology model showed a mostly well-folded C-terminal domain with all helical components within the temperature sensor.<sup>28,39</sup>

Thermo and nociceptive TRP channels have the ability to integrate multiple stimuli, and temperature activation thresholds can be shifted in response to algogenic substances, phospholipid signaling molecules, phosphorylation states, mild acidic conditions, and membrane voltage. A modular model with allosteric gating mechanism of thermo TRP channels was proposed to explain the TRP mechanisms.<sup>40</sup> Current *in vivo* studies on the functions of TRP channels involves mostly the use of transgenic mouse models, providing a productive source of validated targets for future drug discovery.<sup>41</sup> Nevertheless, mouse gene knockouts can be problematic pertaining to pain phenotyping. For example, thermo and pain reception can be compensated by related channels and receptors, and differences between mouse strains can be

significant.<sup>42</sup> Moreover, the lack of knowledge on the detailed mechanisms and structures of TRP channels, particularly the C-terminal domain, severely hampers the ability to understand the mechanistic role of TRP channels in nociception and the development of drugs to target TRP channels.<sup>43</sup> TRPV1 is the only member of the TRP superfamily that has been targeted in the treatment of pain, bladder, and gastrointestinal diseases.<sup>44</sup> The minimal construct of the TRPV1 possessed the temperature-sensing segment (residues 727-752), but not the regulatory PIP<sub>2</sub>/calmodulin binding segment (residues 778-819), suggesting that the temperature sensing and regulatory segments are functionally independent and structurally unrelated. Considering the intrinsically disordered nature of the C-terminal domain, we have studied these two segments as individual peptides as an initial attempt, and combined with molecular dynamics (MD) simulation of the full-length C-terminal domain to integrate the findings of the individual peptides into a more complete model. Here we report our initial NMR spectroscopic characterization of the putative temperature-sensing and PIP<sub>2</sub>-interacting segments of the C-terminal domain of TRPV1 channel at various conditions, complemented by an MD simulation of the complete C-terminal domain at two different temperatures.

### **1.3.3 Materials and Methods**

#### *1.3.3.1 Peptide synthesis*

The C-terminal segment that shows temperature sensitivity of human TRPV1 (hTRPV1) residues 728-753 with sequence QVGYTPDGKDDYRWCFRVDEVNWTW and the putative PIP<sub>2</sub>-interacting



segment of mouse TRPV1 (mTRPV1) protein residues 778-819 with sequence of LRSGRVSGRNWKNFALVPLLRDASTRDRHSTQP<sub>EEVQLKHYT</sub> were synthesized and purified at the Proteomics Resource Center of the Rockefeller University, and their identities were confirmed by mass spectrometry.

### *1.3.3.2 NMR Sample Preparation*

All NMR samples were prepared in 20 mM sodium phosphate buffer, pH 6.6, 150 mM NaCl, in 90%/10% H<sub>2</sub>O/D<sub>2</sub>O solvent. The phospholipids, DHPC, DMPC, DMPG, and brain PIP<sub>2</sub> were purchased from Avanti Polar Lipids, Inc. (Alabaster, AL). A 15% stock bicelle solution was formed at a molar ratio of 0.53 DHPC:0.27 DMPC:0.20 DMPG in the above buffer. The hTRPV1 727-752 peptide (temperature sensor) was dissolved in the above buffer to a final concentration of 4.0 mg/ml. The mTRPV1 778-819 peptide (PIP<sub>2</sub> interacting segment) was prepared in the buffer and in the bicelle solution in the absence and presence of 4 mol% brain PIP<sub>2</sub>. The final peptide concentration in all samples was 3.3 mg/ml and final lipid concentration was 5%.

### *1.3.3.3 NMR Spectroscopy*

All NMR spectra were acquired on a Bruker Avance 900 MHz spectrometer, equipped with a cryogenically cooled TCI-probe, operating at a <sup>1</sup>H frequency of 900.154 MHz. Standard two-dimensional NOESY pulse sequence was used for samples without lipid bicelles, and a  $\omega_2$ -selective NOESY pulse sequence, in which the final excitation pulse was replaced by an E-BURP2 pulse selective for the frequency region of 6.5 – 10.5 ppm, was used for samples containing lipid bicelles.

The NOESY mixing times were set to 100, 200, and 300 ms. 4096×1024 complex data points were collected in each experiment with spectral widths of 11682.243 Hz (or 12.978 ppm) in both dimensions. 16 transients were collected for each 2D increment. The experiments were performed at 25, 35, and 45 °C (298, 308, and 318 K). All spectra were processed using NMRPipe<sup>31</sup> and analyzed and displayed using NMRViewJ.<sup>44</sup>

#### *1.3.3.4 Molecular Dynamics Simulations*

A BLAST search indicated that two proteins are structurally homologous to TRPV1 C-terminal domain, G684-K839, with PDB ID 2HE7<sup>45</sup> homologous to the proximal end and 2R5K homologous to the distal end. A homology model was built upon these two proteins using program Modeller version 9.11<sup>46</sup> The homology model was then minimized and equilibrated using molecular dynamics simulation package NAMD version 2.9<sup>20</sup> at 298 K and 318 K, respectively. The trajectories were simulated for 10 ns at 2 fs time step using periodic boundary conditions for water solvent under constant temperature/pressure and variable volume conditions. The restart frequency was set to 1 ps (every 500 steps) in the simulations. Periodic boundary conditions enable computer simulations to perform and analyze a small number of particles in a system rather than the complete system in bulk. The structural equilibrations were assessed using graphical presentation tool VMD version 1.91<sup>47</sup> and the structures were visualized using PyMOL version 1.5.<sup>87</sup>

## 1.3.4 Results

### *1.3.4.1 NMR spectroscopy of TRPV1 temperature-sensing segment (Q728-W753)*

The 300-ms mixing time NOESY spectra (amide-aromatic region) of the hTRPV1 temperature-sensing segment, residues Q728-W753, at different temperatures (298, 308, and 318 K) are shown in Figure 4.

This segment displays extended, strand-like, secondary structural feature, with inter-chain N-H/N-H ( $d_{\text{NN}}$ ) NOE cross peaks observed at room temperature. Upon increase in temperature, the three valine residues exhibit the most significant shifts, while the single tyrosine residue also shifts continuously. New interactions between valine methyl groups and aromatic residues are appearing only at elevated temperatures (308 and 318 K), whereas the inter-chain  $d_{\text{NN}}$  NOE cross peaks are disappearing at high temperatures. These observations indicate that upon increase in temperature, the temperature sensing segment experiences significant conformational change, and the hydrophobic core interactions are reorganizing in response to temperature change. The conformational changes at the temperature sensing segment are likely transferred to the transmembrane domain under the regulation at the PIP<sub>2</sub> binding segment.

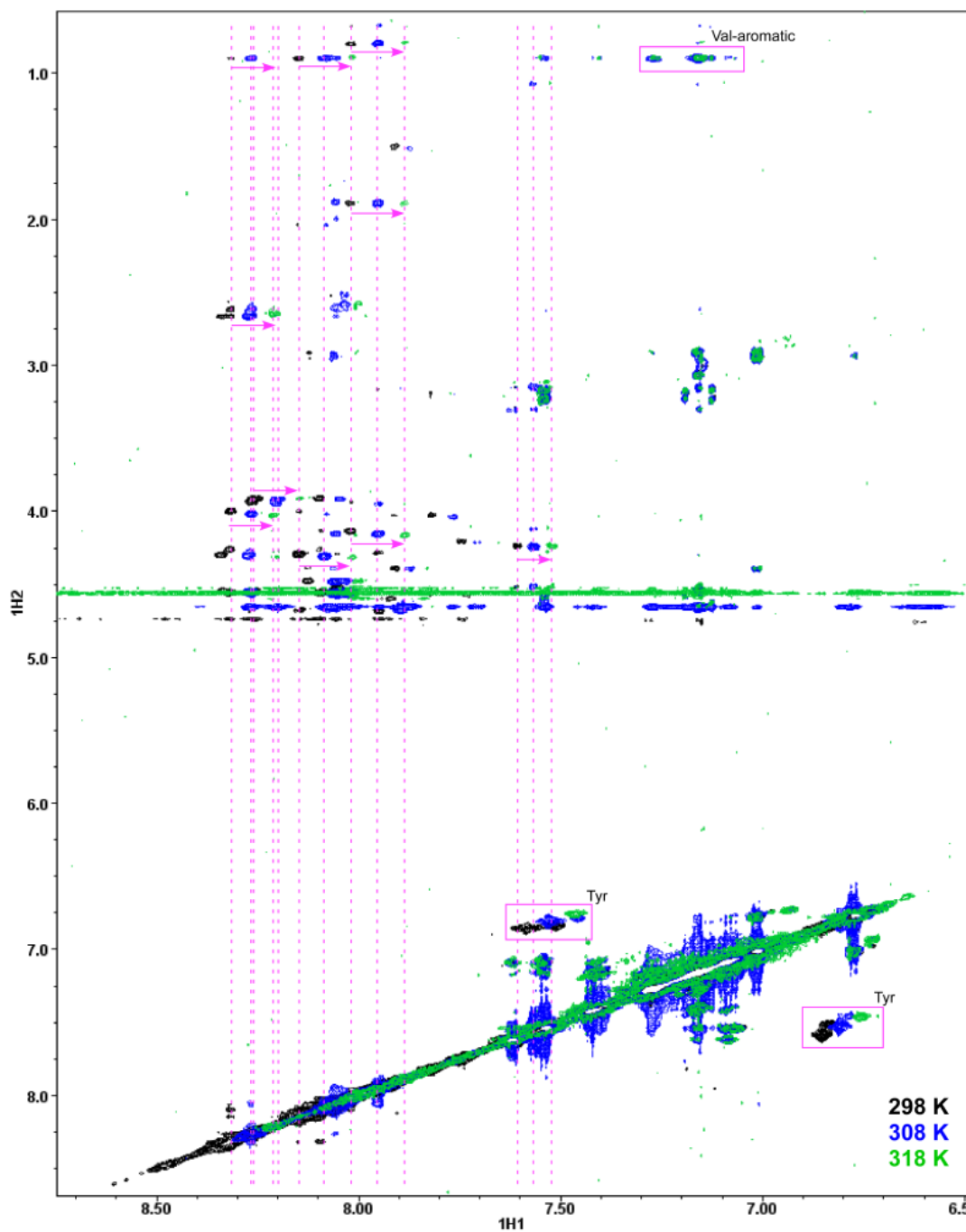


**Figure 4: Overlaid NOESY Spectra of TRPV1 Q727-752** Figure 4 depicts an overlaid NOESY spectra of human TRPV1 residues Q727-W752, the putative temperature sensing segment, at temperatures of 25, 35, and 45 °C. The arrows indicate resonance shift of all three valine residues upon increase in temperature, and boxes highlight aromatic-valine interactions and shifts in Tyr resonances in response to temperature change.

#### *1.3.4.2 NMR spectroscopy of TRPV1 PIP<sub>2</sub>-binding segment (residues L778-T819)*

The hTRPV1 PIP<sub>2</sub>-interacting peptide is largely unstructured in phosphate buffer without lipids in the temperature range of 25-45°C, with the exception of a short stretch of residues 811-815, where a helical structure is evidenced by the sequential  $d_{NN}$  NOEs (Figure 5A and C). In the presence of lipid bicelles (0.53 DHPC: 0.27 DMPC: 0.20 DMPG), however, the hTRPV1 peptide undergoes significant conformational change, and a great number of helical elements can be observed by  $d_{NN}$  NOEs, especially when PIP<sub>2</sub> is present (Figure 5B, 5D, and 5E). Although the helical stretch of 811-815 is retained both in phosphate buffer and in lipid bicelles, the resonances have shifted significantly (Figure 5A), indicating a completely different environment experienced by the helix. Comparing the spectra of mTRPV1 in bicelles with and without PIP<sub>2</sub> (Figure 5B), many peaks are broadened in the hTRPV1 spectrum when PIP<sub>2</sub> is absent, indicating an intermediate exchange between the lipid bicelles and mTRPV1 peptide, while these peaks are clearly visible when PIP<sub>2</sub> is present in the sample, suggesting a reinforced interaction between the peptide and PIP<sub>2</sub>. The broadened peaks in the absence of PIP<sub>2</sub> mostly come from the helical stretch of 790-794, situated in the middle of the key residues R786, K789, and R798, suggesting an essential role of these residues in mediating PIP<sub>2</sub> interaction through an induced conformational change in this region.

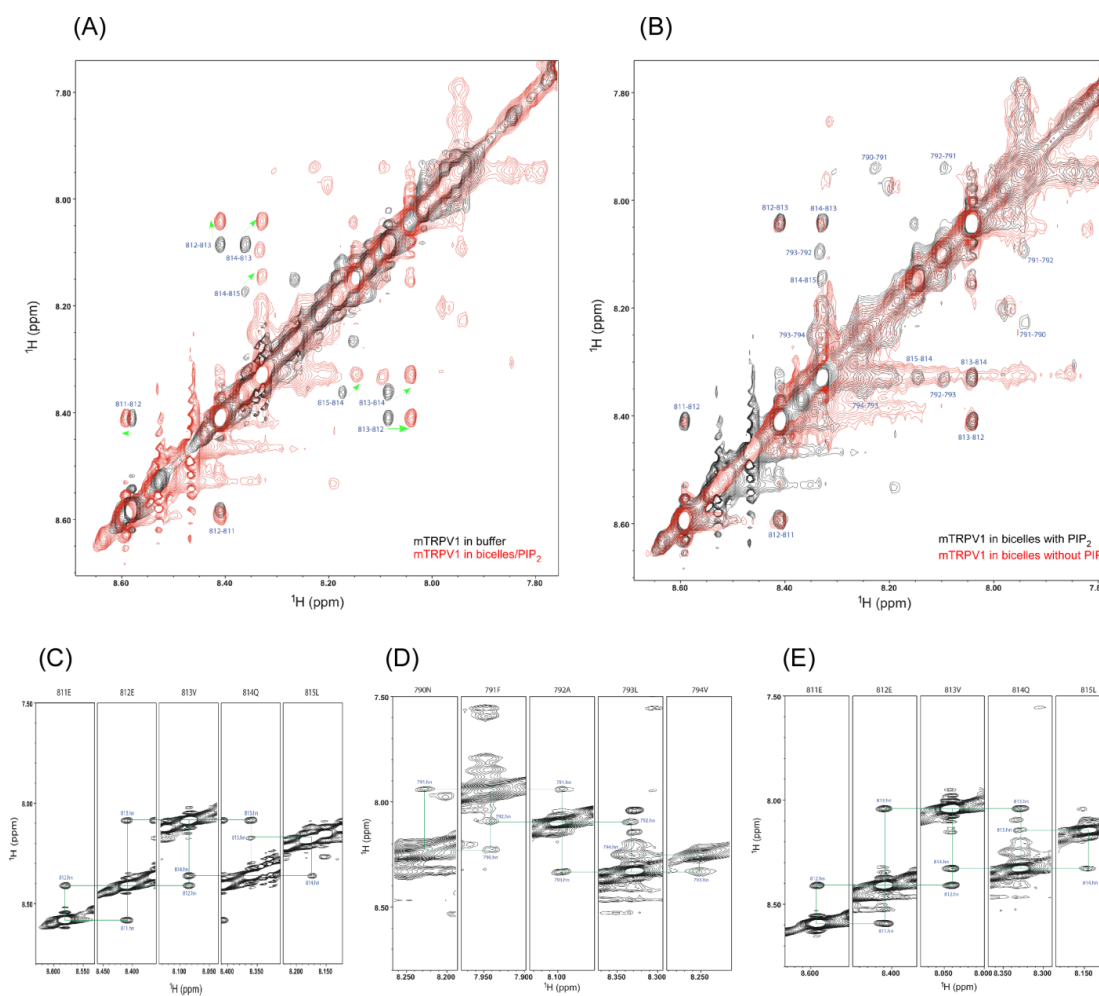


**Figure 5: NOESY Spectra of mTRPV1 778-819.** Figure 5 illustrates NOESY spectra of mTRPV1 778-819 peptide (A) Overlay of the  $d_{\text{NN}}$  region of the peptide in buffer and in lipid bicelles with  $\text{PIP}_2$ ; (B) Overlay of the  $d_{\text{NN}}$  region of the peptide in lipid bicelles with and without  $\text{PIP}_2$ ; (C)  $d_{\text{NN}}$  connectivity of the helical stretch 811-815 without bicelles/ $\text{PIP}_2$ ; (D)  $d_{\text{NN}}$  connectivity of the helical stretch 790-794 in lipid bicelles with  $\text{PIP}_2$ ; (E)  $d_{\text{NN}}$  connectivity of the helical stretch 811-815 in lipid bicelles with  $\text{PIP}_2$ .

### 1.3.4.3 Molecular dynamics simulations of TRPV1 C-terminal domain

A homology model for TRPV1 C-terminal domain, residues G684-K839, was built from 2HE7 (FERM domain of EPB41L3) and 2R5K (Pentamer Structure of Major Capsid protein L1 of Human Papilloma Virus type 11) structures that cover the full sequence of TRPV1 C-terminal domain. The sequence alignment between TRPV1 C-terminal domain and 2HE7 and 2R5K sequences is illustrated in Figure 6. Five homology structures were generated by Modeller<sup>46</sup>, and the model with lowest objective function (molpdf) value and DOPE assessment score was selected for additional molecular dynamics simulations using NAMD<sup>20</sup> package at 298 and 318 K, respectively. The MD models at both temperatures were properly equilibrated over 10 ns simulations, as indicated by the absence of vacuum holes between identical periodic images and small changes in volume over time of the simulated structures.

```

2HE7      257  PNHTKELEDKVIELHKSHRGMPAEEAMHFTENAKKLSMYGVDLHHAKDSEVEIMLGVC
hTRPV1   684  GETVNKLAQESKNIWKLQRAITILDTEKSFLEKCMRKA-----FRSCKLLQVGYT
2R5K
-----

2HE7      317  ASGLLIYRDRLRINRFAPKVLKISYKRNNFYTKIRPGEFEQFESTIGFKLPNHRAAKRL
hTRPV1   733  PDGKDDYRWCFRVDEVNWT-----WNTNVTGIINDEPGNCEGVKRITLSFSLRSSRVSGRH
2R5K     225  -----LFFVLRKEQMFARH
-----

2HE7      377  WK-----
hTRPV1   788  WKNFAL-----VELLREASARDROSAQPEEVYLRQFSGSLKPEDAEVFKSPAASGEK
2R5K     239  FFNRAAGTVGEPVDDLLVKGGNRNSVASSIYVHTPSGSLVSSEAQLFNKP-----

```

**Figure 6: Sequence alignment of human TRPV1 C-terminal.** Figure 6 contains the sequence alignment of human TRPV1 C-terminal domain (residues 684-839) with PDB 6les 2HE7 and 2R5K. Identical residues are shaded black and similar residues are shaded grey. /e alignment E-values are 1.3 for 2HE7 and 4.3 for 2R5K.

Although there is a homology model of the full length TRPV1,<sup>39</sup> the validity of this model is questionable. This model showed a mostly structured C-terminal domain, while the most recent experimental structure suggested a disordered domain. In addition, our experimental results do not support the C-terminal domain features reported in the model. The most discrepancy lies in the temperature sensor: our data

indicates an extended secondary structure, which was confirmed by a  $\beta$ -strand observed in the cryo-EM structure, while the model suggested a helical structure for the same region. Our models for the TRPV1 C-terminal domain, shown in Figure 7, are, in general, consistent with the NMR experimental data, and are complementary to the cryo-EM experimental structure, which provided limited information on the C-terminal domain. Our model structures at both temperatures show two helices at the proximal C-terminal domain, consisting of the conserved TRP box and the TRP domain that would link to the putative transmembrane segment. These two helices represent the coiled-coil domain, and are responsible for channel oligomerization. Down to the distal part of the C-terminal domain, both the temperature sensor (residues 727 -752, green) and the regulatory PIP<sub>2</sub>-binding segment (residues 778 – 819, blue) are largely unstructured, with the exception of a short stretch of  $\alpha$ -helix in the PIP<sub>2</sub>-binding segment (Figure 7A), at room temperature (25°C). The non-polar residues within the temperature sensor (grey, space filled) are not close to each other in three-dimensional space. At channel activating temperature (45°C), the non-polar residues in the temperature sensor reorganize to form a hydrophobic core, consistent with NMR data that shows the appearance of NOE cross peaks between aromatic and valine residues. The formation of the hydrophobic core induces conformational change in the heat sensor, and extended antiparallel  $\beta$ -sheets are formed. At elevated temperature, additional conformational changes are also observed in the regulatory PIP<sub>2</sub>-binding segment as the con-formation becomes more extended in this region and a short stretch of helix also forms (Figure 7B). In addition, the coiled-coil structure along the TRP box and TRP domain changes the relative orientations between the two



helices, indicating a conformational change migrating from the temperature sensor into the transmembrane segment.

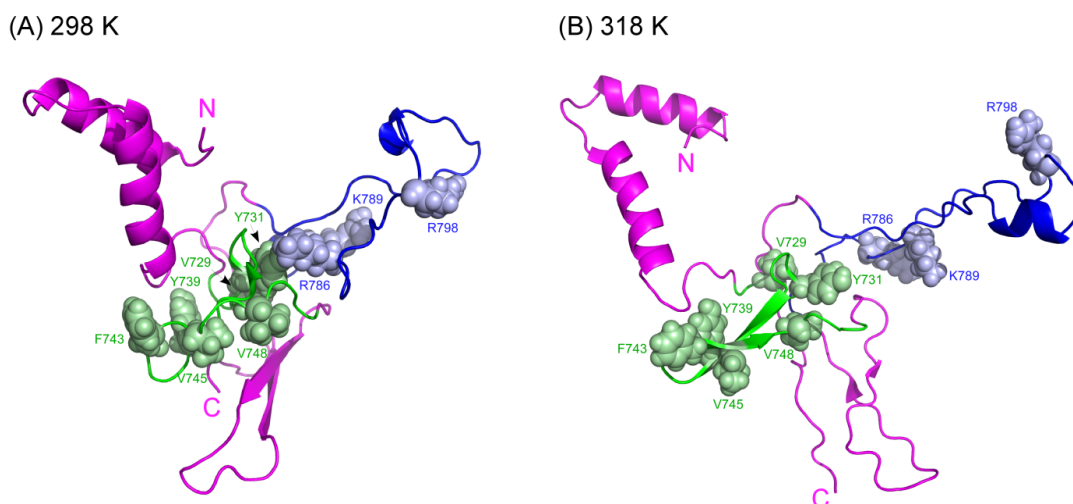


**Figure 7: computational models of TRPV1 C-terminal domain at 298 K (A) and 318 K (B).** The temperature sensor (728 – 753) is colored green, and the regulatory PIP<sub>2</sub>-binding segment (778 – 819) is blue. The key residues forming the hydrophobic core (pale green) in the temperature sensor and the residues essential for PIP<sub>2</sub> binding (light blue) in the regulatory segment are shown as space-filling model.

### 1.3.5 Discussion

Temperature sensing TRP channels are modular, allosterically controlled, multifunctional protein sensors that can integrate a wide variety of stimuli, including temperature, acidic pH, cell membrane voltage, and intracellular Ca<sup>2+</sup> levels, respond to chemical agonists, alcohols, and endogenous cannabinoids, and induce hyperesthesia under nociceptive, inflammatory, and neuropathic conditions. The functions and responses of TRP channels are also strictly regulated by membrane-associated second messengers (such as PIP<sub>2</sub>) and phosphorylation states. Therefore, it is important to characterize the structures and conformations of the C-terminal domain in response to temperature and PIP<sub>2</sub> regulation, key information currently lacking from the literature. This study reports our initial attempt in obtaining structural

information and conformational changes of the TRPV1 C-terminal domain at atomic details under channel activating conditions.

At room temperature, both our NMR spectra and molecular dynamics (MD) model show that most regions of the C-terminal domain, including the heat sensor and PIP<sub>2</sub>-regulatory segments, appear unstructured with the exception of two helices around the conserved TRP box and TRP domain, a coiled-coil segment responsible for the oligomerization of TRPV1 channel, consistent with the recent cryo-EM structure of TRPV1 showing an  $\alpha$ -helical TRP domain<sup>28</sup>. At channel activating temperature (45 °C), our NMR experimental data and the MD model demonstrated a dramatic conformational change at the heat sensor, involving the formation of various hydrophobic valine-aromatic interactions, accompanied by increasing in the  $\beta$ -strand components in this segment. This C-terminal  $\beta$ -strand component was also observed in the cryo-EM structure<sup>28</sup>, which is an important interaction point to the N-terminal domain. This change of conformation at the heat sensor propagates throughout the C-terminal domain, including the PIP<sub>2</sub>-interacting segment and the coiled-coil structural motif, and eventually activates the channel and opens the pore in the transmembrane segment.

Our experimental NMR results, consistent with our MD models, also show that the TRPV1 PIP<sub>2</sub>-interacting segment is intrinsically unstructured in the temperature range of 25-45 °C; only a short stretch of helical structure in this segment was revealed in the MD model, which was also observed in the NMR experiments. The TRPV1 PIP<sub>2</sub>-binding segment seemed to be able to interact with the lipid bicelles, which consists of 80% neutral lipids (DHPC and DMPC) and 20% negatively

charged lipids (DMPG). The TRPV1 C-terminal domain contains several clusters of basic residues (Lys and Arg) that are positively charged under experimental conditions (pH 6.6), including a segment near the TRP box and TRP domain (residues 694-721) and the putative PIP<sub>2</sub>-interacting segment (residues 778-819). These positively charged basic residue patches may possibly interact with the negatively charged DMPG lipid through electrostatic interactions, but such interactions are largely non-specific, as evidenced by the broadened NOE cross peaks in the presence of lipid bicelles without PIP<sub>2</sub> (Figure 5B). Only in the presence of 4% PIP<sub>2</sub> (-4 charge under experimental conditions) in the lipid bicelles, the PIP<sub>2</sub>-interacting segment undergoes significant conformational changes, clearly adopting secondary structures, as illustrated by the shifts and appearance of new NOE cross peaks (Figure 5B). We believe that the PIP<sub>2</sub>-interacting segment is involved in a specific, electrostatic interaction with the PIP<sub>2</sub> molecule. This observation agrees with early studies on other PIP<sub>2</sub>-binding peptides (such as MARCKS) that these basic membrane-bound peptides only sequester multivalent (such as PIP<sub>2</sub>), but not monovalent (such as PG or PS) acidic lipids.<sup>47,48</sup>

### **1.3.6 Concluding Remarks**

TRPV1, a multifunctional ion channel protein, is an important drug target for novel analgesics and potential modulators of the effects of substances of abuse, including alcohol and illicit drugs. However, the lack of essential structural information on TRP channels greatly limits the understanding of the channel functions and mechanisms in mediating relevant biological processes and physiological effects. Here we report our

experimental NMR studies and MD simulations in revealing potential structure-activity relationship of the TRPV1 C-terminal domain. In conclusion, the C-terminal domain is largely unstructured under normal conditions (25 °C), with the exception of the proximal TRP box and TRP domain region, which forms a helical coiled-coil structure, and is responsible for the oligomerization of the channel. At channel activating temperature (45 °C), the temperature sensor (residues 727 – 752) adopts an extended secondary structure with the formation of a hydrophobic core involving several valine and aromatic residues within the sensor. The structural changes at the temperature sensor induce a substantial conformational change throughout the C-terminal domain, and transmit into the transmembrane segment to activate the channel. The PIP<sub>2</sub>-interacting segment (residues 778 – 819) is also intrinsically unstructured, although a short stretch of  $\alpha$ -helix was observed. This segment specifically interacts with PIP<sub>2</sub> (-4 charge) electrostatically through clusters of basic residues, but does not interact with monovalent lipid, such as DMPG used in this study or POPS as in the actual mammalian plasma membrane. Our study confirms the important roles of the C-terminal domain in temperature sensing and PIP<sub>2</sub>-regulation of the TRPV1 channel functions, and provides structural insights into the mechanisms of the C-terminal domain in mediating these stimuli. Although a high-resolution cryo-EM structure of a minimum TRPV1 construct is now available, this structure lacked the regulatory PIP<sub>2</sub>-binding segment of the C-terminal domain, and besides the  $\alpha$ -helix of the TRP domain and a  $\beta$ -strand within the temperature sensor, limited information was available for the functionally critical C-terminal domain in this experimental structure. Our models of the full C-terminal domain, complementary to

the experimental structure, therefore, provide key information in understanding the channel functions.

### **1.3.7 Acknowledgments**

We thank Proteomics Resource Center of the Rockefeller University for syntheses and characterizations of TRPV1 peptides, and the New York Structural Biology Center for high field NMR instrument time. We are also grateful for various funding and fellowships from the Eric F. Ross Research Foundation, Independent College Fund of New Jersey, New Jersey Space Grant Consortium/NASA, and University Research Council of Seton Hall University.

## ***1.4 Structural Affect on C-terminal Domain of TRPV1 at Varying Temperatures***

### **1.4.1 Methodology**

In order to further expand on how temperature and PIP<sub>2</sub> binding affect TRPV1 activation, the complete monomer C-terminal domain model was generated. Since there is limited published structure data on the C-terminal domain, DNA STAR Lasergene and Modeller<sup>46</sup> were used in order to create the C-terminal domain using a homology model. A BLAST search was conducted and the homology model was created using rat isolated K<sub>v</sub>1.2, a potassium channel voltage gated protein; its structure was determined using X-ray crystallography and was published under Protein Data Bank ID 2R9R.<sup>36</sup> In order to insert the C-terminal domain into a lipid membrane mimicking the environment of TRPV1, an S6  $\alpha$ -helix was created. This was accomplished by aligning the S6  $\alpha$ -helix sequence from the TRPV1 with 2R9R<sup>36</sup> using DNA STAR Lasergene. The  $\alpha$ -helix was constructed using PyMOL using the amino acid sequence **GETNKIAQESKNI**.<sup>87</sup> After this structure was created, the  $\alpha$ -helix was attached to the C-terminal domain in order to produce one joined structure using Modeller.<sup>46</sup> The complete amino acid sequence of the combined structure of the S6  $\alpha$  helices and the C-terminal domain is as follows:

MGDLEFTENYDFKAVFIILLAYVILTYILLNMLIALMGETVNKIAQESKNIW  
 KLQRAITILDTEKSFLKCMRKAFRSGKLLQVGYTPDGKDDYRWCFRVDEVN  
 WTTWNTNVGIINEDPGNCEGVKRTLFSLSRVSGRHWKNFALVPLLREAS  
 ARDRQSAQPEEVYLRQFSGSLKPEDAIEVFKSPAASGEK\*

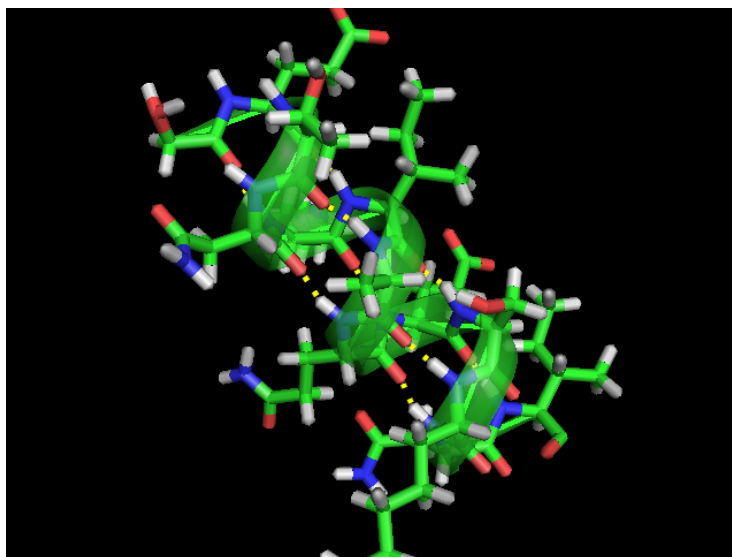


Figure 8: TRPV1 created S6  $\alpha$  helix created using PyMOL visualized using VMD<sup>47,87</sup>

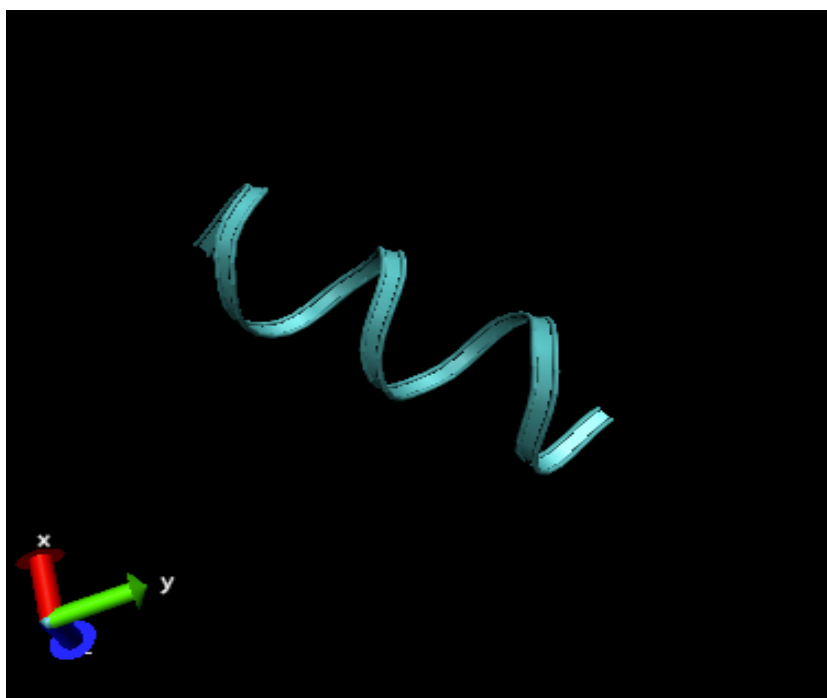


Figure 9: TRPV1 created S6  $\alpha$  helix visualized using VMD<sup>47</sup>

Once the S6-CTD complex as created, six homology structures were generated by Modeller<sup>46</sup>, and the model with lowest objective function (molpdf) value and DOPE assessment score was selected for additional molecular dynamics simulations using NAMD<sup>20</sup> package. Figure 10 below contains an overlay of structures 1, 3 and 4. The overlaid structures are very similar however structure 1 had the straightest  $\alpha$ -helix. Since this structure is going to be inserted into a lipid membrane, this structure was chosen.

**Table 1: Modeller Results**

Filename	molpdf	molpdf	DOPE score
S6CTD.B99990001.pdb	1290.52087	12609.74707	-0.92686
S6CTD.B99990002.pdb	1257.61279	12544.09082	0.96651
S6CTD.B99990003.pdb	1119.74719	-12529.54395	0.96981
S6CTD.B99990004.pdb	1183.25500	-12529.69727	0.92234
S6CTD.B99990005.pdb	1255.80859	-12353.58203	0.81043



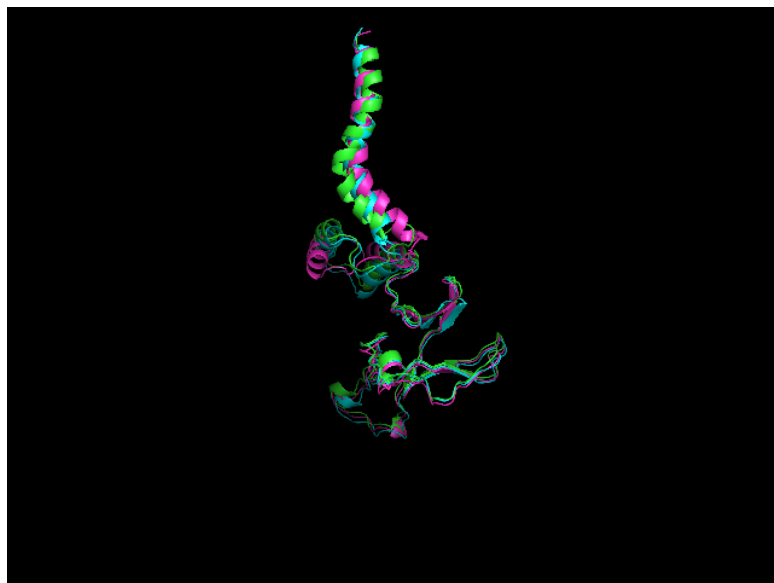


Figure 10: Overlay of C-terminal domain structures 1,3, and 4 visualized using VMD<sup>47,87</sup>



Figure 11: C-terminal domain highlighting secondary structure motifs visualized using VMD<sup>47,87</sup>

## 1.4.2 Lipid Membrane Generation

TRPV1 is a lipid membrane therefore in order to properly simulate the protein and obtain necessary structure-function information on the channel, the associated protein domains must be inserted into a lipid membrane. The lipid membrane was created by CHARMM-GUI<sup>50</sup>, an Internet based graphical user interface that creates, equilibrates and generates necessary input files for many different simulation programs, including CHARMM<sup>50</sup> and NAMD<sup>20</sup>. A heterogeneous lipid membrane was created via the insertion method utilizing the membrane-building feature. The following numbers of lipid components were chosen in order to create a membrane that would be large enough for protein insertion: 60 POPC, 43 POPE and 21 POPS. The focus of this particular study was the effect of temperature on the C-terminal domain of TRPV1; PIP<sub>2</sub> was not included in the lipid membrane.

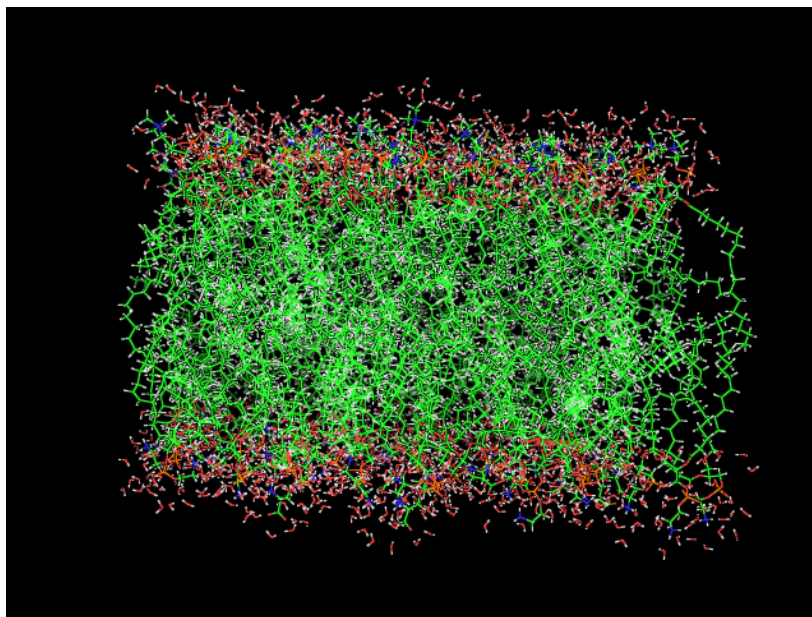


Figure 12: Lipid Membrane created by CHARMM-GUI<sup>50</sup> visualized using VMD<sup>47</sup>

A PSF file for the lipid membrane and the CTD-S6 complex were generated utilizing CHARMM topology file, which contain the atom names, types, bonds and partial charges for each residue type. Specifically, topology file `top_all36_lipid.inp` was used in order to create the PSF file for the lipid membrane and `top_all36_protein.inp` was used to create the PSF file for the C-terminal domain.<sup>53-55</sup>

### 1.4.3 Protein Insertion

Protein insertion was completed using VMD<sup>47</sup> and a published script known as `combine.tcl`. The protein and membrane were aligned and then combined into one PDB structure.

```
#!/usr/local/bin/vmd
# join (parts of) protein complex with a membrane

# set echo on for debugging
echo on

# need psfgen module and topology
package require psfgen
topology top_all27_prot_lipid.inp

# load structures
resetpsf
readpsf membrane.psf
coordpdb membrane.pdb
readpsf protein_only.psf
coordpdb protein_psfgen.pdb

# can delete some protein segments if needed
#set pseg2del { "D" "E" "F" "G" "H" }
set pseg2del { }
foreach seg $pseg2del {
    delatom $seg
}

# write temporary structure
set temp "temp"
writepsf $temp.psf
writepdb $temp.pdb
```

```

# reload full structure (do NOT resetpsf!)
mol load psf $temp.psf pdb $temp.pdb

# select and delete lipids that overlap protein:
# any atom to any atom distance under 0.8A
# (option: heavy atom to heavy atom distance under 1.3A)
set sellip [atomselect top "resname POPC"]
set lseglip [lsort -unique [$sellip get segid]]
foreach lseg $lseglip {
  # find lipid backbone atoms
  set selover [atomselect top "segid $lseg and within 0.8 of
protein"]
  # delete these residues
  set resover [lsort -unique [$selover get resid]]
  foreach res $resover {
    delatom $lseg $res
  }
}
foreach res { } {delatom $LIP1 $res}
foreach res { } {delatom $LIP2 $res}

# select and delete waters that overlap protein:
set selwat [atomselect top "resname TIP3"]
set lsegwat [lsort -unique [$selwat get segid]]
foreach lseg $lsegwat {
  set selover [atomselect top "segid $lseg and within 3.8 of
protein"]
  set resover [lsort -unique [$selover get resid]]
  foreach res $resover {
    delatom $lseg $res
  }
}
foreach res { } {delatom $WAT1 $res}
foreach res { } {delatom $WAT2 $res}

# write full structure
writepsf protein_and_membrane.psf
writepdb protein_and_membrane.pdb

# clean up
file delete $temp.psf
file delete $temp.pdb

# non-interactive script:  vmd -dispdev text < combine.tcl >
combine.log
quit

```

Once combined, a new PSF file was created for the compiled structure followed by solvation and ionization. The completed system was ionized with a salt concentration of 0.15M NaCl.

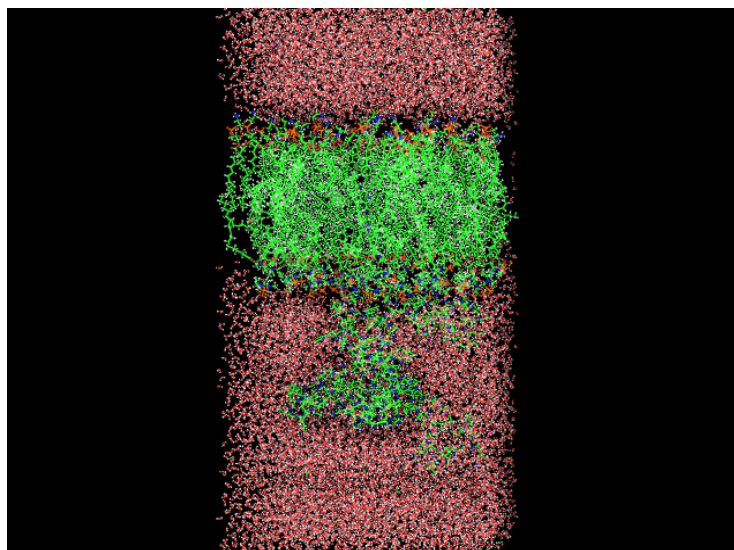


Figure 13: Solvated and Ionized C-terminal Domain inserted into a lipid membrane visualized using VMD<sup>47</sup>

#### 1.4.4 Molecular Dynamics Simulations

As previously stated, TRPV1 is activated by temperature greater than 43°C. Performing MD simulations at 300K and 400K using CHARMM force fields and NAMD<sup>20</sup> scalable molecular dynamics package further assessed temperature affect on TRPV1. Simulations were performed under periodic boundary conditions. VMD<sup>47</sup> was utilized to view the simulations and perform additional calculations.

In order to determine if the structure was properly equilibrated and to potentially evaluate protein flexibility, VMD<sup>47</sup> was employed in order to perform a Root Mean Squared Deviation. According to the VMD tutorial guide, RMSD is defined as a measure of the distance between two structures:

$$RMSD = \frac{\sqrt{\sum_{e_0}^{t_f} (r(t) - r(t_0))^2}}{N}$$

Where  $N_{\text{atoms}}$  is the number of atoms whose positions are being compared and  $r_i(t)$  is the position of atom  $i$  at time  $t$ .

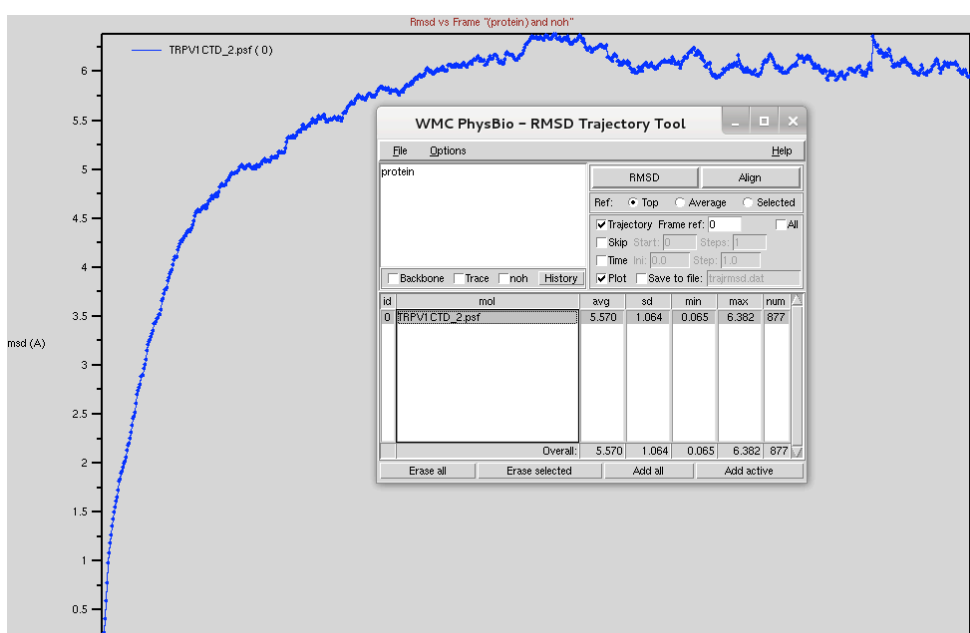


**Figure 14: Simulation RMSD created and displayed using VMD<sup>47</sup>**

The Figure above shows a vast increase in the RMSD value at the start of the simulation. As the simulation time increases, the angstrom change in the RMSD value becomes negligible. This implies the system is properly equilibrated and production runs can be initiated.

Production runs were performed at both 300K and 400K under NPT conditions. Isobaric-Isothermal Ensemble, or NPT, is characterized by a fixed number of atoms (N), pressure (P) and temperature (T). The structure below highlights the  $\alpha$ -helices in red, the  $\beta$ -sheets in yellow loops in green and the pink area represent the putative temperature-sensing region.

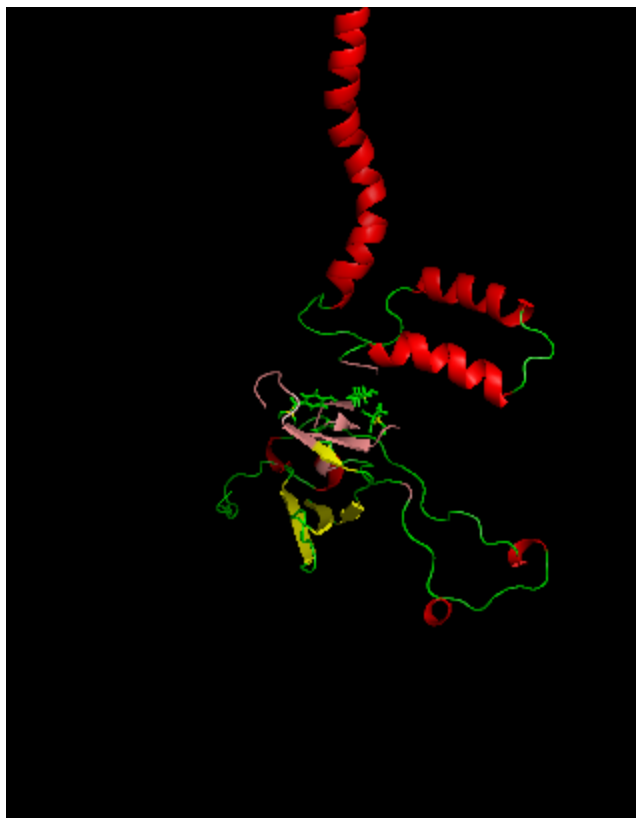


**Figure 15: C-terminal domain highlighting the secondary structure and temperature sensing region using VMD<sup>47</sup>**

The overlay below highlights the last frame structure differences between the simulations performed at 300K and 400K, respectively. In order to properly highlight the potential changes that occurred in the C-terminal domain at the different temperatures, the lipid membrane, water and ions were removed from the overlay. In the Figure below, the final frame of the simulation at 300K is in green and at 400K is

highlighted in red. In addition, the overlay in Figure 16 contains the starting and ending frames for the simulation at 400K. The starting frame is highlighted in red and the ending frame is highlighted in pink.

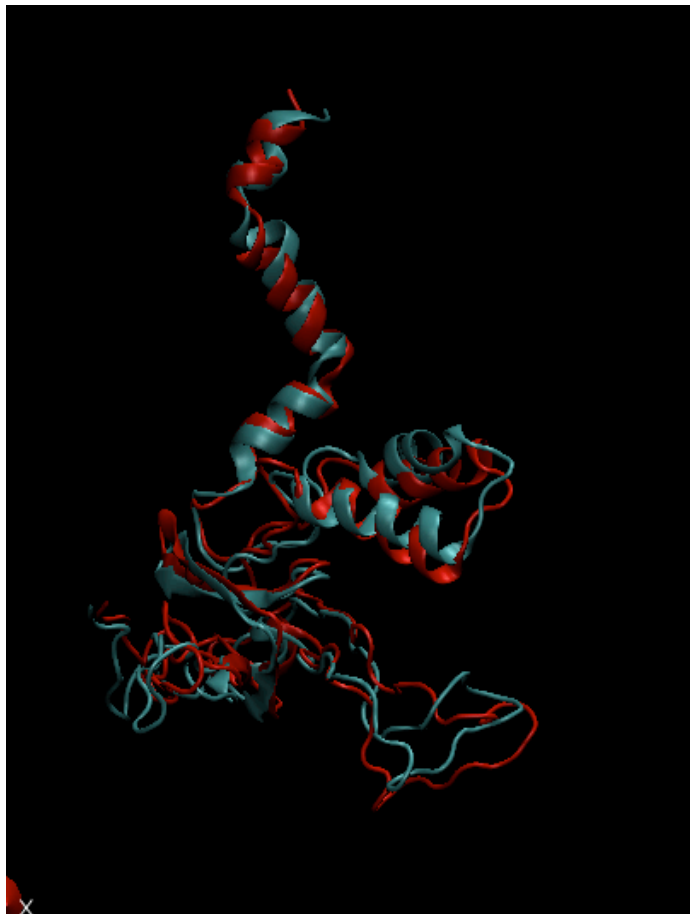


**Figure 16: Overlay of C-terminal domain at 300K(red) and 400K(green) visualized using VMD<sup>47</sup>**



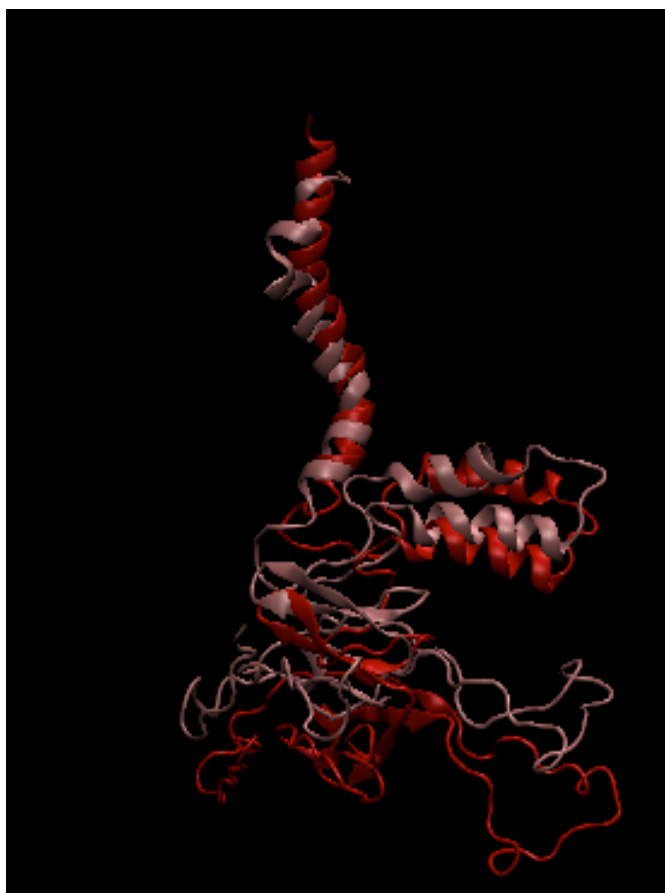


**Figure 17: Overlay of C-terminal domain 400K starting frame (red) and ending frame (pink) visualized using VMD<sup>47</sup>**

### **1.4.5 C-terminal domain Experiment Results**

As compared with the previous experimental results, the temperature-sensing region contains unstructured portions as well as  $\beta$ -turns. A slight conformational change was observed between the 300K and 400K simulations specifically in the unstructured sections of the C-terminal domain. A more extreme temperature increase may be required in order to observe a more dramatic conformational change. In addition, temperature alone may not cause a large conformational change in the

protein; the conformational change may be increased by the addition of a second channel activator such as PIP<sub>2</sub>.

## ***1.5 C-terminal Domain Experiments with PIP<sub>2</sub>***

### **1.5.1 PIP<sub>2</sub> insertion with C-terminal domain and S6 helix**

PIP<sub>2</sub> was inserted into the pdb file containing the CTD-S6 helix complex employing the combine.tcl script.

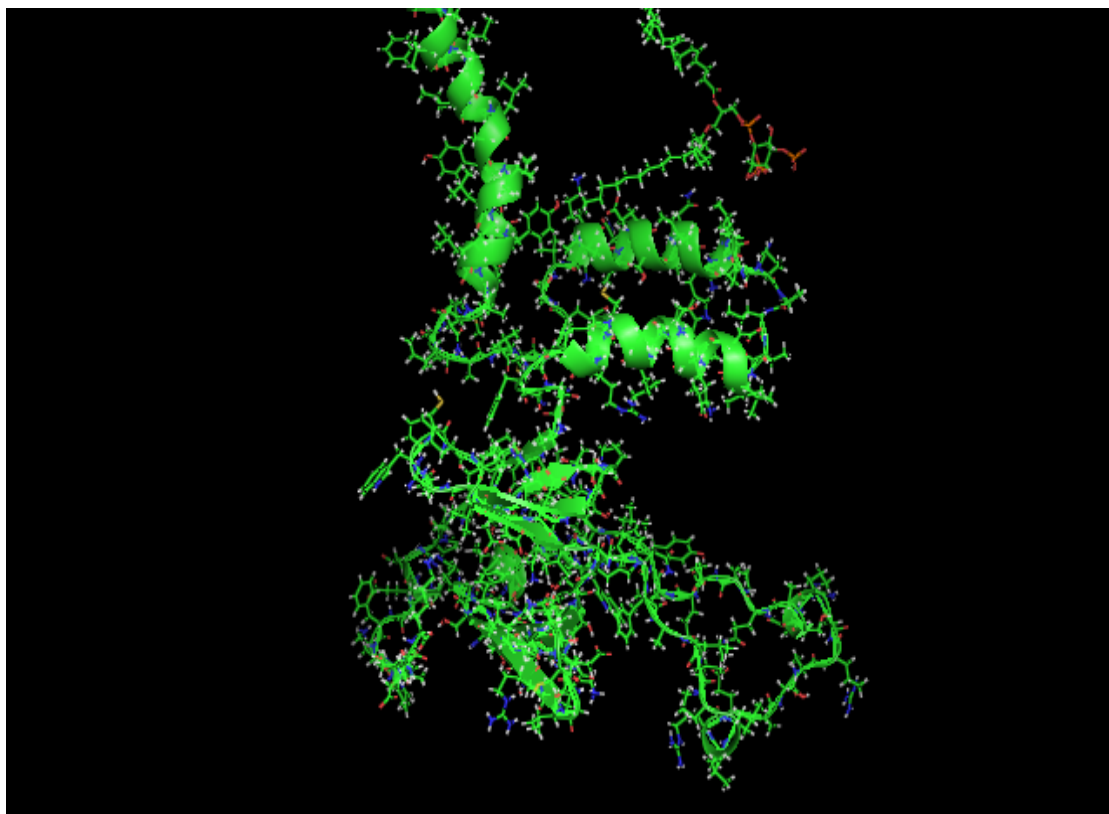


**Figure 18:** C-terminal domain and S6 helix complex with the addition of 1 molecule of PIP<sub>2</sub> visualized using VMD<sup>47</sup>

One molecule was placed in an arbitrary position in the upper left hand corner of the PDB file, highlighted in Figure 18 above. A docking study utilizing the program AutoDock<sup>78,79</sup> was performed in order to determine the optimal location for PIP<sub>2</sub> as well as provide insight on a PIP<sub>2</sub> binding pocket.

## 1.5.2 AutoDock

### 1.5.2.1 AutoDock Experiment Rationale and Methodology

AutoDock<sup>78,79</sup> is a suite of automated docking tools designed to determine the most thermodynamically stable binding location for ligands or small molecules binding to receptors.<sup>78,79</sup> In this case PIP<sub>2</sub> is the functional ligand and CTD-S6 complex is the receptor. In Figure 19 below, a simulated model containing 1 molecule of PIP<sub>2</sub> using AutoDock<sup>78,79</sup> location and “best guess” location were performed at both 300K and 400K.

### 1.5.2.2 AutoDock Results

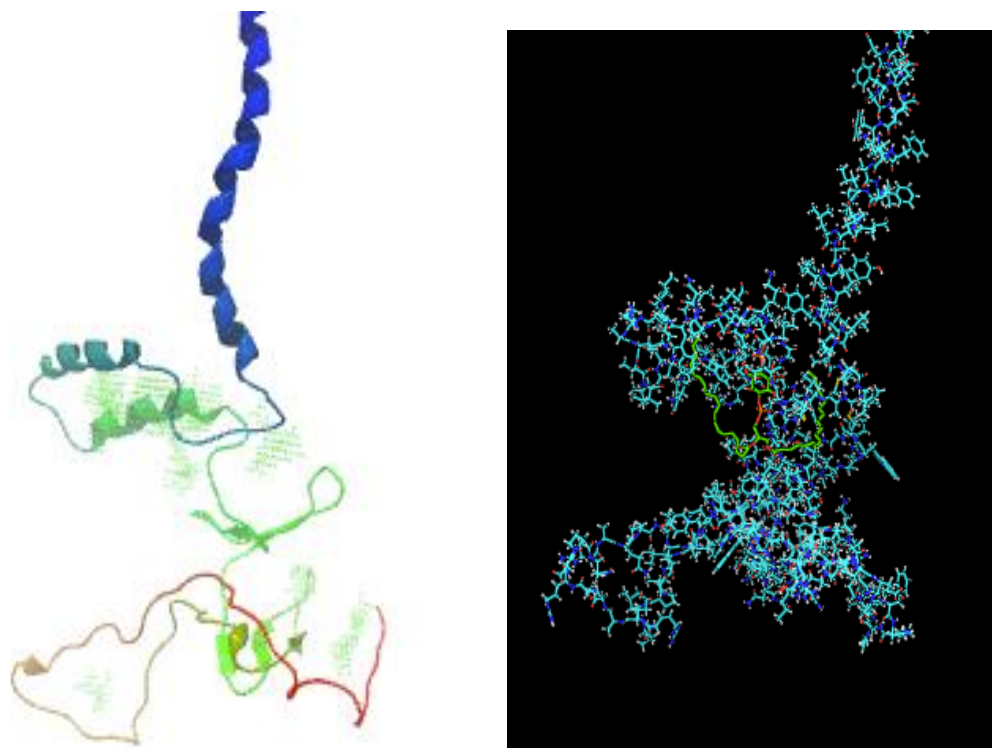


Figure 19: AutoDock binding study results<sup>78,79</sup>

### 1.5.2.3 AutoDock Result Table

**Table 2: AutoDock Result Table**

mode	affinity   (kcal/mol)	dist from best mode   rmsd l.b.   rmsd u.b.	
-----+-----+-----+-----			
1	-6.1	0.000	0.000
2	-6.1	2.639	7.693
3	-6.0	3.052	8.119
4	-5.9	2.182	6.601
5	-5.9	5.323	10.923
6	-5.7	2.508	6.566
7	-5.6	2.361	5.803
8	-5.6	5.022	10.812
9	-5.6	4.972	9.237

### 1.5.2.4 Autodock Discussion

AutoDock binding study implies the highest probability of PIP<sub>2</sub> binding occurs in the  $\alpha$ -helix section of the C-terminal domain. At physiological pH, PIP<sub>2</sub> possesses a -4 charge, therefore it was hypothesized that PIP<sub>2</sub> would bind to a region of the C-terminal domain that contained protonated, positively charged amino acids such as arginine, lysine and histidine. The theoretical binding section contains limited positively charged amino acids. Therefore, the data suggests that the interaction between PIP<sub>2</sub> and the CTD occurs not through a binding pocket but through electrostatic interactions.

## ***1.6 Temperature and PIP<sub>2</sub> Binding Experiments Utilizing the Complete Tetramer***

### **1.6.1 Introduction**

High-resolution structures of TRPV1 ion channel were determined using state-of-the-art single particle cryo-electron microscopy (cryo-EM) technique, and distinct conformations were revealed upon activation of the channel.<sup>5,28</sup> These structures provided detailed information on the arrangement of the transmembrane section, including the ion passage pore and the cytosolic N-terminal domain, including the ankyrin repeats. However, not included in PDB 3J5P<sup>5</sup> is about half of the cytosolic C-terminal domain specifically residues 684-839.<sup>4,5</sup> The inability to obtain more definitive structure information on the C-terminal domain implies that it is not only largely unstructured but that it also undergoes a significant conformation change upon channel activation. In order to obtain pertinent channel activation information focusing on the C-terminal domain: four homology created C-terminal domains will be attached to the published transmembrane section of 3J5P.<sup>5</sup> Specifically the most thermodynamically stable C-terminal domain will be attached to each transmembrane monomer. Once combined, the C-terminal domain was inserted into a lipid bilayer, solvated and ionized. Simulations were performed in the presence and absence of PIP<sub>2</sub> at varying temperatures in order to determine if both temperature and the functional ligand are required for channel activation.

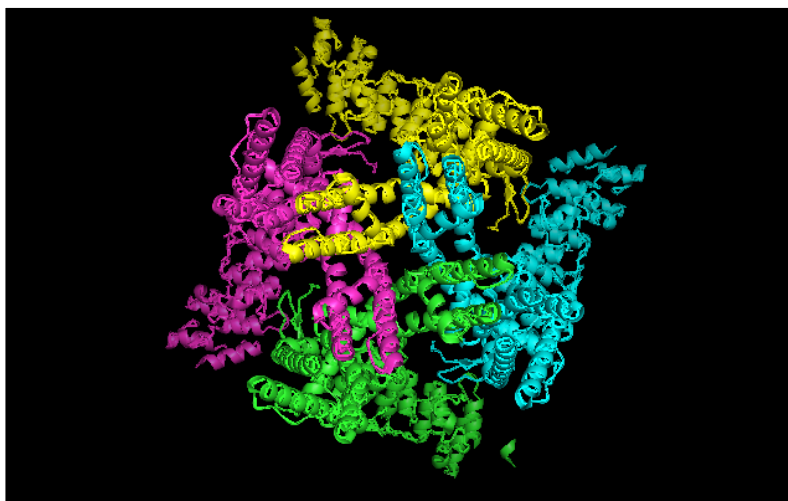


Figure 20: Top View of the transmembrane domain of TRPV1 created in VMD<sup>47</sup>



Figure 21: Side View of the transmembrane domain of TRPV1 created in VMD<sup>47</sup>

## 1.6.2 Methodology and Experiments

### 1.6.2.1 C-terminal Domain attachment to Transmembrane Domain

In Figures 20 and 21 above each monomer is highlighted in a different color. The most thermodynamically stable C-terminal domain, as determined by Modeller<sup>46</sup>, was added to the distal end of each monomer. Utilizing VMD<sup>47</sup> and the combine.tcl

script that can be found in **Section 1.4.3** performed the addition of the C-terminal domain to each transmembrane monomer.

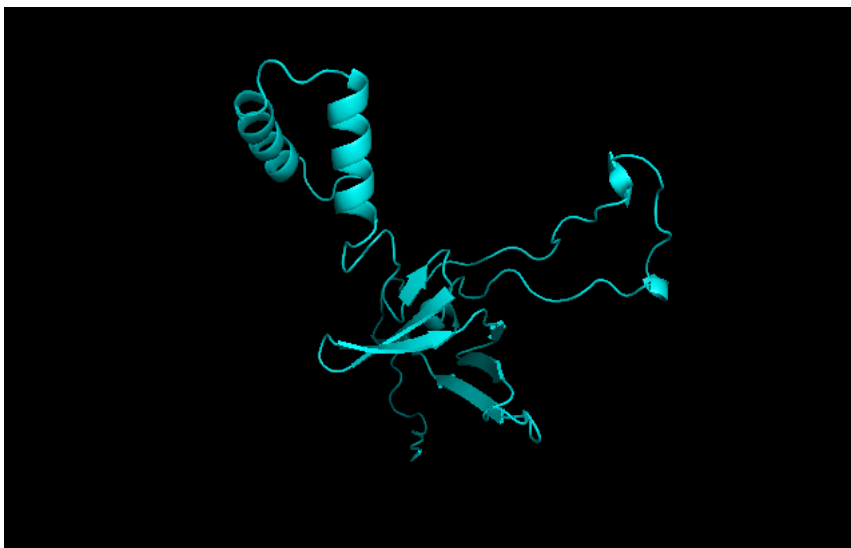


**Figure 22: Representation of the most thermodynamically stable, newly created C-terminal domain visualized using VMD<sup>47</sup>**

The completed TRPV1 transmembrane section plus four C-terminal domains is illustrated below in Figure 23. The protein CHARMM<sup>53-55</sup> topology file, `top_all36_protein.inp`, was chosen in order to create a viable TRPV1 transmembrane and C-terminal domain PSF structure file.<sup>53-55</sup>

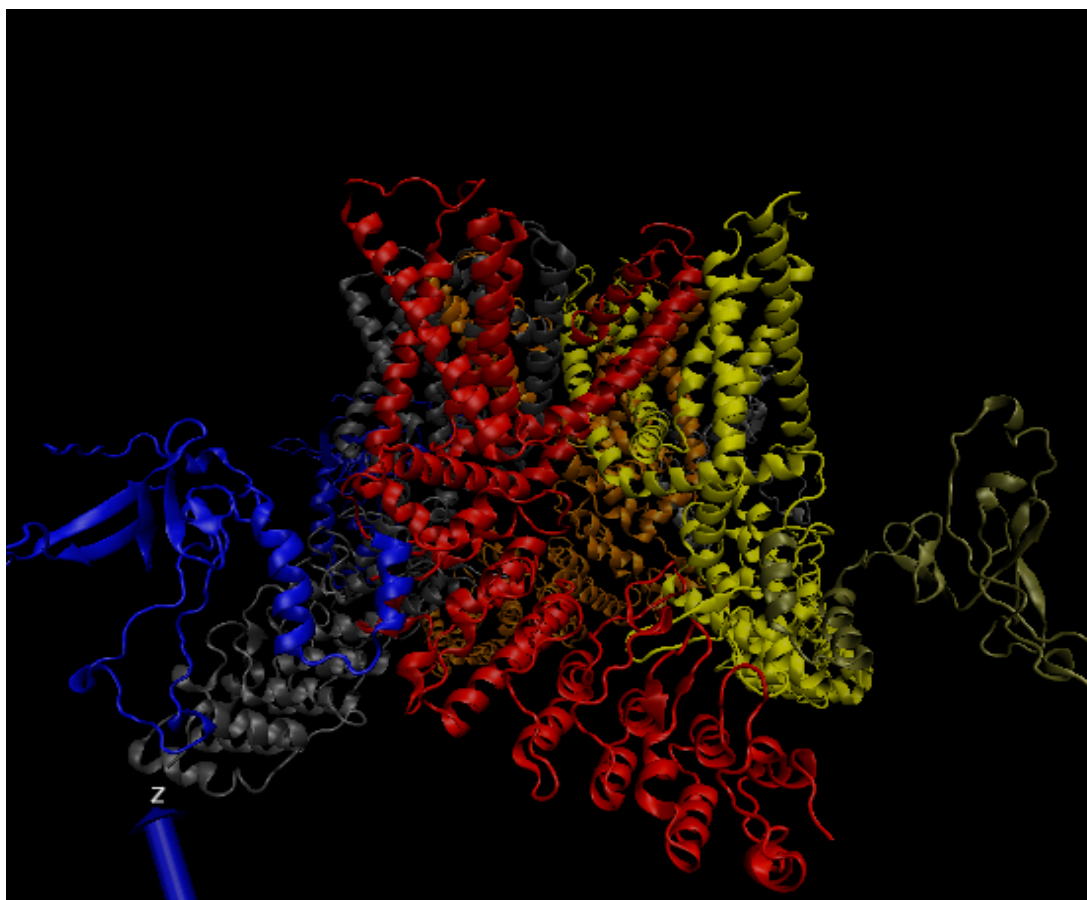


Figure 23: The completed TRPV1 transmembrane section plus four CTD visualized using VMD<sup>47</sup>

#### 1.6.2.2 Lipid Membrane Generation

Several lipid membrane structures were generated using the CHARMM-GUI<sup>50</sup> Internet graphical user interface. The chosen generated lipid membrane created full and complete coverage of the transmembrane section of TRPV1. The membrane was comprised of 400 POPC molecules, 300 POPE molecules, 150 POPS molecules and no PIP<sub>2</sub> molecules. The system was solvated and ionized to 0.15M NaCl. Since the system was equilibrated by CHARMM-GUI<sup>50</sup> it was confirmed that CHARMM<sup>51</sup> had an inositol compatible topology and parameter file. A PSF file was created using two CHARMM<sup>53-55</sup> force fields `top_all36_lipid.inp` and `toppar_all36_lipid_inositol.inp`. In order for `toppar_all36_lipid_inositol.inp` to be accurate for creating a PSF and



eventually running a simulation using the parameter section of the file, a few sections were updated. The CHARMM<sup>51</sup> created inositol force field contains the name SAPI, stearyl arachidonyl phosphatidylinositol-4,5-bisphosphate, rather than PIP<sub>2</sub>. In addition, some of the atom types contained more than 4 characters, such as CC3161 and OC311. This creates an issue when generating a PSF; the charges are shifted to the right 1 or 2 spaces resulting in an incorrect final total charge. All atoms types were altered to 4 or less characters for both the topology and parameter files.

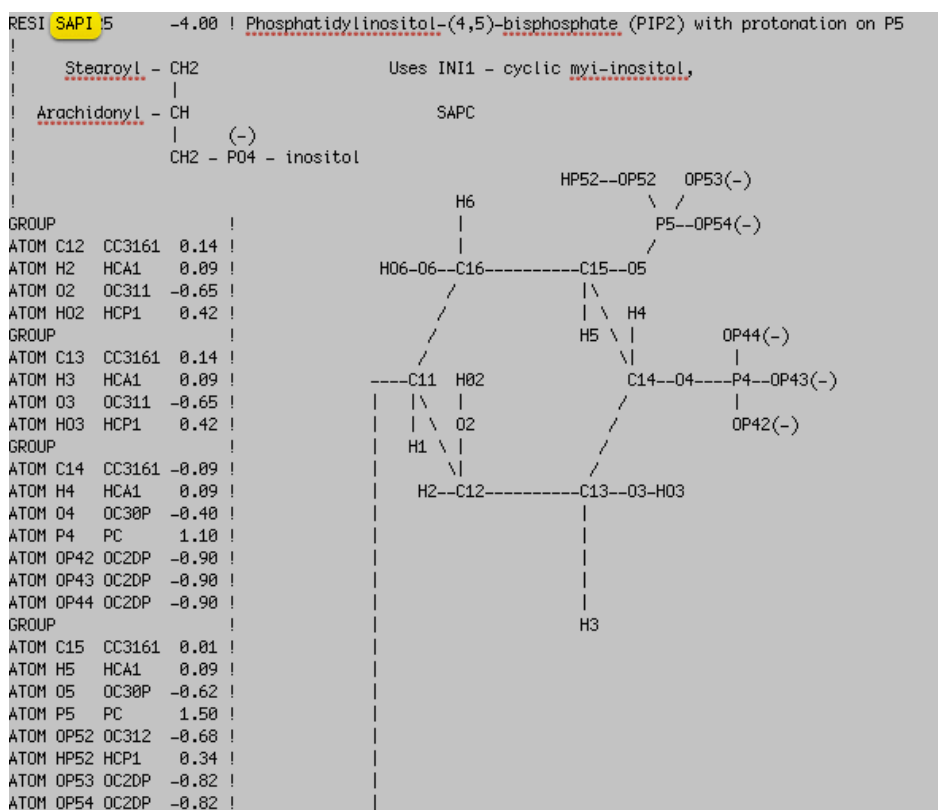


Figure 24: Original topology file for PIP<sub>2</sub><sup>51</sup>

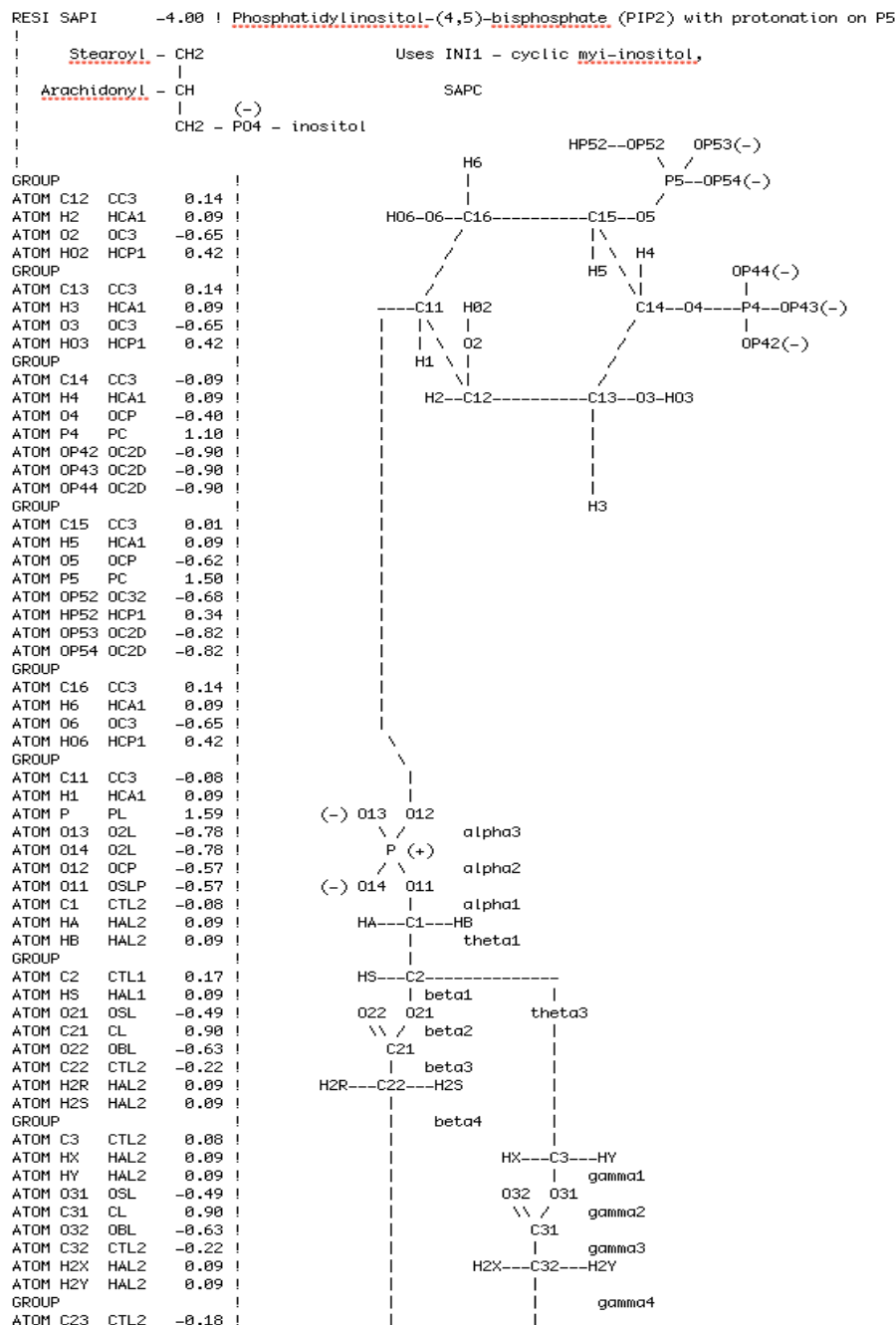


Figure 25: Updated topology file for PIP<sub>2</sub><sup>51</sup>

Figure 26, highlights the PIP<sub>2</sub> molecules in the PSF file using the VDW representation in VMD<sup>47</sup>. Clearly illustrated in the lipid membrane below are all of the PIP<sub>2</sub> molecules.

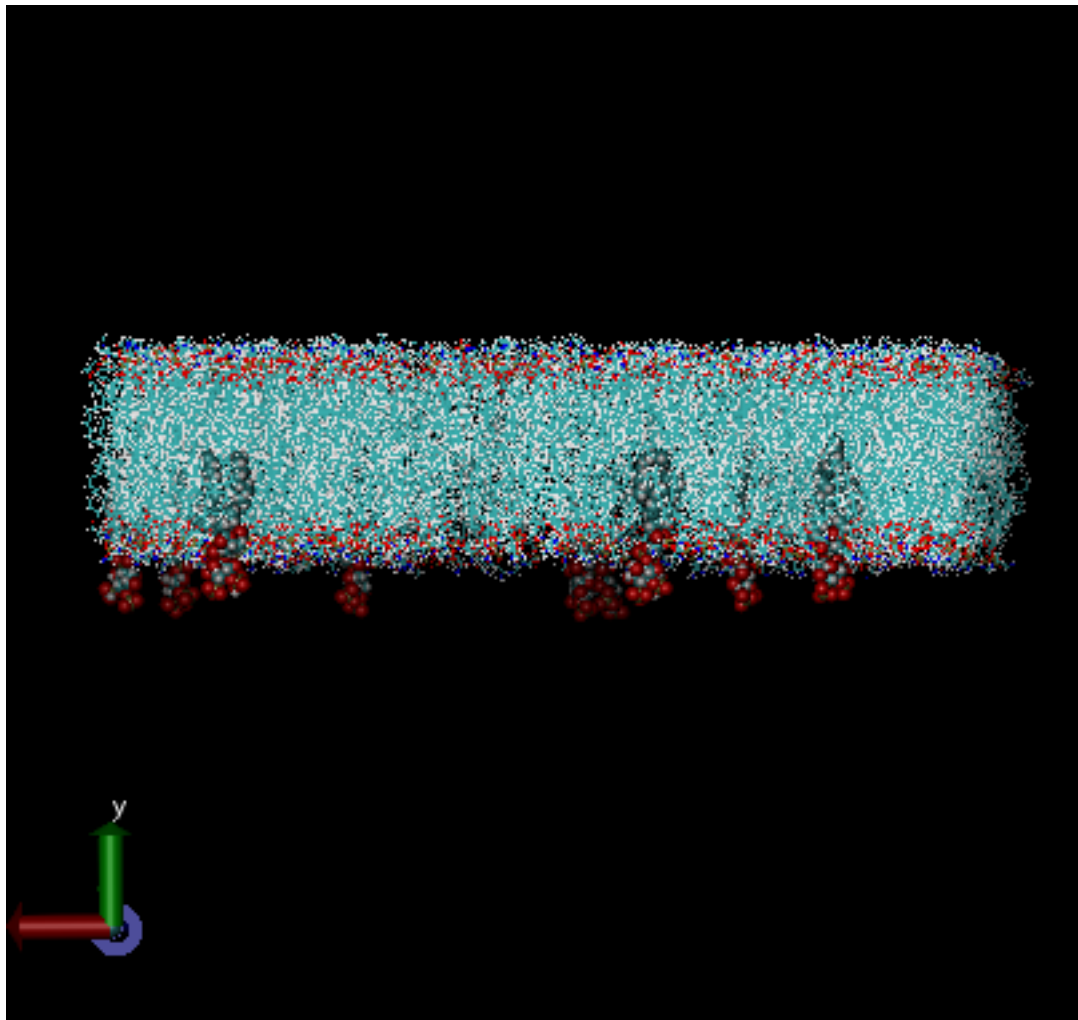


Figure 26: Lipid Membrane created using CHARMM-GUI<sup>50</sup> with PIP<sub>2</sub> visualized using VMD<sup>47</sup>

### 1.6.2.3 Protein Insertion into Lipid Membrane

The completed transmembrane domain with four attached C-terminal domain was inserted into the lipid membrane containing 10 PIP<sub>2</sub> molecules. The combine.tcl script was utilized in order to combine the transmembrane domain and lipid membrane into one PDB file. The combine.tcl script contains lines to delete overlapping atoms this included one PIP<sub>2</sub> molecule; a total of 9 PIP<sub>2</sub> molecules are present in the final structure. The most important feature of the combined structure is the C-terminal domain are not in contact with the lipid membrane; this inhibits a potential atom velocity error from occurring during the simulation. Once combined several CHARMM topology files were employed in order to create a corresponding PSF file: top\_all36\_carb.inp, top\_all36\_lipids.inp, top\_all36\_carb.inp, and top\_all36\_lipid\_inositol.inp.<sup>53-55</sup>

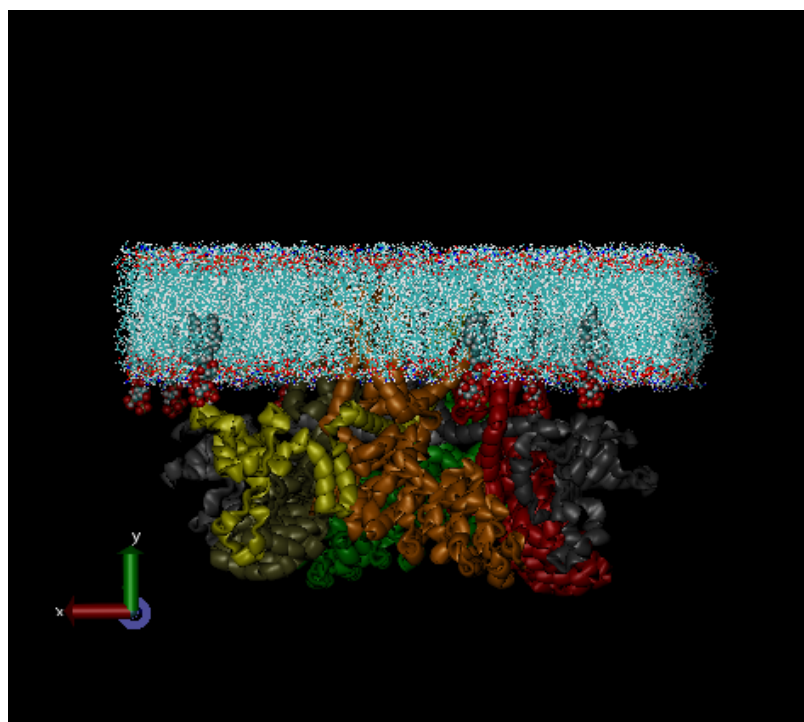


Figure 27: Transmembrane section inserted into lipid membrane visualized using VMD<sup>47</sup>

#### 1.6.2.4 Solvation and Ionization

The combined structure was then solvated and ionized. Figure 28, outlines the solvation parameters. The solvation box size did not completely cover the lipid membrane; this ensures that the water molecules will not enter the adjoining cell. Final structure was ionized to a concentration of 0.15M NaCl. The complete and final structure is illustrated in Figure 29. In addition, Figure 30 displays the same structure with the removal of the water molecules. Figure 31, highlights the top view; this view clearly displays the lipid molecules that were deleted due to protein insertion.

The screenshot shows the 'Solvate' dialog box in VMD. The parameters are as follows:

- Input:**  Waterbox Only
- PSF:** C:/Users/KRaymond/Dropbox/V1\_sapi
- PDB:** C:/Users/KRaymond/Dropbox/V1\_sapi
- Rotate to minimize volume    Rotation Increment (deg): 10
- Selection for Rotation:** all
- Output:** solvate\_lipidsaprotein18a
- Segment ID Prefix:** WT
- Boundary:** 5
- Box Size:**  Use Molecule Dimensions
 

Min: x:	-75	y:	-50	z:	-75
Max: x:	75	y:	50	z:	68
- Box Padding:**

Min: x:	0	y:	35	z:	0
Max: x:	0	y:	35	z:	0
- Use nonstandard solvent
 

Solvent box PDB:	
Solvent box PSF:	
Solvent box topology:	
Solvent box side length:	
Solvent box key selection:	

Figure 28: Solvation parameters obtained from VMD<sup>47</sup>

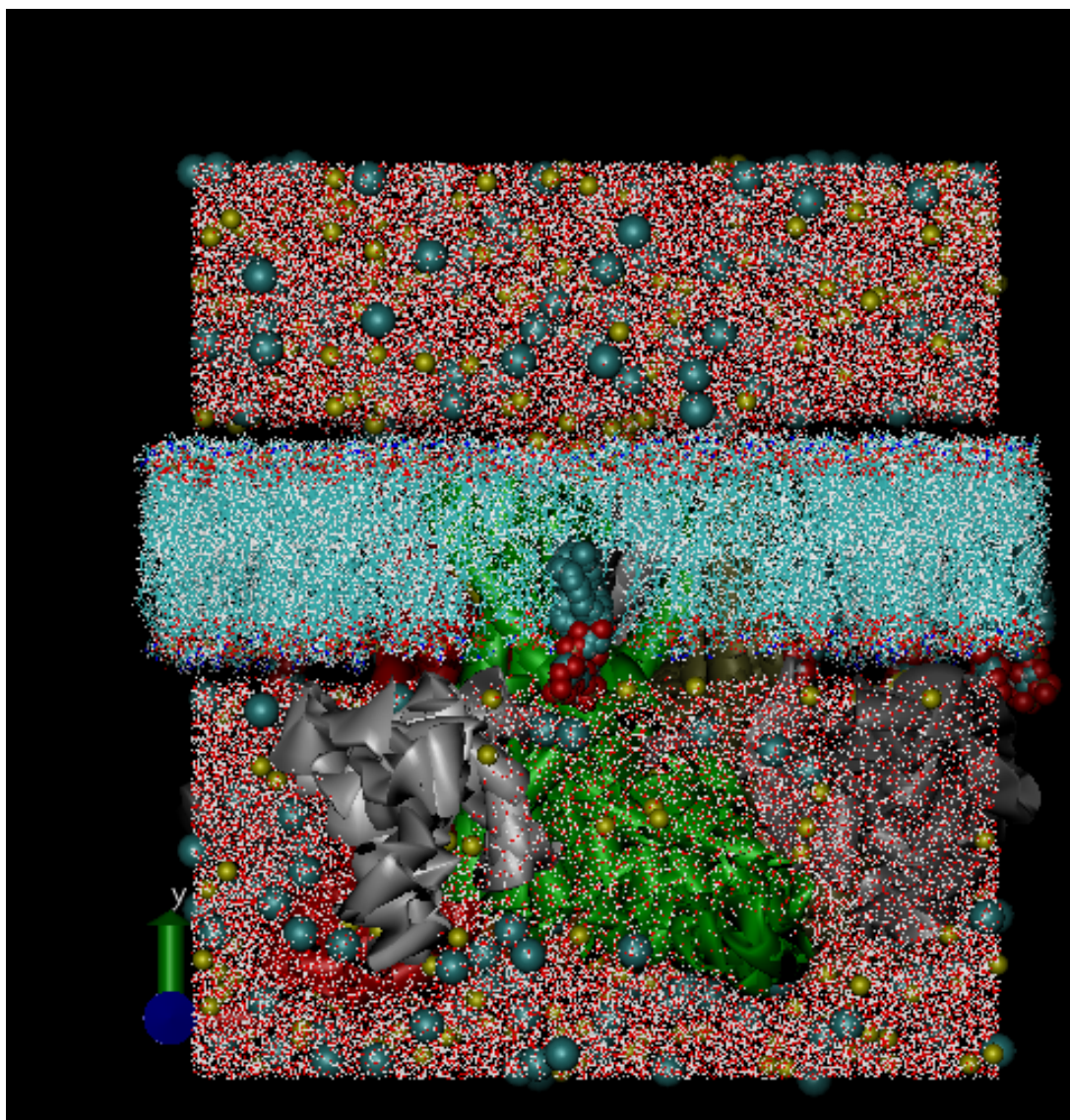


Figure 29: Snapshot of complete TRPV1 structure visualized using VMD.<sup>47</sup>

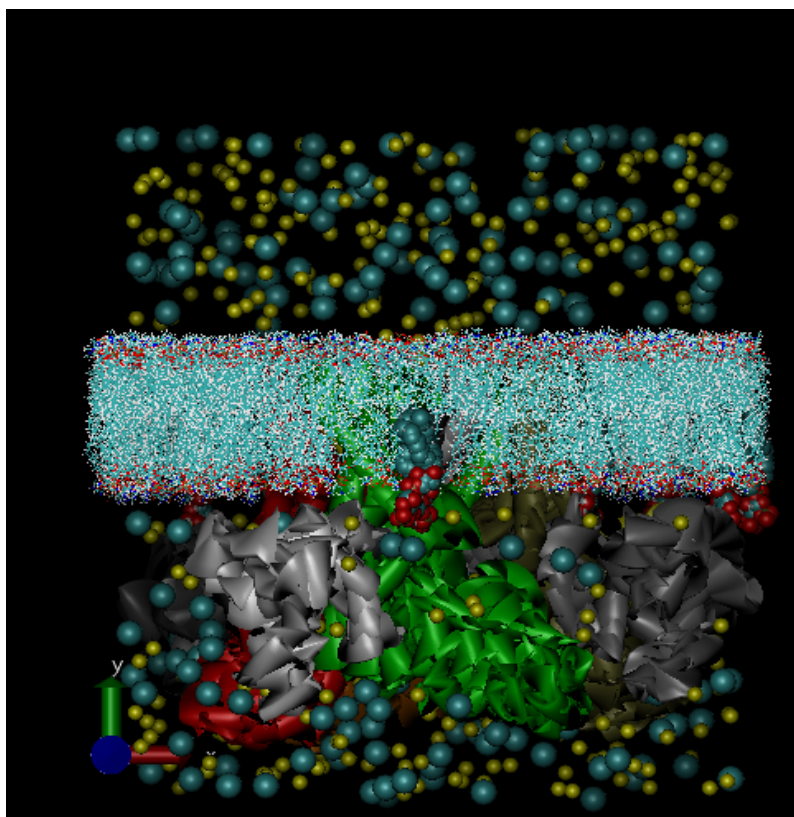


Figure 30: Snapshot of complete TRPV1 structure with water removed visualized using VMD.<sup>47</sup>

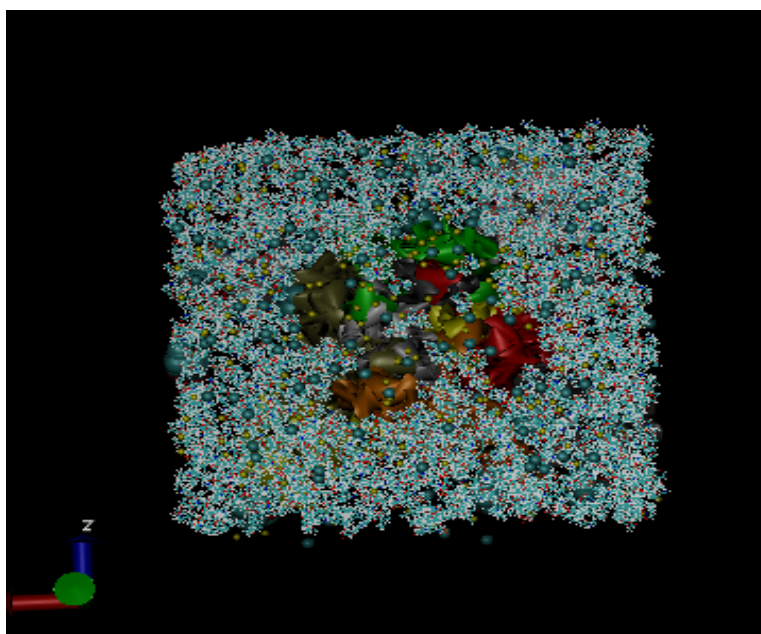


Figure 31: Snapshot of complete TRPV1 structure with water removed top view visualized using VMD.<sup>47</sup>

The same structure was created without PIP<sub>2</sub> as a control.

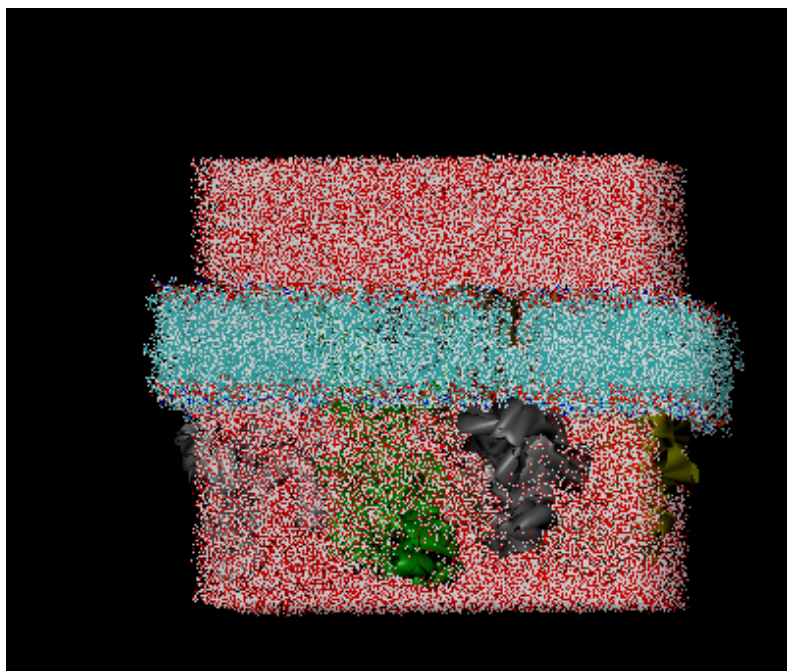


Figure 32: VMD snapshot final control structure without PIP<sub>2</sub> visualized using VMD.<sup>47</sup>

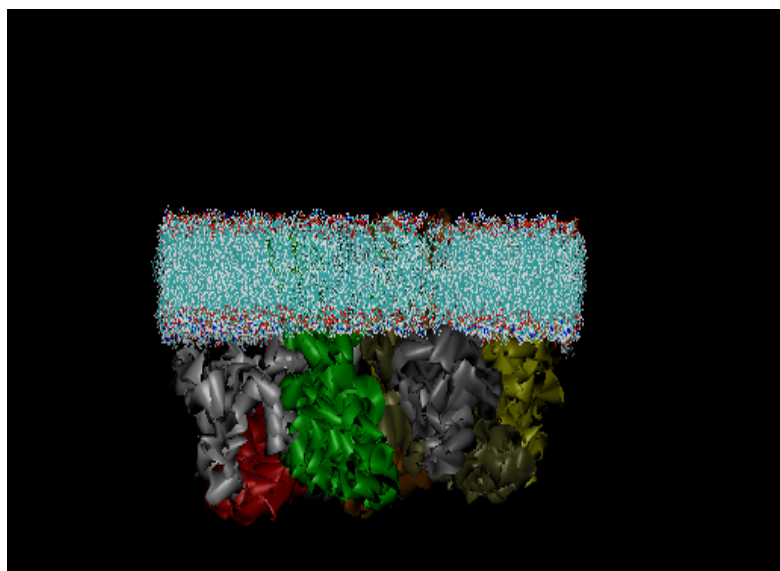


Figure 33: Snapshot of complete TPRV1 control structure with water removed visualized using VMD<sup>47</sup>



### 1.6.3 Simulation Results

#### 1.6.3.1 Control Results

Simulations were performed on both the final control structure (containing no PIP<sub>2</sub>) and the final structure containing PIP<sub>2</sub>. Simulations were minimized prior to production runs. The control structure configuration file was generated at both 300K and 400K. Each of the parameter files that directly correspond with the topology files utilized to generate the PSF files were inputted into the configuration file.

Simulations were performed at NPT conditions and were performed using a time step of 1.0. The rigid bonds were set to all and the steps per cycle were set at 10. The minimization configuration file did not employ Periodic Boundary Conditions, PBC, but they were utilized for the production runs. The box size for PBC was determined using VMD<sup>47</sup>:

Table 3: Box size for PBC

<b>cellBasisVector1</b>	<b>183.5</b>	<b>0</b>	<b>0</b>
<b>cellBasisVector2</b>	<b>0</b>	<b>179.3</b>	<b>0</b>
<b>cellBasisVector3</b>	<b>0</b>	<b>0</b>	<b>117.7</b>
<b>cell origin</b>	<b>13.03</b>	<b>19.84</b>	<b>9.45</b>

The PME Grid Size for the control was set to 256 for the x, y, and z-axes.

Simulations of the control system were performed for 10ns at both 300K and 400K. Figure 34, contains an overlay of the final frame of each simulation performed

at 300K and 400K. The final frame for simulation performed at 300K is in grey while the final frame for the 400K simulations is in blue.

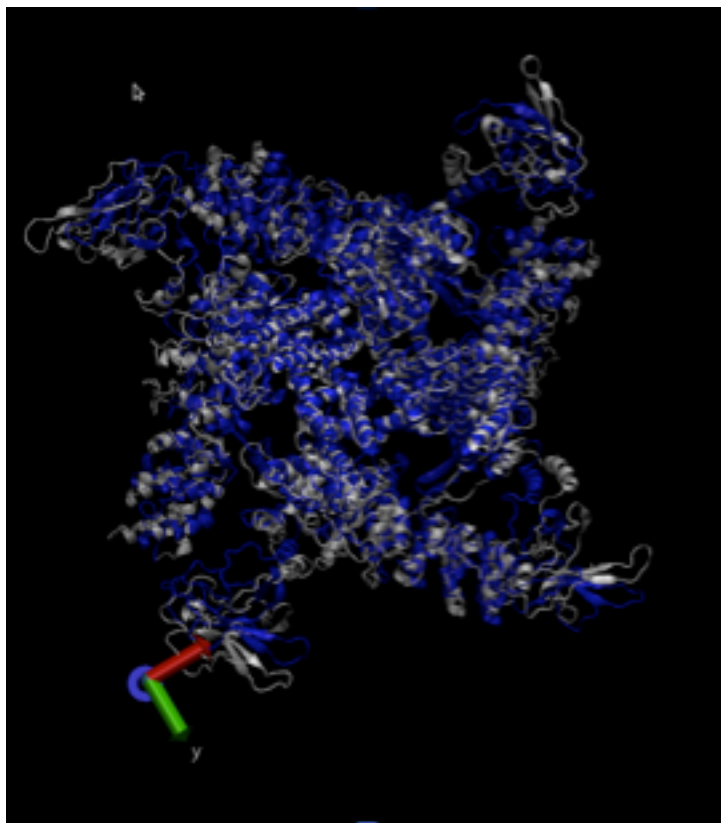
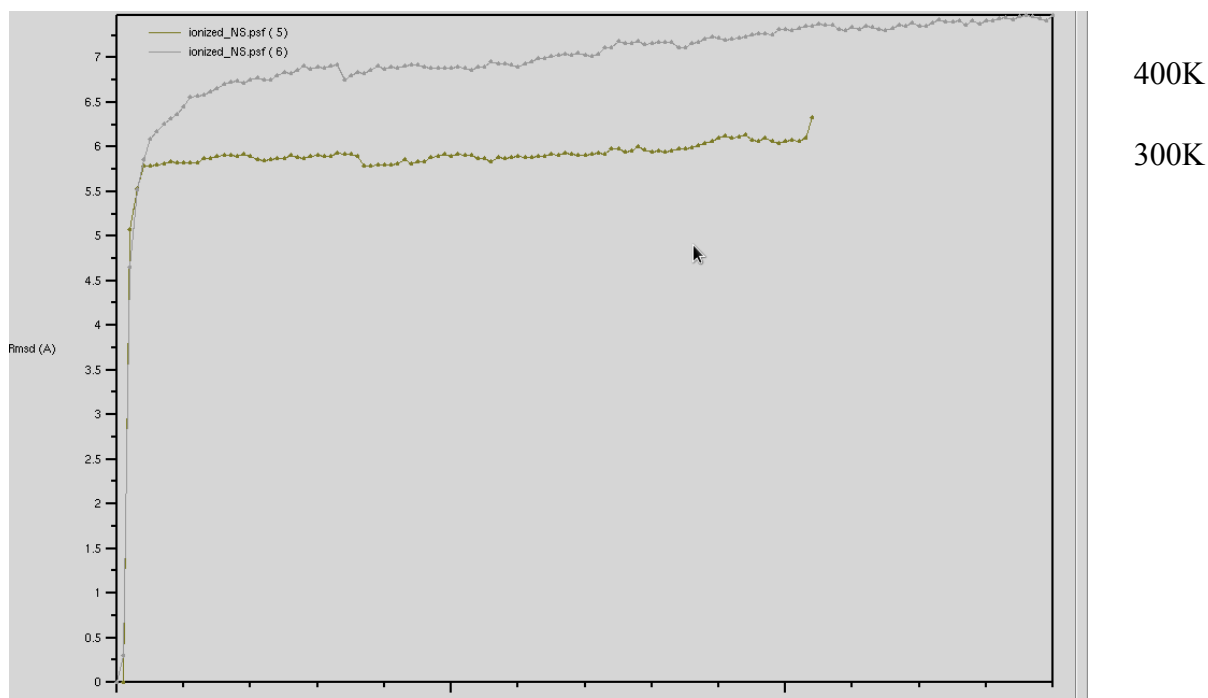


Figure 34: Snapshot of overlay containing final frame of simulations performed at 300K and 400K visualized using VMD<sup>47</sup>

There is a slight conformational change, particularly in the C-terminal domain regions, between the two structures. Based on this and the experiments performed previously, it appears that an additional channel activator (or perhaps much higher temperature) is required in order to observe a significant conformational change. Upon further review of the experiments results, based on the RMSD values, the 400K simulations does not appear fully equilibrated. The compilation of simulations performed at 300K shows an initial rapid increase in angstrom deviation followed by a flat, stable angstrom change; this implies that the system is properly equilibrated. On the contrary, the compilation of simulations performed at 400K never reaches a

flat, stable angstrom change; implying that even after 10ns of simulations the system is not properly equilibrated.



**Figure 35: RMSD of compilation of simulations performed at 300K and 400K created and visualized using VMD<sup>47</sup>**

### 1.6.3.2 Simulations of Complete Structure containing $PIP_2$

Simulations were performed in the same manner consistent with the simulations performed in the control experiments. Several simulations were initiated however an atoms moving too quickly error caused the simulations to terminate. In order to alleviate the atom velocity errors several adjustments were made to the configuration file including: melting the lipid tails, temperature gradient, and fixed protein during minimization and relaxed atoms during production runs. The only significant difference between the control experiments and the experiments performed in this section are the presence of 9  $PIP_2$  molecules in the lipid membrane. It is hypothesized

that the root cause of the simulation errors is based on the large negative charge of the PIP<sub>2</sub> molecules.

Melting of lipid tails were accomplished by fixing all of the atoms except the lipid tails; including water, ions, protein and lipid head groups. The beta column, located in the pdb file, values were adjusted from 0 to 1 in order to fix the atoms. The PDB file was then updated to include .fix at the end of the file name in order to differentiate between the fixed atom version and the original file. Additionally, temperature gradient was achieved by adding the following lines into the configuration file.

**Table 4: Temperature gradient in Configuration File**

reassignTemp	25
reassignIncr	5
reassignHold	300
reassignFreq	1000

The successful equilibration simulation with all the atoms fixed, minus the lipid tails, and the temperature gradient provided a successful restart point. In the next equilibration restart run, all of the lipid component were not fixed; followed by the relaxing the water and ions. In the final simulations, the protein remained fixed.



**Figure 36: Snapshot of TRPV1 and PIP<sub>2</sub> in 10ns simulation visualized using VMD.<sup>47</sup>**

### *1.6.3.3 Results from PIP<sub>2</sub> experiments*

Successful completion MD simulations on complete TRPV1 structure in its membrane bound environment. Simulations were performed in the presence of PIP<sub>2</sub> and without PIP<sub>2</sub> as a control. An observed conformation change occurred 300K and 400K simulations particularly in the unstructured C-terminal domain. Longer and additional experiments are needed in order assess how PIP<sub>2</sub> affects the conformation of TRPV1.

## ***1.7 Additional and Future Experiments***

In order to obtain additional and pertinent information pertaining to the conformational change that occurs in the C-terminal domain upon channel activation longer MD simulation needs to be performed on TRPV1 in order to ensure proper equilibration. In addition, an increase temperature to 500K and 600K to see if greater conformational change occurs in pore region with and without PIP<sub>2</sub> present in the lipid membrane. Lastly, using the information obtained in the temperature study of the control molecule, perform temperature studies on TRPV1 with PIP<sub>2</sub> in the membrane.

## ***1.8 Concluding Remarks***

TRPV1, a non-selective ion channel protein, is an important drug target for novel analgesics, asthma and diabetes. Currently, there is a lack of structural information in regards to not only TRPV1 but other TRP channel proteins; the limited structural information greatly inhibits our ability to design novel medications for a variety of diseases. Based on the MD simulations performed on the CTD the following conclusions were established:

1. Experimental results suggest that temperature and PIP<sub>2</sub> are required for a conformational change to occur.
2. Additionally, the CTD experiments confirmed that CTD is largely unstructured and undergoes a significant potentially significant conformational change. Specifically, the temperature sensor (residues 727 -752) and the

regulatory PIP<sub>2</sub>-binding segment (residues 778 – 819,) are largely unstructured.

3. Additional CTD experiments showed as compared with previous data, the temperature-sensing region contains unstructured portions as well as  $\beta$ -turns.
4. Based on MD simulations, a slight conformational change observed between 300K and 400K simulations.
5. CTD binding study experiments suggested PIP<sub>2</sub> binds to alpha helix section of CTD; even though there is a limited presence of hydrophobic amino acids present in “binding pocket”. Data therefore, suggests electrostatic interactions are responsible for PIP<sub>2</sub> binding to TRPV1 CTD.
6. MD simulations were performed on the complete TRPV1 structure in its membrane bound environment. Based on simulations, the CTD undergoes a conformational change between 300K and 400K.

## **CHAPTER II**

*Structural Analysis of Proline Mimics using Computational  
Techniques*



## Abstract

Proline is unlike any other natural amino acid; it is the only amino acid that contains a pyrrolidine ring structure and is a secondary amine.<sup>56</sup> Pseudoproline was derived in order to address the solubility and aggregation difficulties that can arise when performing Fmoc solid phase synthesis of peptides.<sup>60</sup> The presence of pseudoproline in a peptide overcomes aggregation by disrupting helices and  $\beta$ -sheets; leading causes in peptide aggregation.<sup>60</sup> Derived from serine, cysteine or threonine via cyclo-condensation reaction with aldehydes or ketones, pseudoproline is commercially available, however, it undergo peptide synthesis through SPPS. A new proline mimic be utilized by SPPS; additionally, it is hypothesized to also decrease aggregation and increase solubility. The proposed mechanism for the proline mimic increased stability is due to a hypothesized formation of stable  $\beta$  hairpin turn during peptide synthesis. Density functional theory (DFT) calculations were performed in order to determine the equilibrium constant (K) and total energy of peptides containing proline, pseudoproline or the proline mimic. Molecular dynamic simulations were used in order to generate theoretical Ramachandran plots, which provided essential insight into the secondary structure of all three peptides.

## ***2.1 Introduction***

Solid phase peptide synthesis, SPPS, was developed in order to efficiently add peptides to a growing polypeptide chain via a solid support.<sup>56</sup> Solid phase peptide synthesis is accomplished by attaching the first amino acid to a solid polymer via a covalent bond, followed by subsequent addition of additional amino acids, ending with the removal of the peptide from the solid support.<sup>56</sup> BOC and Fmoc protecting groups were added to the procedure in order to increase purity; with SPPS purity decreased with the amount of coupling steps.

Proline is a non-essential amino acid that contains a unique cyclic side chain that accounts for its conformational rigidity.<sup>59</sup> The presence of the cyclic side chain creates a limited backbone dihedral angle range =  $-65^\circ$  and because its bulky size inhibits  $\alpha$ -helix formation in a polypeptide. One last consequence of proline's bulky side chain is cannot act as a hydrogen bond donor; when bound as an amide in a polypeptide there is no available hydrogen available to engage in hydrogen bonding. Proline's inherent rigidity breaks up both  $\alpha$ -helices and  $\beta$ -sheets; both known causes of aggregation and low solubility in peptide synthesis.<sup>59</sup>

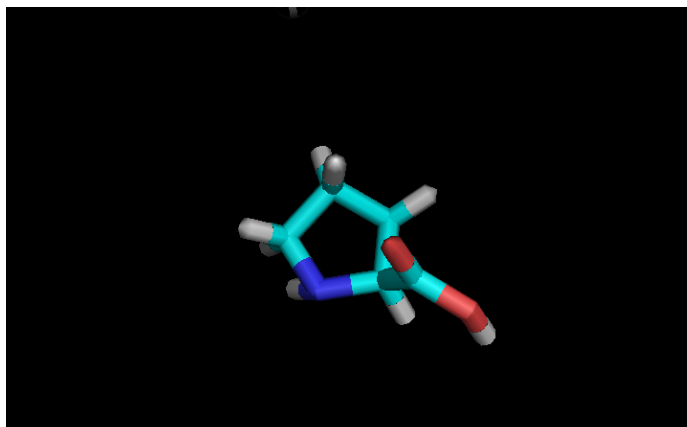


Figure 37: Proline Structure created and visualized in Avogadro.<sup>67</sup>

### 2.1.1 Proline Conformations

Amino acids form almost exclusively *trans* isomers in peptide bonds; the exception is proline, which can also exist in the *cis* form in polypeptides.<sup>58</sup> In addition to forming *cis* and *trans* isomers, proline can also adapt an *exo* or *endo* ring pucker conformation.<sup>58,86</sup> It is well documented and understood that isomer preference in peptide bonds for the *trans* isomer is due to steric hindrance.<sup>57</sup> The Raines lab has put forth an additional theory; his team explains that steric hindrance is not the sole explanation for the *trans* conformation preference.<sup>57</sup> Raines and his team state the  $n \rightarrow \pi^*$  interaction between the oxygen of the peptide bond and the adjacent carbonyl carbon in the polypeptide chain also plays a vital role in this preference.<sup>57</sup> The *trans* conformation stability leads to an increased  $\beta$ -turn stability resulting in a hypothesized increase in total energy and overall peptide stability.

Figure 38 below illustrates a proline structure that adapted a *trans* configuration.

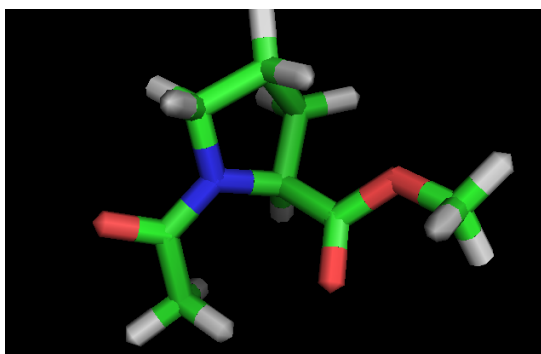


Figure 38: Proline amino acid in *trans* configuration created and visualized using Avogadro<sup>67</sup>

### 2.1.2 Pseudoproline and $\beta$ -Turns

Pseudoproline, synthesized from serine, threonine or cysteine, is an amino acid derivative designed to enhance solubility and decrease aggregation during solid phase peptide synthesis (SPPS).<sup>60</sup> The structure of pseudoproline differs from proline in the position 4; pseudoproline contains an oxygen while proline contains a carbon.

Pseudoproline, like proline, has the ability to form a kink the peptide backbone.<sup>60</sup> The formation of the kink is responsible for decreasing aggregation in peptide synthesis.<sup>60</sup>

Pseudoproline is commercially available however it cannot be utilized on a solid support as in Fmoc SPPS.

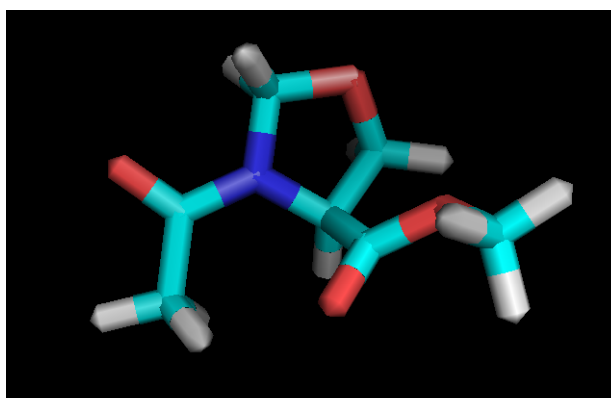
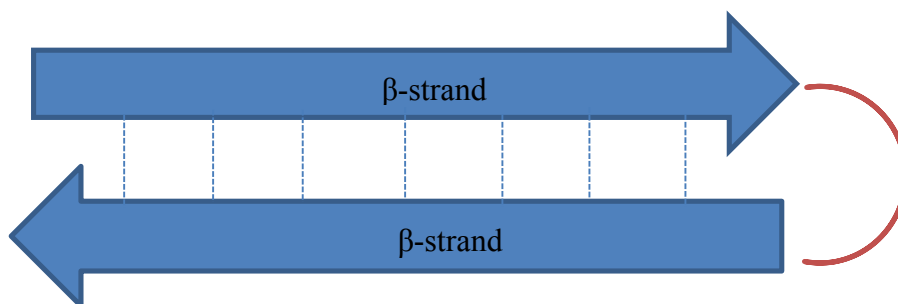


Figure 39: Pseudoproline *trans* isomer created and visualized in Avogadro<sup>67</sup>

Reverse turns are vaguely defined as a secondary structure motif that occurs when a polypeptide chain changes directions.<sup>61</sup>  $\beta$ -Turns, also known as  $\beta$ -hairpin turns, are reverse turns in which a hydrogen bond occurs between the  $i$  and  $i + 3$  residues therefore at least four residues need to be present for a  $\beta$ -turn to be present.<sup>61</sup> A  $\beta$ -hairpin occurs when a  $\beta$ -turn lies between two  $\beta$ -strands.<sup>61</sup> Figure 40, shows an example of both a  $\beta$ -turn highlighted by arrows and an N-terminal  $\beta$ -hairpin highlighted in red. The formation of a  $\beta$ -turn is hypothesized to stabilize the synthesized peptide.



**Figure 40:** An illustration of an anti-parallel  $\beta$ -turn highlighted by arrows and a hairpin turn highlighted in red. Hydrogen bonding is represented by the dotted lines.

### 2.1.3 Proline Mimic

Dr. Raj's team synthesized a new proline mimic; hypothesized to decrease aggregation, increase solubility and can be used in Fmoc SPPS. The team's rationale was stabilization provided by the *trans* isomer of the proline mimic would result in large total energy and ultimately lead to the formation of stable  $\beta$ -hairpin turn in a peptide. The structure is similar to proline in that it contains nitrogen in the cyclic ring structure but it also contains an oxygen in carbon 4 position, as is found in pseudoproline. The newly synthesized proline mimic also contains a carbonyl group

adjacent to the oxygen located in the cyclic ring; which can adopt either *cis* or *trans* conformation to the carbonyl group adjacent to the  $\alpha$ -amino group.

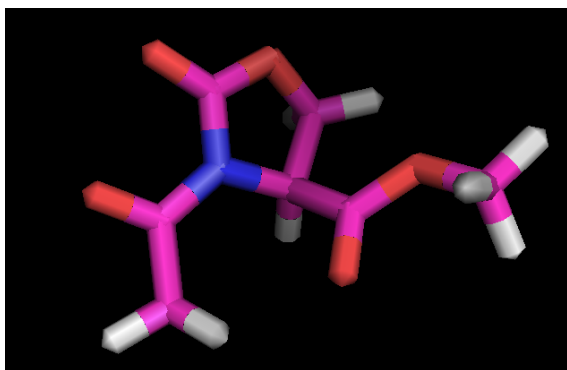


Figure 41A: Proline Mimic *cis* isomer created in Avogadro.<sup>67</sup>

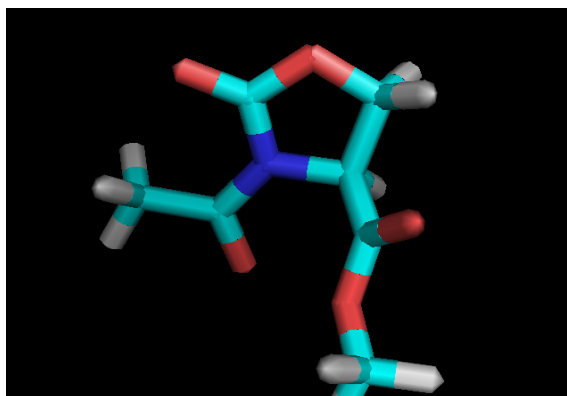


Figure 41B: Proline Mimics *trans* isomer created in Avogadro.<sup>67</sup>

## 2.2 Rationale for Studying Peptides

The use of peptide synthesis, particularly Fmoc SPPS, gained traction due to an increase in synthetic peptides role in drug development and delivery. Currently, therapeutic peptides are currently studied in order to investigate potential treatments for cancer, diabetes, obesity, allergies, and cardiovascular disease.<sup>63</sup> Addition of proline, pseudoproline, or the newly synthesized proline mimic likely increases solubility and decreases aggregation. The potential stabilization of the *trans*

configuration of the proline mimics structure, leading to the stable secondary  $\beta$ -hairpin, and therefore a stable peptide is the rational for studying these peptides.

## 2.3 Methodology

### 2.3.1 Amino Acid, Peptide Generation and GAMESS Analysis

Proline, pseudoproline and proline mimic were models were created. In the Figures below, the different potential conformations are highlighted with a dotted line. For simplicity reasons, a methyl group was added to the C and N terminus of each structure.

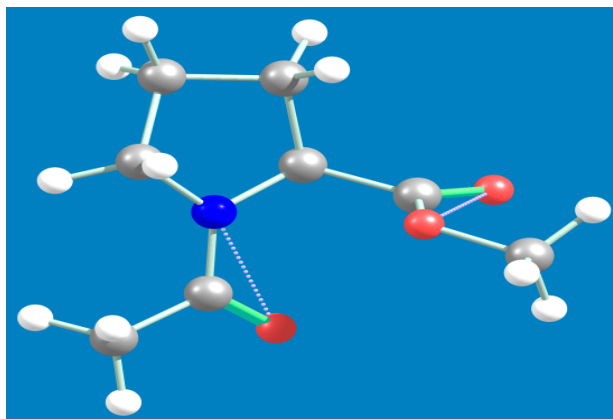


Figure 42: Structure of proline highlighting potential conformations

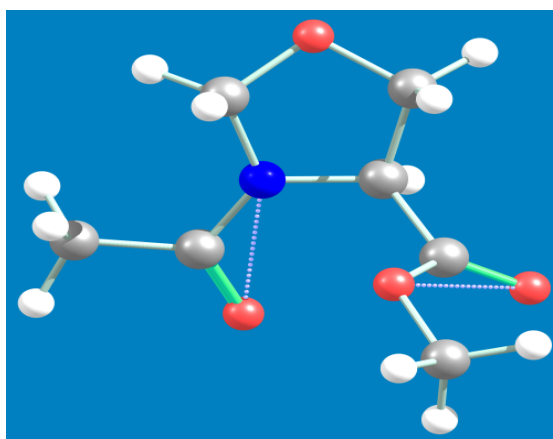


Figure 43: Structure of pseudoproline

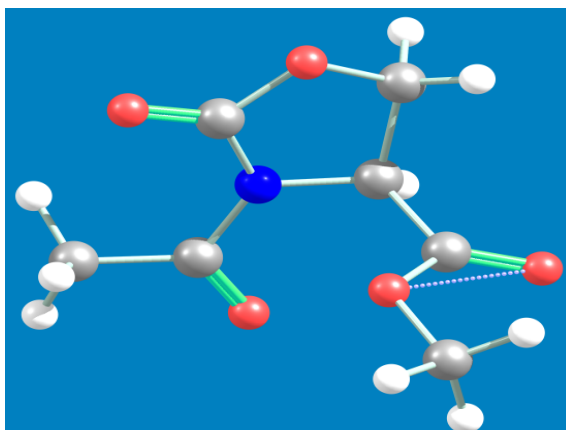


Figure 44: Structure of proline mimic

General Atomic and Molecular Electronic Structure System, GAMESS, was utilized to perform density functional theory, DFT, calculations on six peptides focusing on proline, pseudoproline, and proline mimic molecules. Molecules were analyzed using restricted open-shell Hartee-Fock (ROHF) theory. The B3LYP functional was utilized for all the molecules with the 6-N311++ G(2d, p) basis set. The complete GAMESS input is in Table 5.

Table 5: GAMESS Input

BASIS	GBASIS=311	NGAUSS=6	NDFUNC=1	NPFUNC=1
CONTROL	SCFTYP=ROHF	RUNTYP=OPTIMIZE	DFTTYP=B3LYP	MAXIT=150
SYSTEM	MWORDS=3			
STATPT	OPTTOL=0.0001		NSTEP=150	



GAMESS results can be seen in Tables 6-8. Columns 1 and 2 outline which ring (*endo* or *exo*) and which conformation (*cis* or *trans*) was analyzed. GAMESS provides an energy output in Ha; energy can be converted from Ha to eV; 1 Ha = 27.2116 eV. GAMESS output in Ha is in column 3 and the conversion to eV's is in Column 4. The change in energy between ring and conformation is Column 5. Equilibration constant K was calculated:  $K=e^{-\Delta E/kT}$ .

**Table 6: GAMESS Result Table Proline**

Ring	Chain	Etot (ha)	Etot (eV)	$\Delta E_{tot}$	K(trans/cis)	K(endo/exo)	Etot (kcal/mol)	$\Delta E(en-ex)$	$\Delta E(trans-cis)$
endo	cis	-592.9541	-16135.229	0.03356	3.6629	2.4333	-372087.1328	-0.2430	-0.7739
endo	trans	-592.9553	-16135.263			1.5033	-372087.9067		
exo	cis	-592.9532	-16135.206	0.04601	5.9288		-372086.6026	-0.5301	-1.0611
exo	trans	-592.9549	-16135.252				-372087.6637		

**Table 7: GAMESS Result Table Pseudoproline**

Ring	Chain	Etot (ha)	Etot (eV)	$\Delta E_{tot}$	K(trans/cis)	K(endo/exo)	$\Delta E_{tot}$ (kcal/mol)	$\Delta E(en-ex)$	$\Delta E(trans-cis)$
endo	cis	-628.8533179	-17112.1049	0.0025	0.9068	3.8019	-394614.4139	-0.3182	0.0583
endo	trans	-628.853225	-17112.1024			1.7054	-394614.3556		
exo	cis	-628.8520491	-17112.0704	-0.0182	2.0217		-394613.6177	-0.7962	-0.4197
exo	trans	-628.8527179	-17112.0886				-394614.0373		

**Table 8: GAMESS Result Table Proline Mimic**

<b>Chain</b>	<b>Etot (Ha)</b>	<b>Etot (eV)</b>	<b><math>\Delta</math>Etot</b>	<b>K(trans/cis)</b>	<b>Etot (kcal/mol)</b>	<b><math>\Delta</math>E(trans-cis)</b>
cis	-702.892	-19126.8076	-0.381	2528315.293	-441074.548	-8.78924
trans	-702.906	-19127.1887			-441083.337	

In order to complete MD simulations, several peptides were created each containing either proline, pseudoproline or proline mimic residue. Each peptide was created using Avogadro.<sup>67</sup> For simplicity purposes, glycine (GLY) was chosen to be added to each side of either proline, pseudoproline or proline mimic. Six peptides in total were created: GPG, GpseudoprolineG, GprolinemimicG, GGPGG, GGSSGG, GGMimicGG. In the case of GGSSGG, serine was chosen because pseudoproline is derived from serine and there are established CHARMM parameter and topology files for serine. Figures 45-50 below highlight the structures created in Avogadro that will be used in the simulations.<sup>67</sup>

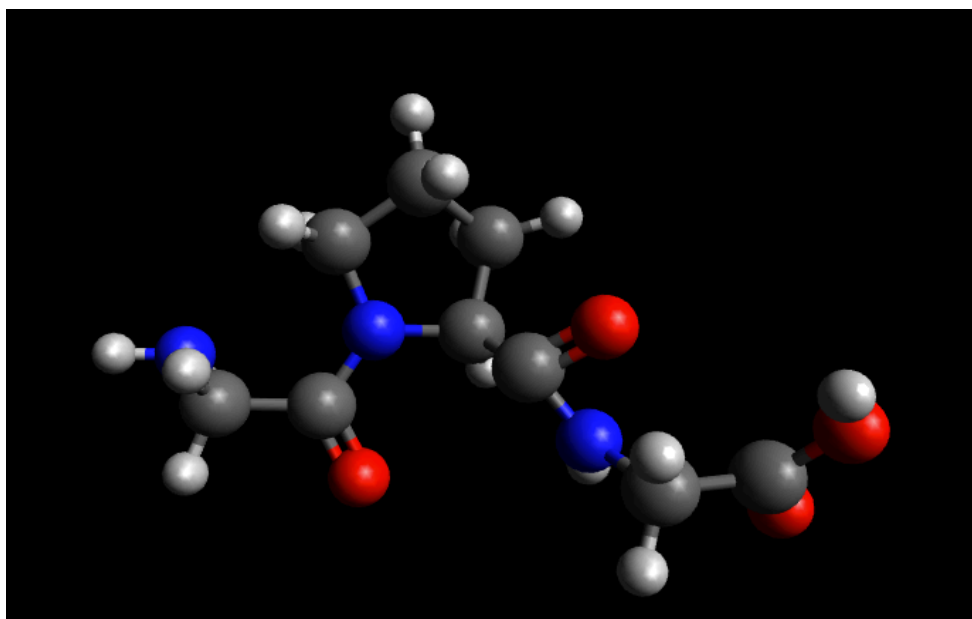


Figure 45: Avogadro created peptide, GPG.<sup>67</sup>

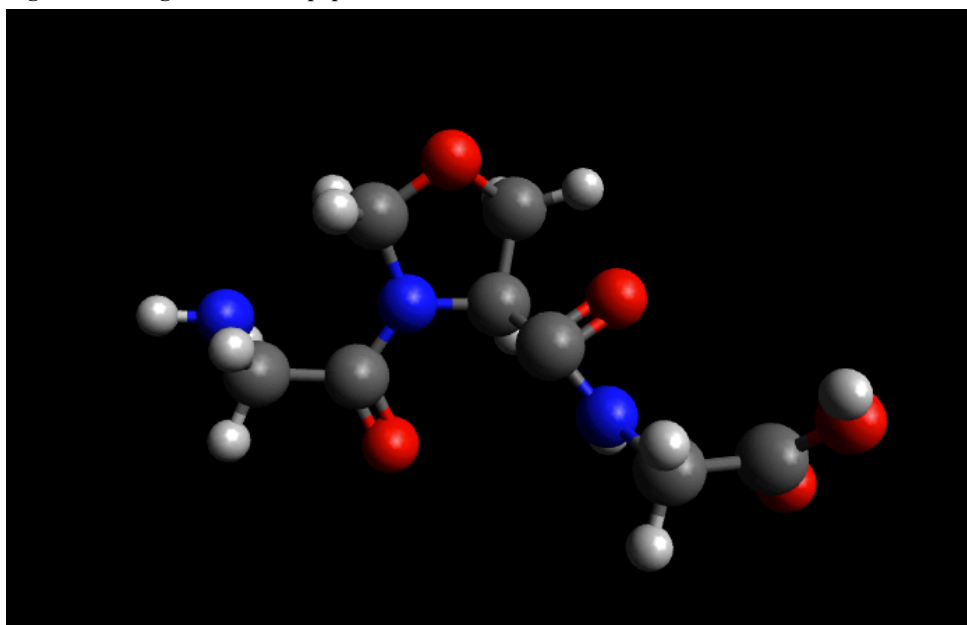


Figure 46: Avogadro created peptide, GPseudoprolineG<sup>67</sup>

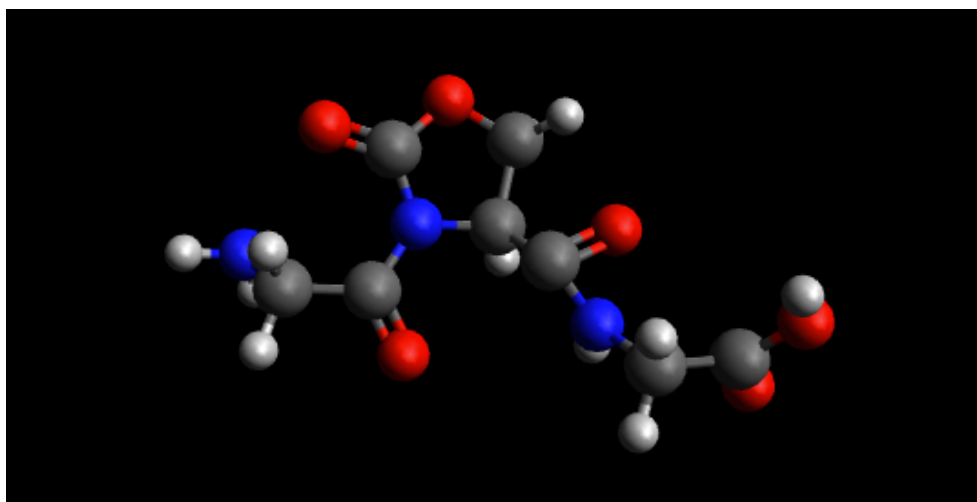


Figure 47: Avogadro created peptide, GProlineMimicG<sup>67</sup>

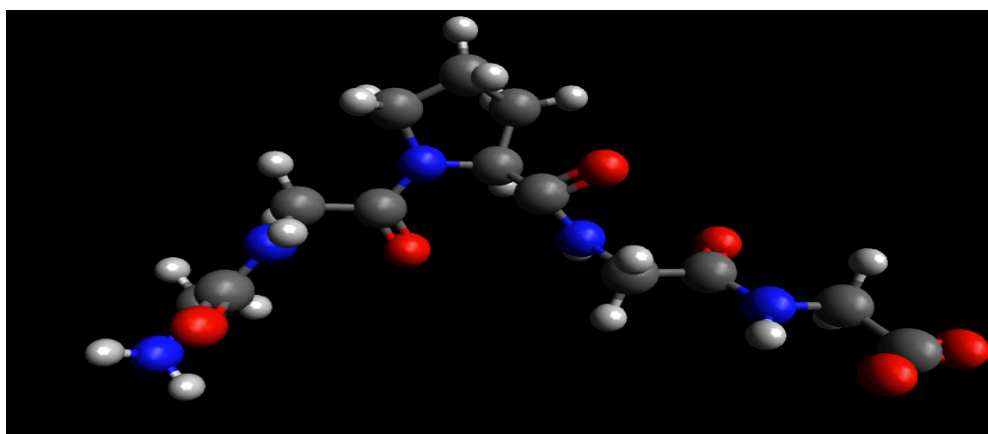


Figure 48: Avogadro created peptide, GGPGG<sup>67</sup>

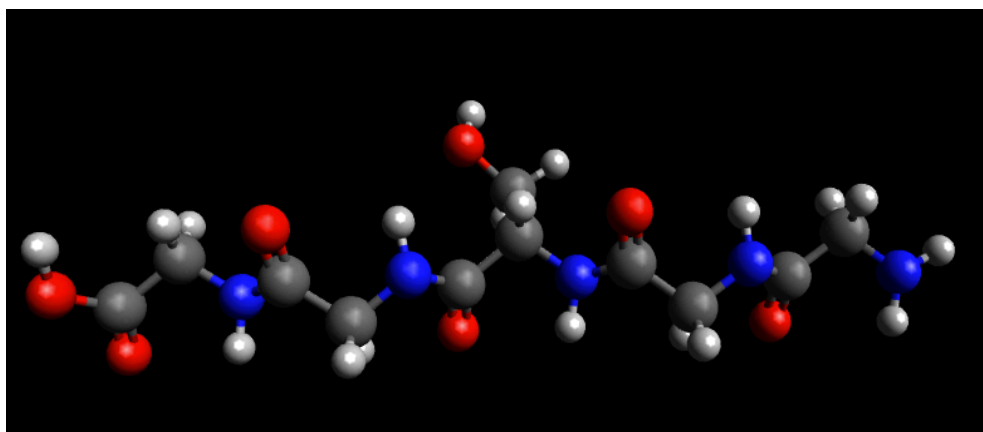


Figure 49: Avogadro created peptide, GGS GG<sup>67</sup>

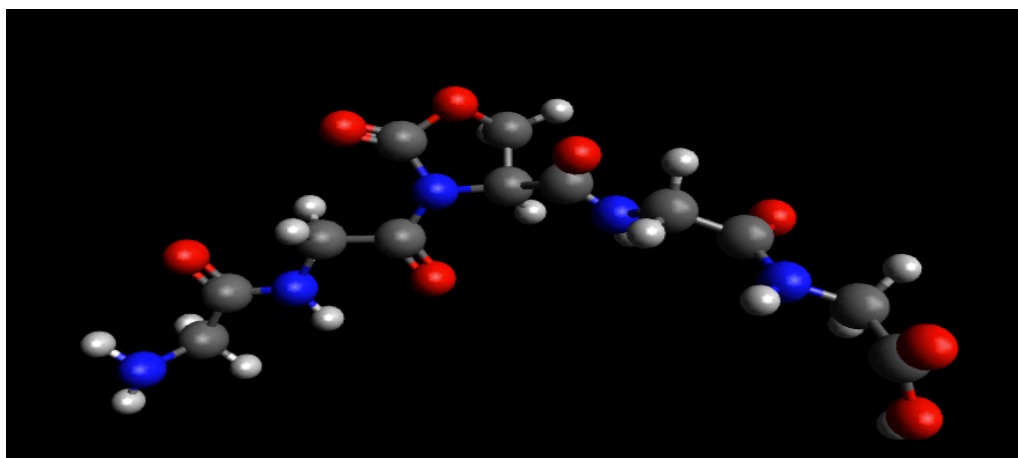


Figure 50: Avogadro created peptide, GGProlinMimicGG<sup>67</sup>

### 2.3.2 Structure Analysis

MD simulations were performed in order to assess secondary structure motifs; specifically in Avogadro generated peptides GGP GG, GGS GG and GGMimicGG. Each peptide was solvated and ionized using 0.15M NaCl and simulated under NPT conditions for at least 10ns. In order to perform MD simulation on the proline mimic structure, transferability was used in order to create a new topology and corresponding parameter file. Upon simulation completion a Ramachandran plot was generated in order to determine which secondary structure motifs were present in each peptide; specifically interested in an  $\alpha$ -helix,  $\beta$ -turn or  $\beta$ -sheets are present in each molecule.

#### 2.3.2.1 Ramachandran Plot

Protein secondary structure can be predicted based on backbone torsion angles  $\phi$ , angle around the  $\alpha$ -carbon, and  $\psi$ , angle around the N- $\alpha$ -carbon. Figure 51 below illustrates angles  $\phi$  and  $\psi$  present in a peptide backbone.

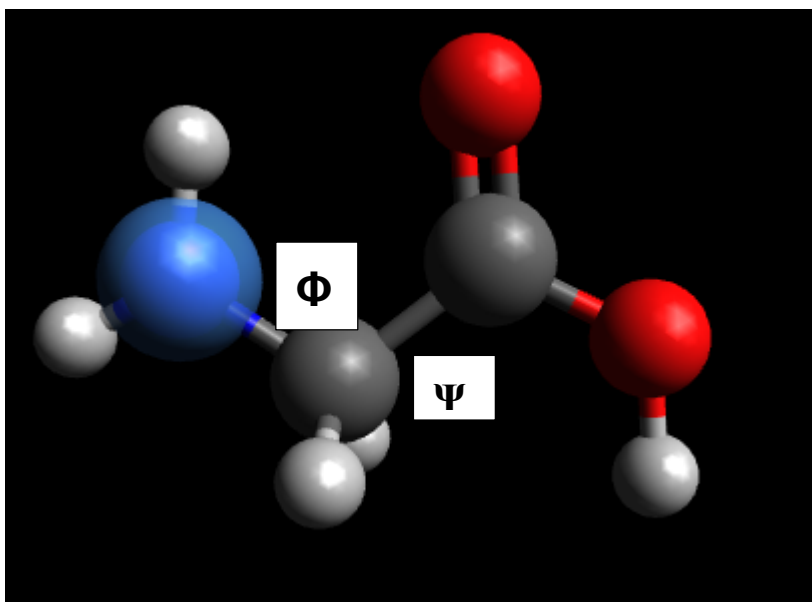


Figure 51: Angles  $\phi$  and  $\psi$  present in a peptide backbone created and visualized in Avogadro<sup>67</sup>

Ramachandran plot<sup>66</sup> is a scatter plot of the bond angles between each pair of residues. An example Ramachandran plot is shown in Figure 52.

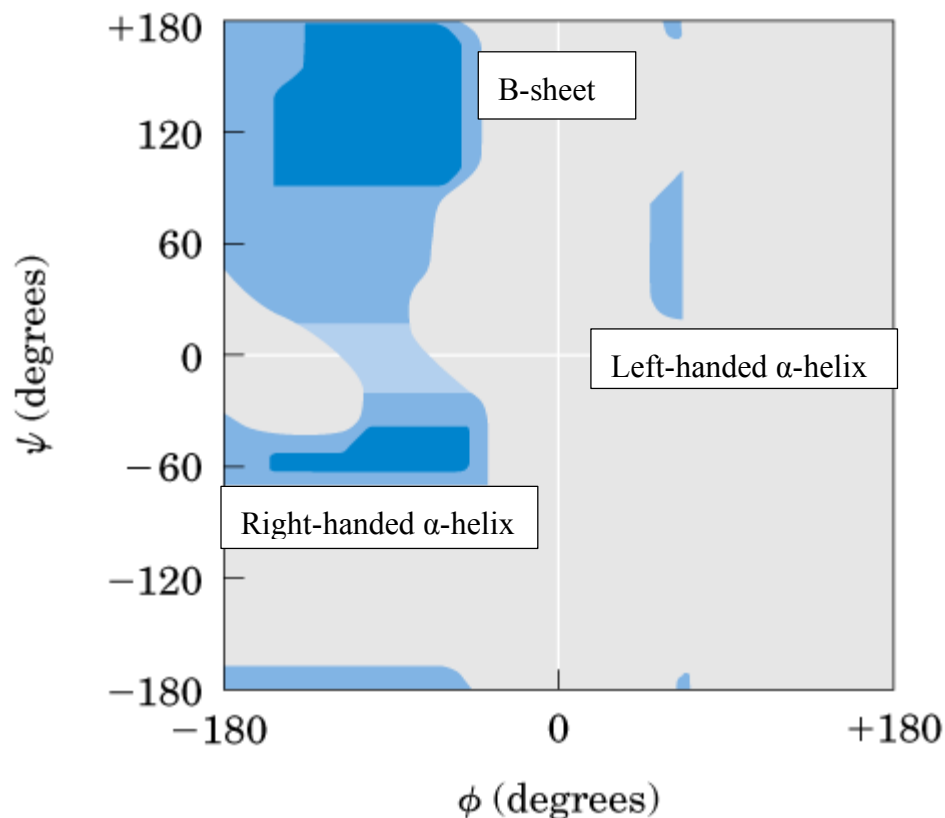


Figure 52: Ramachandran Plot Example for Alanine <sup>85</sup>

As illustrated in the Ramachandran plot above, residues containing a left handed  $\alpha$ -helix rotated around  $\Psi=+60^\circ$ ,  $\Phi=+45^\circ$  while a right-handed  $\alpha$ -helix rotate around  $\Psi=-45^\circ$ ,  $\Phi=+45^\circ$

Once the simulations were completed, VMD was utilized in order to visualize the theoretical Ramachandran plots.<sup>47</sup> Each plot is focused around proline, pseudoproline or proline mimic. The plots can be seen Figures 53-55. In addition, a contour plot was created in order to highlight the densely populated area of the proline mimic Ramachandran plot.

### 2.3.2.2 Peptide Ramachandran Plots

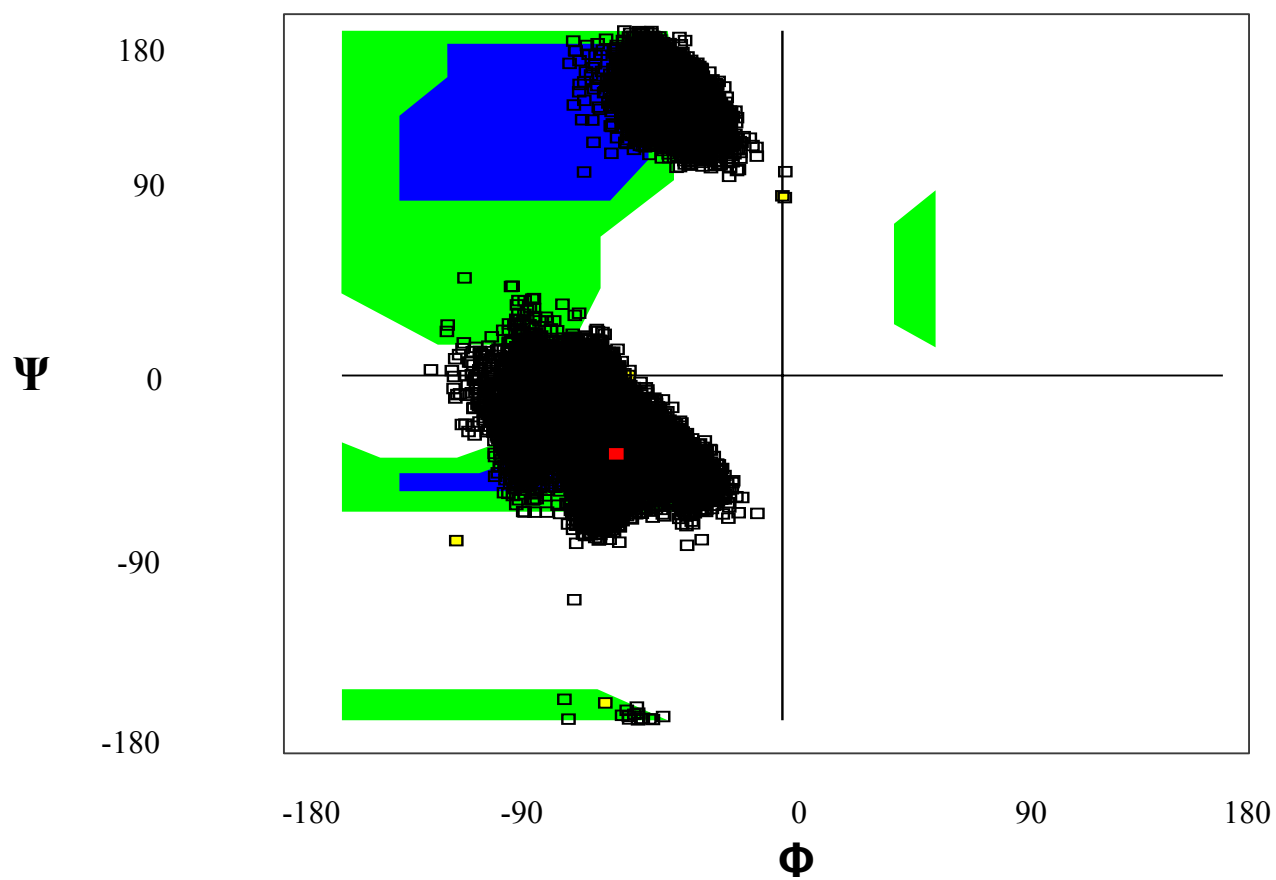


Figure 53: Ramachandran plot focused on Proline in GGPGG peptide



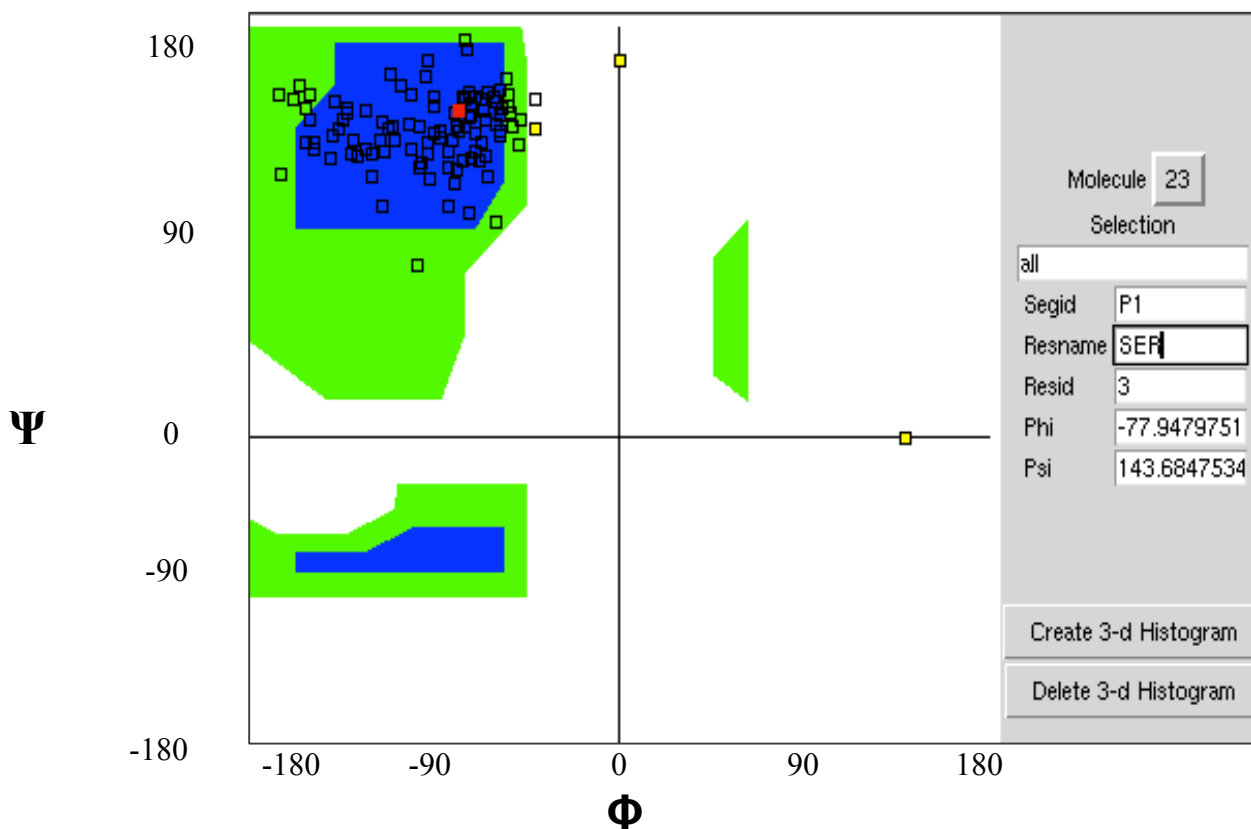


Figure 54: Ramachandran plot focused on Proline in GGSGG peptide

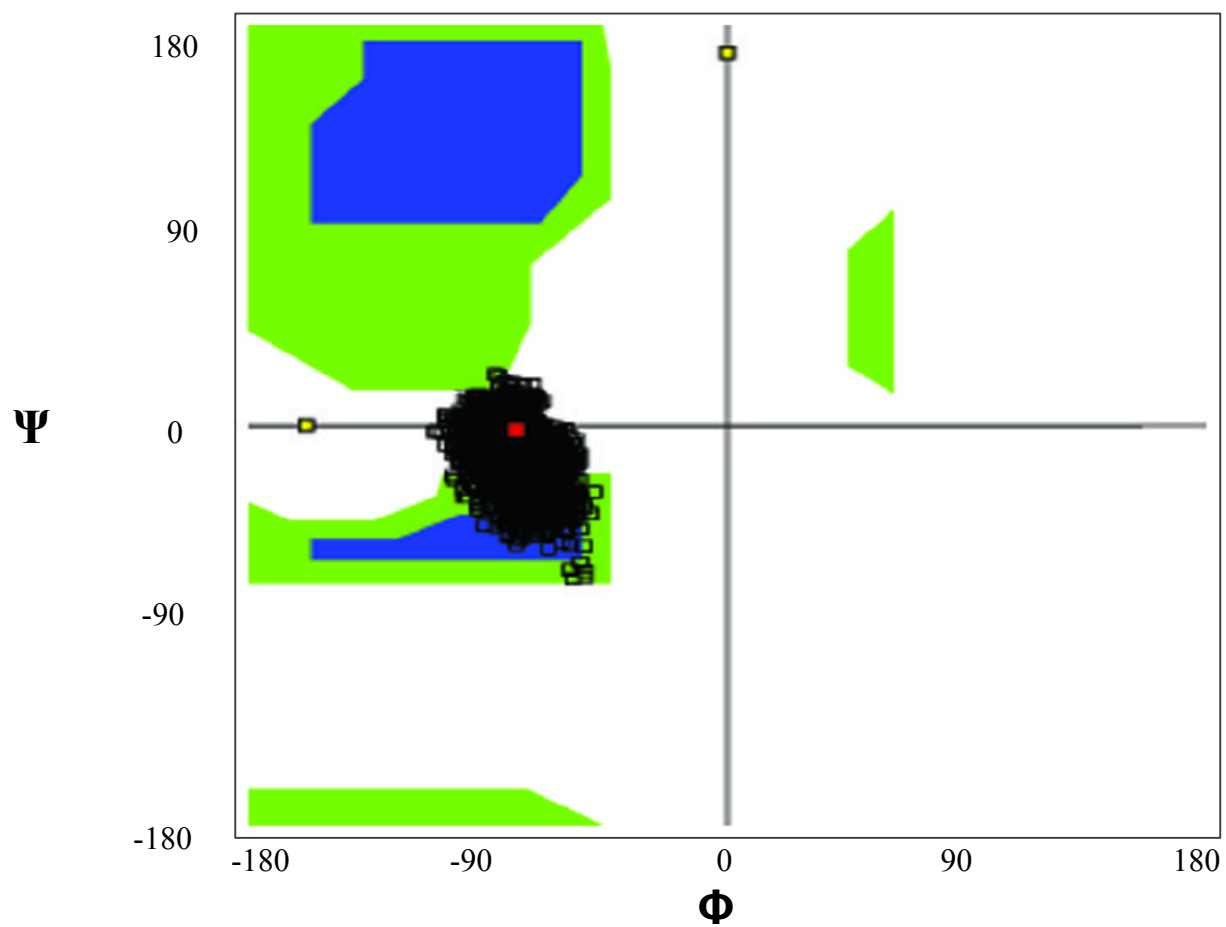
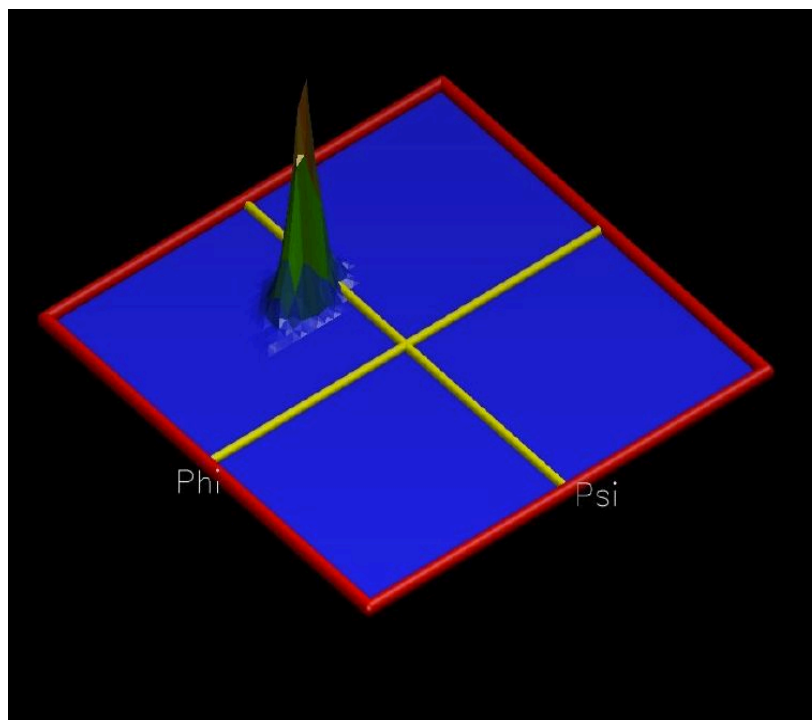


Figure 55: Ramachandran plot focused on Proline in GGMimicGG peptide



**Figure 56: Contour plot based on proline mimic Ramachandran Plot**

### *2.3.2.3 Results Ramachandran Plot*

The Ramachandran plots created for both proline and serine, are consistent with expected and previously reported results. At first glance, the GGMimicGG secondary structure motif appeared to be an  $\alpha$ -helix however upon further review it appeared to be a  $\beta$ -hairpin turn. Figure 57, highlights the  $\beta$ -hairpin turn motif in a Ramachandran plot.

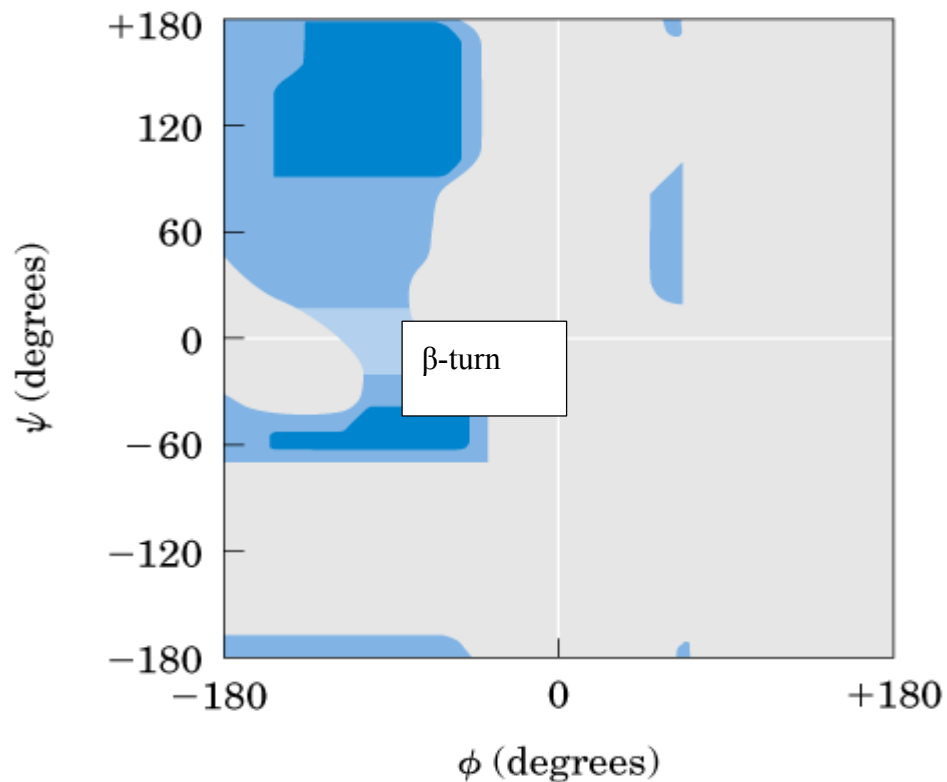


Figure 57: Ramachandran plot focusing on  $\beta$ -hairpin turn<sup>85</sup>

MD simulations resulted in the proline mimic containing peptide contains  $\phi$  and  $\Psi$  angles are  $-79.22$  and  $-2.02$  respectively. Values that are consistent with expected  $\phi$  and  $\Psi$  angles for a peptide containing a  $\beta$ -turn.



Figure 58: Figure illustrating  $\phi$  and  $\Psi$  angles of proline mimic structure

Structural analysis performed via classical MD simulations provided pivotal insight into the secondary structure of the newly created proline mimic residue present in a peptide. The theoretical Ramachandran plots confirm the hypothesis that the newly synthesized proline mimic structure in a peptide forms a stabilizing  $\beta$ -hairpin turn.

## ***2.4 Concluding Remarks***

Proline mimic structure was synthesized in order to decrease aggregation, increase solubility and increase peptide synthesis efficiency. Energy calculations performed by GAMESS<sup>9,10</sup> provided a total energy and dissociation constant (K) 10 fold higher than proline or pseudoproline; data that eludes to the increased stability of the proline mimic structure. Completed classical MD simulations provided valuable insight into the secondary structure of a peptide containing proline mimic and its vast stability improvement as compared with proline or pseudoproline. MD simulations resulted in the proline mimic containing peptide contains  $\phi$  and  $\Psi$  angles are -79.22 and -2.02 respectively; consistent with the theoretical values of approximately -90 and 0, respectively. Peptide synthesis that includes the proline mimic structure should dramatically increase efficiency and peptide stabilization.

## References:

1. Jara-Oseguera, A., Nieto-Posadas A., et al. Molecular Mechanisms of TRPV1 Channel Activation. *The Open Pain Journal*. **2010**, *3*, 68-81.
2. Clapham, D. E. TRP Channels as Cellular Sensors. *Nature*. **2003**, *426* (6966), 517-524.
3. Frenandez-Ballester, G.; Ferrer-Montiel, A. Molecular Modeling of the Full-length Human TRPV1 Channel in Closed and Desensitized States. *J. Membrane Biology*. **2008**, *223*, 161-172.
4. Raymond, K.A.; Twomey, E.C.; Wei, Y. Characterization of Temperature-Sensing and PIP<sub>2</sub>-Regulation of TRPV1 Ion Channel at the C-terminal domain using NMR Spectroscopy and Molecular Dynamics Simulations. *J. of Integrated Omics*. **2014**, *4*(2), 79-86.
5. Liao, M; Cao, E; Juilus, D; Cheng, Y. Structure of th TRPV1 Ion Channel Determined by Electron Cryo-Microscopy. *Nature*. **2013**, *504* (7478), 107-112.
6. Zweifel, M.E.; Leahy ,D.J.; Hughson, F.M.; Barrick, D. Structure and Stability of the Ankyrin Domain of the *Drosophila* Notch Receptor. *Protein Sci*. **2003**, *12*(11), 2622-2632.
7. Lishko, P.V; Procko, E.; Jin, X; Phelps, C.B; Gaudel, R. The Ankyrin Repeats of TRPV1 Bind Multiple Ligands and Modulate Channel Sensitivity. *Neuron*. **2007**, *54*(6), 905-918.
8. Salazar, H; Jara-Oseguera, A.; Hernandez-Garcia, E.; Llorente, I.; Arias-Olguin, I.; Soriano-Garcia, M.; Islas, L.D.; Tosenbaum, T. Structural Determinants of Gating in the TRPV1 Channel. *Nat. Struct. Mol. Biol*. **2009**, *16*(7), 704-710.
9. Stein, A.T.; Ufret-Vincenty, C.A.; Hua, L.; Santa, L.F.; Gordon, S, E. Phosphoinositide 3-Kinase Binds to TRPV1 and Mediates NGF-stimulated TRPV1 Trafficking to the Plasma Membrane. *J. Gen. Physiol*. **2006**, *128*(5), 509-522.
10. Vlachova, V.; Teisinger, J.; Susankova, K.; Lyfenko, A.; Ettrich, R.; Vyklicky, L. Functional role of C-terminal Cytoplasmic Tail of Rat Vanilloid Receptor 1. *J. Neurosci*. **2003**, *23*, 1340 – 1350.
11. Liu,B.; Ma,W.; Ryu, S; Qin, F. Inhibitory Modulation of Distal C-terminal on Protein Kinase C-dependent Phospho-regulation of Rat TRPV1 Receptors. *J Physio*. **2004**, *560*, 627–638.
12. Prescott, E.D.; Julius, D. A Modular PIP<sub>2</sub> Binding Site as a Determinant of Capsaicin Receptor Sensitivity. *Science* **2003**, *300*, 1284 –1288.
13. Lee, J.H.; Lee, Y.; Ryu, H; Kang, D.W. ; Lee, J.; Lazar, J.; Pearce, L.V.; Pavlyukovets, VA.; Blumberg, P.M.; Choi, S. Structural Insights into Transient Receptor Potential Vanilloid Type 1 (TRPV1) from Homology Modeling, Flexible Docking, and Mutational Studies. *J Comput Aided Mol Des*. **2011**, *25*(4), 317-27.
14. Jara-Oseguera, A.; Simon, S. A.; Rosenbaum, T. TRPV1: on the Road to Pain Relief. *Current Molecular Pharmacology*. **2008**, *1*(3), 255–269.
15. O’Neill, J.; Brock, C.; Olesen, A. E.; Andresen, T.; Nilsson, M.; Dickenson, A. H. Unraveling the Mystery of Capsaicin: A Tool to Understand and Treat Pain. **2012**, *Pharmacological Reviews*, *64*(4), 939–971.

16. Voets, T.; Talavera, K.; Owsianik, G.; Nilius, B. Sensing with TRP Channels. Sensing with TRP channels. *Nat. Chem. Biol.* **2005**, *1*(2), 85-92.
17. Patapoutian, A.; Peier, A. M.; Story, G. M.; Viswanath, V. ThermoTRP Channels and Beyond: Mechanisms of Temperature Sensation. *Nat. Rev. Neurosci.* **2003**, *4*(7), 529-539.
18. Bandell, M.; Macpherson, L. J.; Patapoutian, A. From Chills to Chilis: Mechanisms for Thermosensation and Chemesthesis via ThermoTRPs. *Curr. Opin. Neurobiol.* **2007**, *17*(4), 490-497.
19. Cortright, D. N.; Szallasi, A. TRP Channels and Pain. *Current Pharmaceutical Design.* **2009**, *15*(15), 1736-1749.
20. Phillips, J. C.; Braun, R.; Wang, W.; Gumbart, J.; Tajkhorshid, E.; Villa, E.; Chipot, C.; Skeel, R. D.; Kalé, L.; Schulten, K. Scalable Molecular Dynamics with NAMD. *J. of Comput. Chem.* **2005**, *26*(16), 1781-1802.
21. Patapoutian, A.; Tate, S.; Woolf, C. Transient Receptor Potential Channels: Targeting Pain at the Source. *J. Nat. Rev. Drug Discov.* **2009**, *8*(1), 55-68.
22. Benedikt, J.; Teisinger, J.; Vyklicky, L.; Vlachova, V. Ethanol Inhibits Cold-Menthol Receptor TRPM8 by Modulating its Interaction with Membrane Phosphatidylinositol 4,5-bisphosphate. *J. Neurochem.* **2007**, *100*(1): 211-224.
23. Matta, J. A.; Cornett, P. M.; Miyares, R. L.; Abe, K.; Sahibzada, N.; Ahern, G. P. General Anesthetics Activate a Nociceptive Ion Channel to Enhance Pain and Inflammation. *Proceedings of the National Academy of Sciences.* **2008**, *105*(25), 8784-8790.
24. Trevisani, M.; Smart, D.; Gunthorpe, M. J.; Tognetto, M.; Barbieri, M.; Campi, B.; Amadesi, S.; Gray, J.; Jerman, J. C.; Brough, S. J.; Owen, D.; Smith, G. D.; Randall, A. D.; Harrison, S.; Bianchi, A.; Davis, J. B.; Geppetti, P. Ethanol Elicits and Potentiates Nociceptor Responses via the Vanilloid Receptor-1. *Nat. Neurosci.* **2002**, *5*(6), 546.
25. Cornett, P. M.; Matta, J. A.; Ahern, G. P. General Anesthetics Sensitize the Capsaicin Receptor Transient Receptor Potential V1. *Molecular Pharmacology.* **2008**, *74*, 1261-1268.
26. Ellingson, J.; Silbaugh, B.; Brassler, S. Reduced Oral Ethanol Avoidance in Mice Lacking Transient Receptor Potential Channel Vanilloid Receptor 1. *Behav. Genet.* **2009**, *39*(1), 62-72.
27. Blednov, Y. A.; Harris, R. A. Deletion of Vanilloid Receptor (TRPV1) in Mice Alters Behavioral Effects of Ethanol. *Neuropharmacology.* **2009**, *56*(4), 814-820.
28. Brauchi, S.; Orta, G.; Salazar, M.; Rosenmann, E.; Latorre, R. A Hot-Sensing Cold Receptor: C-terminal Domain Determines Thermosensation in Transient Receptor Potential Channels. *J. Neurosci.* **2006**, *26*(18): 4835-4840.
29. Brauchi, S.; Orta, G.; Mascayano, C.; Salazar, M.; Raddatz, N.; Urbina, H.; Rosenmann, E.; Gonzalez-Nilo, F.; Latorre, R. Dissection of the components for PIP<sub>2</sub> activation and Thermosensation in TRP channels. *Proc. Natl. Acad. Sci. U. S. A.* **2007**, *104*(24), 10246-10251.
30. Suh, B. C.; Hille, B. Regulation of Ion Channels by Phosphatidylinositol 4,5-bisphosphate. *Curr. Opin. Neurobiol.* **2005**, *15*(3), 370-378.

31. Liu, B. Y.; Qin, F. Functional control of cold- and menthol-sensitive TRPM8 ion channels by phosphatidylinositol 4,5-bisphosphate. *Journal of Neuroscience* **2005**, *25*, 1674.
32. Rohacs, T.; Lopes, C. M. B.; Michailidis, I.; Logothetis, D. E. PI(4,5)P<sub>2</sub> regulates the activation and desensitization of TRPM8 channels through the TRP domain. *Nature neuroscience* **2005**, *8*(5), 626-634.
33. Prescott, E. D.; Julius, D. A Modular PIP<sub>2</sub> Binding Site as a Determinant of Capsaicin Receptor Sensitivity. *Science* **2003**, *300*(5623), 1284-1288.
34. Liu, B. Y.; Zhang, C. G.; Qin, F. Functional Recovery from desensitization of Vanilloid Receptor TRPV1 Requires Resynthesis of Phosphatidylinositol 4,5-bisphosphate. *J. of Neurosci.* **2005**, *25*(19), 4835-4843.
35. Lukacs, V.; Thyagarajan, B.; Varnai, P.; Balla, A.; Balla, T.; Rohacs, T. Dual Regulation of TRPV1 by Phosphoinositides. *J. Neurosci.* **2007**, *27*(26), 7070-7080.
36. Long, S. B.; Campbell, E. B.; MacKinnon, R. Crystal Structure of a Mammalian Voltage-dependent Shaker Family K<sup>+</sup> channel. *Science*. **2005**, *309*(5736), 897-903.
37. Zagotta, W. N.; Olivier, N. B.; Black, K. D.; Young, E. C.; Olson, R.; Gouaux, E. Structural basis for modulation and agonist specificity of HCN pacemaker channels. *Nature*. **2003**, *425*(6954), 200-205.
38. Latorre, R.; Brauchi, S.; Orta, G.; Zaelzer, C.; Vargas, G. ThermoTRP channels as modular proteins with allosteric gating. *Cell Calcium*. **2007**, *42*(4-5), 427-438.
39. Zambrowicz, B. P.; Sands, A. T. Knockouts model the 100 best-selling drugs--will they model the next 100? *Nat Rev Drug Discov* **2003**, *2*(1), 38-51.
40. Hatcher, J. P.; Chessell, I. P. Transgenic Models of Pain: A Brief Review. *Curr Opin Investig Drugs* **2006**, *7*(7), 647-652.
41. Latorre, R.; Zaelzer, C.; Brauchi, S. Structure-functional Intimacies of Transient Receptor Potential Channels. *Q Rev Biophys.* **2009**, *42*, 201-246.
42. Szallasi, A.; Cortright, D. N.; Blum, C. A.; Eid, S. R. The Vanilloid Receptor TRPV1: 10 years from Channel Cloning to Antagonist Proof-of-Concept. *Nat Rev Drug Discov* **2007**, *6*(5), 357-372.
43. Delaglio, F.; Grzesiek, G.; Vuister, W.; Zhu, G.; Pfeifer, J.; Bax, A. NMRPipe: a multidimensional spectral processing system based on UNIX pipes. *J Biomol. NMR* **1995**, *6*(3), 277-293.
44. Johnson B.A.; Blevins, R.A. NMR View: A Computer Program for the Visualization and Analysis of NMR Data. *J. Biomol NMR*. **1994**, *4*(5), 603-614.
45. Busam, R.D.; Thorsell, A.G.; Flores, A.; Hammarstrom, M.; Persson, C.; Obrink, B.; Hallberg, B.M. Structural basis of tumor suppressor in lung cancer 1 (TSLC1) binding to differentially expressed in adenocarcinoma of the lung (DAL-1/4.1B). *J Biol Chem*. **2011**, *6*, 4511-4516.



46. Fiser, A.; Sali, A.; Charles W.; Carter, Jr.; Robert, M. S. Modeller: Generation and Refinement of Homology-based Protein Structure Models. *Methods Enzymol.* **2003**, *374*, 461-491.
47. Humphrey, W.; Dalke, A.; Schulten, K. VMD: Visual Molecular Dynamics. *J. Mol. Graph.* **1996**, *14*(1), 33-38.
48. Golebiewska, U.; Gambhir, A.; Hangyás-Mihályiné, G.; Zaitseva, I.; Rädler, J.; McLaughlin, S. Membrane-bound Basic Peptides Sequester Multivalent (PIP<sub>2</sub>), but Not Monovalent (PS), Acidic Lipids. *Biophys. J.* **2006**, *91*(2), 588-599.
49. McLaughlin, S.; Murray, D. Plasma membrane Phosphoinositide Organization by Protein Electrostatics. *Nature.* **2005**, *438*(7068), 605-611.
50. S. Jo; T. Kim; V.G. Iyer; Im, W. CHARMM-GUI: A Web-based Graphical User Interface for CHARMM. *J. Comput. Chem.* **2008**, *29*(11), 1859-1865.
51. Brooks B.R.; Brooks, C.L.; MacKerell, A.D.; Nilsson, L.; Petrella, R.J.; Roux, B.; Won, Y.; Archontis, G.; Bartels, C.; Boresch, S.; Caflisch, A.; Caves, L.; Cui, Q.; Dinner, A.R.; Feig, M.; Fischer, S.; Gao, J.; Hodoseck, M.; Im, W.; Kuczera, K.; Lazaridis, T.; Ma, J.; Ovchinnikov, V.; Paci, E.; Pastor, R.W.; Post, C.B.; Pu, J.Z.; Schaefer, M.; Tidor, B.; Venable, R. M.; Woodcock, H. L.; Wu, X.; Yang, W.; York, D.M.; Karplus, M. CHARMM: The Biomolecular Simulation Program. *J. Comput. Chem.* **2009**, *30*, 1545-1614.
52. Lee, J.; Cheng, X.; Swails, J.M.; Yeom, M.S.; Eastman, P.K.; Lemkul, J.A.; Wei S.; Buckner, J.; Jeong, J.C.; Qi, Y.; S. Jo; Pande, V.S.; Case, D.A.; Brooks, C.L.; MacKerell, A.D.; Klauda, J.B.; Im, W. CHARMM-GUI Input Generator for NAMD, GROMACS, AMBER, OpenMM, and CHARMM/OpenMM Simulations using the CHARMM36 Additive Force Field. *J. Chem. Theory Comput.* **2016**, *12*, 405-413.
53. Klauda, J.B.; Venable, R.M.; Freites, J.A.; O'Connor, J.W.; Tobias, D.J.; Mondragon-Ramirez, C.; Vorobyov, I.; MacKerell, Jr., A.D.; Pastor, R.W. Update of the CHARMM All-Atom Additive Force Field for Lipids: Validation on Six Lipid Types. *J. Phys Chem B.* **2010**, *114*(23), 7830-7843.
54. Best, R.B.; Zhu, X.; Shim, J.; Lopes, P.E.M.; Mittal, J.; Feig, M.; MacKerell Jr., A.D. Optimization of the Additive CHARMM All-Atom Protein Force Field Targeting Improved Sampling of the Backbone phi, psi and side-chain chi1 and chi2 Dihedral Angles. *J. Chem. Theory Comput.* **2012**, *8*, 3257-3273.
55. MacKerell, Jr., A. D.; Bashford, D.; Bellott, M.; Dunbrack Jr., R.L.; Evanseck, J.D.; Field, M.J.; Fischer, S.; Gao, J.; Guo, H.; Ha, S.; Joseph-McCarthy, D.; Kuchnir, L.; Kuczera, K.; Lau, F.T.K.; Mattos, C.; Michnick, S.; Ngo, T.; Nguyen, D.T.; Prodhom, B.; Reiher, III, W.E.; Roux, B.; Schlenkrich, M.; Smith, J.C.; Stote, R.; Straub, J.; Watanabe, M.; Wiorkiewicz-Kuczera, J.; Yin, D.; Karplus, M. All-atom Empirical Potential for Molecular Modeling and Dynamics Studies of Proteins. *J. Phys Chem B.* **1998**, *102*, 3586-3616.
56. Mothes, C.; Caumes, C; Guez, A.; Boulet, H.; Gendrineau, T.; Darses, S.; Delsue, N.; Moumne, R.; Oswald, B.; Lequin, O.; Karoyan, P. 3-Substituted Prolines: From Synthesis to Structural Applications, from Peptides to Foldamers. *Molecules*, **2013**, *18*, 2307-2327.
57. Hinderaker, M.P. and Raines, R.T. An electronic effect on protein structure. *Protein Science.* **2003**, *12*, 1188-1194.

58. Pandey, A.K.; Naduthambi, D.; Thomas, K.M.; Zondio, N.J. Proline Editing: A General and Practical Approach to the Synthesis of Functionally and Structurally Diverse Peptides. Analysis of Steric versus Stereoelectronic Effects of 4-Substituted Prolines on Conformation within Peptides. *J Am Chem Soc.*, **2014**, *135*(11), 4333-4363.
59. Williamson, M.P. The Structure and Function of Proline-Rich Regions in Proteins. *Biochem. J.* **1994**, *297*, 249-260.
60. Wöhr, T.; Wahl, F.; Nefzi, A.; Rohwedder, B.; Sato, T.; Sun, X.; Mutter, M. Pseudo-Prolines as a Solubilizing, Structure-Disrupting Protection Technique in Peptide Synthesis. 1996, *118*, 9218-9227.
61. Marcelino, A. M. C.; Gierasch, L. M. Roles of  $\beta$ -Turns in Protein Folding: From Peptide Models to Protein Engineering. *Biopolymers*. **2008**, *89*(5), 380–391.
62. Merrifield, R. B. Solid Phase Peptide Synthesis. I. The Synthesis of a Tetrapeptide. *J. Am. Chem. Soc.* **1963**, *85*(14), 2149-2154.
63. Chandrudu, S.; Simerska, P.; Toth, I. Chemical Methods for Peptide and Protein Production. *Molecules*. **2013**, *18*, 4373-4388.
64. Schmidt, M. W.; Baldrige, K. K.; Boatz, J. A.; Elbert S. T.; Gordon, M. S.; Jensen, J. H.; Koseki, S.; Matsunaga, N.; Nguyen, K. A.; Su, S. J.; Windus, T. L.; Dupuis, M.; Montgomery, J. A. General Atomic and Molecular Electronic-System, *J. Comput. Chem.* **1993**, *14*, 1347-1363.
65. Advances in electronic structure theory: GAMESS a decade later, M.S.Gordon, M.W.Schmidt Chapter 41, pp 1167-1189, in "Theory and Applications of Computational Chemistry, the first forty years" C.E.Dykstra, G.Frenking, K.S.Kim, G.E.Scuseria, editors Elsevier, Amsterdam, 20.
66. Ramachandran, G.n; Ramakrishnan, C.; Sasisekharan, V. Stereochemistry of polypeptide chain confirmations. *J. Mol. Biol.* **1963**, *7*, 95-99.
67. Hanwell, M.D.; Curtis, D.E.; Lonie, D. C.; Vandermeersch, T.; Zurek, E.; Hutchison, G.R. Avogadro: An advanced semantic chemical editor, visualization, and analysis platform. *Journal of Cheminformatics* **2012**, *4*,17.
68. Nilius, B.; Talavera, K.; Owsianik, G.; Prenen, J.; Droogmans, G.; Voets, T. Gating of TRP channels: a voltage connection? *J Physiol.* **2005**, *567*(1), 35-44.
69. Ramsey, I. S.; Delling, M.; Clapham, D. E. An introduction to TRP channels. *Annu. Rev. Physiol.* **2006**, *68*, 619–647.
70. Venkatachalam, K.; Montell, C. TRP channels. *Annu. Rev. Biochem.* **2007**, *76*, 387–417.
71. Caterina, M.J. Transient receptor potential ion channels as participants in thermosensation and thermoregulation. *Am. J. Physiol. Regul. Integr. Comp. Physiol.* **2007**, *292*, R64–R76.
72. Montell C. The TRP superfamily of Cation Channels. *Sci. STKE.* **2005**, *272*, RE3.
73. Caterina, M.J.; Schumacher, M.A.; Tominaga, M.; Rosen, T.A.; Levine, J.D.; Julius, D. The capsaicin receptor: a heat-activated ion channel in the pain pathway *Nature.* **1997**, *389*, 816–824.

74. Hanson, S.M.; Newstead, S.; Swartz, K.J.; Sansom, M.S.P. Capsaicin Interaction with TRPV1 Channels in a Lipid Bilayer: Molecular Dynamics Simulation. *Biophys J.* **2015**, *108*(6), 1425-1434.
75. Garcia-Sanz, N.; Fernandez-Carvajal, A.; Morenilla-Palao, C.; Planells-Cases, R.; Fajardo-Sanchez, E.; Fernandez-Ballester, G.; Ferrer-Montiel, A. Identification of a Tetramerization Domain in the C Terminus of the Vanilloid Receptor. *The Journal of Neuroscience.* **2004**, *24*(23), 5307–5314,
76. Niemeyer, B.A. Structure-function analysis of TRPV channels. *Naunyn-Schmiedeberg's Arch Pharmacol.* **2005**, *371*, 285–294.
77. Kedei, N.I.; Szabo, T.; Lile, J.D.; Treanor, J.J.; Olah, Z.; Iadarola, M.J.; Blumberg, P.M. Analysis of the native quaternary structure of vanilloid receptor 1. *J Biol Chem.* **2001**, *30*, 28613–28619.
78. Morris, G. M.; Huey, R.; Lindstrom, W.; Sanner, M. F.; Belew, R. K.; Goodsell, D. S.; Olson, A. J. Autodock4 and AutoDockTools4: automated docking with selective receptor flexibility. *J. Computational Chemistry* .**2009**, *16*, 2785-91.
79. Morris, G. M.; Huey, R.; Lindstrom, W.; Sanner, M. F.; Belew, R. K.; Goodsell, D. S.; Olson, A. J. Autodock4 and AutoDockTools4: automated docking with selective receptor flexibility. *J. Computational Chemistry* **2009**, *16*, 2785-91.
80. Khairatkar-Joshi, N.; Szallasi, A. TRPV1 Antagonists: the Challenges for Therapeutic Targeting. *Trends in Molecular Medicine.* **2009**, *15*, 14-22.
81. Peier, A.M.; Moqrich, Z.; Hergarden, A.C.; Reeve, A.J.; Andersson, D.A.; Story, G.M.; Earley, T.J.; Dragoni, I.; McIntyre, P.; Bevan, S.; Patapoutian, A. A TRP Channel that Senses Cold Stimuli and Menthol. *Cell.* **2002**, *108* (5), 705-715.
82. Bautista, D.M.; Movahed, P.; Hinman, A.; Axelsson, H.; Stermer, O.; Hogestatt, E.; Julius, D.; Jordt, S.E.; Zygmunt, P.M. Pungent Products from Garlic Activate the Sensory Ion Channel TRPA1. *PNAS.* **2002**, *102*, 12248-12252.
83. Chen, X.; Wang, Q.; Ni, F.; Ma, J. Structure and Function of Full-length Shaker Potassium Channel Kv1.2 by Normal-Mode-Based X-ray Crystallographic Refinement. *PNAS.* **2010**, *107*, 11352-11357.
84. Pence, H.E; Williams, A. ChemSpider: An Online Chemical Information Resource. *J. Chem.Educ.*, 2010, *87* (11), 1123-1124.
85. Nelson, D.L.; Cox, M.M. *Lehninger Principles of Biochemistry*, 3<sup>rd</sup> ed.; Worth: 2000.
86. Choudhary, A.; Pua, K.H.; Raines, R.T. Quantum mechanical origin of the conformational preferences of 4-thaiproline and its S-oxides. *Amino Acids.* **2011**, *41*, 181-186.
87. The PyMOL Molecular Graphics System, Version 1.8 Schrödinger, LLC.

88. Petrocellis, L.D.; Chu, C.J.; Moriello, A.S.; Kellner, J.C.; Walker, J.M.; Di Marzo, V. Actions of two naturally occurring saturated *N*-acyldopamines on transient receptor potential vanilloid 1 (TRPV1) channels. *British Journal of Pharmacology*. **2009**, *143* (2), 251-256.
-